Stochastic model of high-speed train dynamics for the prediction of long-time evolution of the track irregularities

Nicolas Lestoille

UNIVERSITÉ PARIS-EST

École doctorale Sciences, Ingénierie et Environnement

Thèse de Doctorat

presentée par

Nicolas LESTOILLE

pour obtenir le grade de

Docteur de l'Université Paris-Est

Spécialité : Mécanique

16 Octobre 2015

Stochastic model of high-speed train dynamics for the prediction of long-term evolution of the track irregularities

Jury

Didier CLOUTEAU	Ecole Centrale Paris	Président
Scott COGAN	Université de Franche-Comté	Raporteur
Geert DEGRANDE	KU Leuven	Raporteur
Denis DUHAMEL	Université Paris Est	Examinateur
Christine FUNFSCHILLING	SNCF	Examinateur
Christian SOIZE	Université Paris Est	Directeur de thèse

Acknowledgments

This doctoral thesis arised within the framework of a CIFRE contract between the laboratory MSME at Université Paris Est and the Innovation and Research Department at SNCF. The subject was initiated by SNCF as the following of two doctoral thesis that consisted in identifying the multibody model of the TGV Duplex for the first one, and in constructing the global stochastic model of the track irregularities for the second one.

I would like to thank everybody who contributed to this work, in particular my supervisors at SNCF and at Université Paris Est. At SNCF the thesis was supervised by Christine Funfschilling and at Université Paris Est by Professor Christian Soize. With their strong involvment in this work and their wise advice, they created a very constructive environment for this thesis to bring forward. I would like to thank them for the confidence they have given to me and their support during the three years of my doctoral thesis. The discussions we have, the ideas and the proposals they suggested to me have taken part in a very stimulating environment for this work. I thank them particularly for their unresting availability and for the time spent with me, especially during the redaction of this manuscript. They never refused to explain again what could still be unclear for me. Their involvment in their own job, and their level for requirements and precision, have been for me a source of motivation and contributed to increase my rigor and my autonomy. I also really appreciated their will for having me succeeding in my research work, progressing in the understanding of my subject, and in my writing and scientific skills. They helped me to surpass myself in order to keep progressing in my domain, which makes the richness and the quality of our relations.

I also would like to express my gratitude to all my colleagues at SNCF and at Université Paris Est for their support and for the good time we had. I would like to thank Vinicius Alves Fernandes and Guillaume Perrin for having warmly welcomed me at SNCF. Vinicius Alves Fernandes and Guillaume Perrin have been for me good examples for succeeding in the PhD work. At SNCF, I also involved myself in the organization of the "journée doctorale" (PhD days) and in the PhD student network of SNCF. I would like to thank Elodie Arlaud and Vinicius Alves Fernandes for having shared this experience with me. The time spent together exploring the apparatus of SNCF and organizing this event has given rise to new friendships. I would like to thank all the people with whom I shared an office (or an open space) during my three years of doctoral thesis for the good time we had, in particular Noura Ouhbi, Elodie Arlaud, Olivier Néel at SNCF, Olivier Ezvan, Rémi Capillon, Hussein Nassar, and Corentin Coguenanff at the MSME. Scientific conferences are normal part of a research work, but also they are an opportunity for spending time in an usual frame with colleagues. Especially, a conference in Ajaccio and

one in Graz allowed for having great time with some colleagues of SNCF, and I would like to thank them for it.

Finally, I would like to thank my friends and my family who supported me during this doctoral thesis. The support of my roommates and of my parents has been precious especially while I was writing this manuscript, and I was happy to share with them the difficulties and also the joys of these three years.

Paris, October 2015

Modèle stochastique de la dynamique des trains à grande vitesse pour la prévision de l'évolution à long terme des défauts de géométrie de la voie.

Thèse préparée au laboratoire de Modélisation et Simulation Multi-Echelle :
MSME UMR 8208 CNRS
5, boulevard Descartes
77 454 Marne-la-Vallée
France

Résumé.
Les voies ferrées sont de plus en plus sollicitées : le nombre de trains à grande vitesse, leur vitesse et leur charge ne cessent d'augmenter, ce qui contribue à la formation de défauts de géométrie sur la voie. En retour, ces défauts de géométrie influencent la réponse dynamique du train et dégradent les conditions de confort. Pour garantir de bonnes conditions de confort, les entreprises ferroviaires réalisent des opérations de maintenance de la voie, qui sont très coûteuses. Ces entreprises ont donc intérêt à prévoir l'évolution temporelle des défauts de géométrie de la voie pour anticiper les opérations de maintenance, et ainsi réduire les coûts de maintenance et améliorer les conditions de transport.

Dans cette thèse, on analyse l'évolution temporelle d'une portion de voie par un indicateur vectoriel sur la dynamique du train. Pour la portion de voie choisie, on construit un modèle stochastique local des défauts de géométrie de la voie à partir d'un modèle global des défauts de géométrie et de big data de défauts mesurés par un train de mesure. Ce modèle stochastique local prend en compte la variabilité des défauts de géométrie de la voie et permet de générer des réalisations des défauts pour chaque temps de mesure. Après avoir validé le modèle numérique de la dynamique du train, les réponses dynamiques du train sur la portion de voie mesurée sont simulées numériquement en utilisant le modèle stochastique local des défauts de géométrie. Un indicateur vectoriel et aléatoire est introduit pour caractériser la réponse dynamique du train sur la portion de voie. Cet indicateur est construit de manière à prendre en compte les incertitudes de modèle dans le modèle numérique de la dynamique du train. Pour identifier le modèle stochastique des défauts de géométrie et pour caractériser les incertitudes de modèle, des méthodes stochastiques avancées, comme par exemple la décomposition en chaos polynomial ou le maximum de vraisemblance multidimensionnel, sont appliquées à des champs aléatoires non gaussiens et non stationnaires.

Enfin, un modèle stochastique de prévision est proposé pour prévoir les quantités statistiques de l'indicateur, ce qui permet d'anticiper le besoin en maintenance. Ce modèle est construit en utilisant les résultats de la simulation de la dynamique du train et consiste à utiliser un modèle non stationnaire de type filtre de Kalman avec une condition initiale non gaussienne.

Mots clefs : Défauts de géométrie de la voie, dynamique du train, modélisation stochastique, prévision stochastique, problème inverse statistique.

Stochastic model of high-speed train dynamics for the prediction of long-term evolution of the track irregularities.

Abstract.
Railway tracks are subjected to more and more constraints, because the number of high-speed trains, the train speed, and the train load keep increasing. These solicitations go towards producing track irregularities. In return, track irregularities influence the dynamic response of the train, inducing a degradation of the comfort. To guarantee good conditions of comfort in the trains, railway companies perform maintenance operations of the track, which are very costly. Consequently, it is of great interest for the railway companies to predict the long-term evolution of the track irregularities for a given stretch of track, in order to be able to anticipate the start off of the maintenance operations, and therefore to reduce the maintenance costs and to improve the running conditions.

In this thesis, the long-term evolution of a given track stretch is analyzed through a vector-valued indicator on the train dynamics. For this given track portion, a local stochastic model of the track irregularities is constructed using a global stochastic model of the track irregularities, as well as big data made of experimental measurements of the track irregularities performed by a measuring train. This local stochastic model takes into account the variability of the track irregularities and allows for generating realizations of the track irregularities at each long time. After validating the computational model of the train dynamics, the dynamic responses of the train on the measured track portion are numerically simulated using the local stochastic model of the track irregularities. A vector-valued random indicator is defined to characterize the dynamic responses of the train on the given track stretch. This random indicator is constructed such that it takes into account the model uncertainties in the computational model of the train dynamics. For the identification of the stochastic model of the track irregularities and the characterization of the model uncertainties, advanced stochastic methods such as the polynomial chaos expansion and the multivariate maximum likelihood are applied to non-Gaussian and nonstationary random fields.

Finally, a stochastic predictive model is proposed for predicting the statistical quantities of the random indicator, which allows for anticipating the need for track maintenance. This modeling is constructed using the results of the train dynamics simulation and consists in using a nonstationary Kalman-filter type model with a non-Gaussian initial condition. The proposed model is validated using experimental data from the French railways network for high-speed trains.

Key-words : Track irregularities, train dynamics, stochastic modeling, stochastic prediction, statistical inverse problem.

Contents

Résumé de la thèse

Modèle stochastique de la dynamique des trains à grande vitesse pour la prévision de l'évolution à long terme des défauts de géométrie de la voie

La réponse dynamique d'un train à grande vitesse sur les voies ferrées est influencée par les défauts de géométrie de la voie. Ces défauts de géométrie sont des déformations des rails et sont dus à des défauts dans la structure de la voie, à l'environnement et aux efforts et vibrations induits par le passage des trains. En retour, la dynamique des trains provoque des efforts sur la voie qui augmentent les défauts de géométrie. Ce processus conduit à la dégradation du confort et de la stabilité des trains. Pour garantir le confort et la sécurité des passagers, les entreprises ferroviaires effectuent régulièrement des travaux de maintenance de la voie, qui visent à corriger les défauts de géométrie.

Pour déclencher les opérations de maintenance, les entreprises ferroviaires s'appuient sur des mesures de géométrie de la voie qui sont régulièrement effectuées. Si la mesure d'un défaut de géométrie dépasse un seuil préétabli, une opération de maintenance est lancée. Ces travaux de maintenance sont très coûteux et compliqués à organiser pour les entreprises ferroviaires, qui cherchent donc à anticiper les opérations de maintenance pour optimiser leur politique de maintenance des voies. D'autre part, à cause des non-linéarités du système véhicule-voie, les défauts de géométrie de la voie ne sont pas représentatifs des conditions de confort et de sécurité du train. Il serait donc pertinent de déclencher les opérations de maintenance à partir de critères sur la réponse dynamique du train, et non à partir des défauts de géométrie de la voie. Dans ce contexte, l'objectif de la thèse est de développer un modèle capable de prédire l'évolution à long terme (temps d'évolution de la géométrie de la voie) de la réponse dynamique du train sur une portion de voie donnée.

Après avoir partitionné la voie en portions de longueur égale et de type de courbure donné (alignement, entrée de courbe, courbe, sortie de courbe), l'évolution des défauts de géométrie de la voie est observée et analysée, en utilisant les mesures des défauts de géométrie de la voie réalisées par le train de mesure IRIS 320 sur la ligne à grande vitesse reliant Paris à Marseille. Cette analyse conduit à étudier l'évolution des défauts de géométrie de la voie entre deux opérations de maintenance successives, pour une portion de voie donnée et avec un type de courbure donné. Pour une portion de voie donnée, un modèle stochastique local des défauts de géométrie est construit en adaptant un modèle stochastique global de l'ensemble du réseau. Ce modèle local est identifié à partir de la première mesure des défauts de géométrie de la voie par la méthode du maximum

de vraisemblance en multidimensionnel. Il préserve les propriétés statistiques globales des défauts de géométrie et permet d'observer l'évolution à long terme des défauts de géométrie.

Ensuite, la réponse dynamique d'un train à grande vitesse (TGV Duplex) est simulée avec le logiciel *Vampire* pour la portion de voie considérée. Après post-traitement, les résultats de la simulation sont comparés à des mesures de la réponse dynamique du train réalisées dans un TGV Duplex commercial. Cette comparaison permet de recaler les paramètres du modèle numérique du train. Un indicateur vectoriel et aléatoire est défini pour évaluer la réponse dynamique du train sur la portion de voie donnée. La comparaison entre les indicateurs issus de la mesure et ceux issus de la simulation fait apparaître des incertitudes de modèle, induites par les erreurs de modèle dans le modèle numérique de la dynamique du train. Pour prendre en compte ces incertitudes de modèle, on introduit un bruit multiplicatif dans le calcul des indicateurs, en sortie du modèle numérique de la dynamique du train. Ce bruit, qui est un vecteur aléatoire non gaussien, est caractérisé par sa représentation stochastique réduite, qui est ensuite développée en chaos polynomial gaussien. Les coefficients du chaos sont identifiés en résolvant un problème statistique inverse à partir des réalisations expérimentales de l'indicateur. La prise en compte des incertitudes de modèle permet d'accroître la robustesse de l'indicateur.

La troisième étape consiste à développer un modèle stochastique prédictif pour prédire l'évolution à long terme de l'indicateur sur la réponse dynamique du train. L'indicateur est considéré comme une série chronologique non gaussienne et non stationnaire. De plus, le choix du modèle prédictif est limité par le manque de données expérimentales disponibles : puisque la série est non stationnaire, une seule réalisation est disponible à chaque instant, celle de la mesure. Le modèle stochastique prédictif s'appuie sur un filtre de Kalman non stationnaire et non gaussien et est construit à partir d'une équation différentielle stochastique discrétisée. Pour identifier les paramètres du modèle prédictif, on utilise la méthode des moindres carrés pondérée, dont la fonctionnelle est construite à partir des équations des moments du modèle prédictif. Les équations des moments sont estimées en utilisant les réalisations de l'indicateur qui sont générées par le modèle numérique de la dynamique du train aux instants connus. Pour faciliter la convergence de l'algorithme, l'identification est faite en deux étapes : d'abord en une dimension, sur chaque composante de l'indicateur, puis en multidimensionnel sur l'indicateur vectoriel. Enfin, les paramètres du modèle prédictif qui dépendent du temps sont approximés par des fonctions affines, afin de pouvoir connaître leur valeur dans le futur et de prédire l'évolution de l'indicateur à long terme.

L'ensemble des modèles développés est appliqué à l'étude de l'évolution à long terme de la dynamique du TGV sur une portion de voie donnée de la ligne à grande vitesse entre Paris et Marseille. Le modèle stochastique local des défauts de géométrie est identifié à partir des mesures des défauts de géométrie de la portion de voie donnée, et 2000 réalisations de la portions de voie sont générées pour chaque temps de mesure à long terme. Puis, pour chacun de ces temps de mesure, la réponse dynamique du train est calculée en propageant la variabilité des défauts de géométrie par la méthode de Monte Carlo. Simultanément, 2000 réalisations du bruit de sortie sont générées, ce qui permet

de calculer des réalisations des indicateurs de la réponse dynamique du train pour chaque temps de mesure à long terme. Ces réalisations sont utilisées pour identifier le modèle stochastique prédictif de l'évolution de l'indicateur. On peut ensuite estimer la statistique de l'indicateur dans le long terme pour lequel la mesure des défauts de géométrie de la voie n'est pas encore connue. La pertinence du modèle prédictif est évaluée en utilisant comme temps à long terme un temps pour lequel des mesures expérimentales existent, ce qui permet aussi d'évaluer l'erreur de modèle.

Deux principales avancées scientifiques de la thèse peuvent être soulignées :

- La première est relative au développement de modèles stochastiques avancés, en grande dimension statistique, et appliqués à un problème industriel. Il s'agit de l'adaptation du modèle stochastique global de la géométrie de la voie à un modèle stochastique local, et de la prise en compte des incertitudes de modélisation dans le modèle numérique du train par un bruit multiplicatif en sortie du modèle. Ces modèles stochastiques sont identifiés en résolvant des problèmes statistiques inverses à partir de mesures expérimentales. Des méthodes stochastiques adaptées sont utilisées, comme le maximum de vraisemblance en plusieurs dimensions, et le développement en chaos polynomial pour des vecteurs aléatoires non gaussiens.

- La seconde avancée scientifique correspond à la construction du modèle stochastique prédictif pour une série chronologique (la série des indicateurs) qui est non stationnaire et non gaussienne, pour laquelle peu de données expérimentales sont disponibles. Le modèle de prédiction stochastique est non stationnaire, de type filtre de Kalman avec une condition initiale non gaussienne.

Sur le plan de l'apport pour les industriels, l'évolution à long terme d'une portion de voie ferrée a été modélisée par un modèle stochastique validé. La quantité d'intérêt choisie pour l'évolution est un indicateur aléatoire vectoriel relatif à la réponse dynamique du train sur la portion de voie. La robustesse de cet indicateur est accrue en prenant en compte les incertitudes de modélisation dans le modèle numérique du train. En utilisant le modèle prédictif stochastique, l'évolution de l'indicateur dans le temps peut être prévue, ce qui permet d'anticiper les opérations de maintenance. Un seuil vectoriel de l'indicateur a été introduit à partir des politiques de maintenance actuelles, et contribue à une aide à la décision pour le déclenchement des opérations de maintenance.

Chapter 1

Introduction and objectives

1.1 Industrial context

Railway transport has considerably changed in the recent years: high-speed trains are meant to run ever faster, carrying heavier loads and consuming less energy. Due to the opening to competition, several high-speed trains, such as TGV, ICE, ETR500, etc., for which mechanical properties and structures are different, are likely to run on the same tracks, while they may have been originally designed for specific and different railways networks. At the same time, railway transport has to remain reliable and comfortable. Those items are mainly guaranteed by the dynamic response of the train to the track excitation.

Among the various causes that influence the dynamics of the train-track system, track irregularities are one of the most important factors. The track irregularities are the variations of the vertical and lateral track profiles, due to the rail deformations. They are produced by the vibrations induced by the running trains, by the environment (rain, frost, etc.), or by the track substructure itself (uneven track layers, pipes under the track, etc.). These variations in the track geometry are made possible by deteriorations in the infrastucture, such as the settlement of the track, the ballast loosening, the track slipping, etc. Four track irregularities are distinguished and represented in Figure 1.1: the lateral offset, the vertical offset, the cross level, and the gauge irregularity. In the following, the track irregularities will be denoted by x_1 (lateral offset), x_2 (vertical offset), x_3 (cross level), and x_4 (gauge irregularity). The track irregularities influence the dynamic response of the train, inducing vibrations in the vehicle and reducing the passenger comfort. In return, the dynamic response of the train produces forces on the track, leading to further deterioration of the track and to a reduction of the comfort and of the stability.

To guarantee good conditions of comfort and safety in the trains, railway companies have to monitor the track irregularities, using experimental measurements of the track which are carried out by recording vehicles. The historical recording vehicle used by SNCF is called "Mauzin" car and measures the track irregularities thanks to the height differences between its independent wheelsets. For the high-speed lines, SNCF has developed a recording high-speed train called "IRIS 320" (see Figure 1.2), which inspects the track geometry by inserting in the commercial operation of trains. The experimental

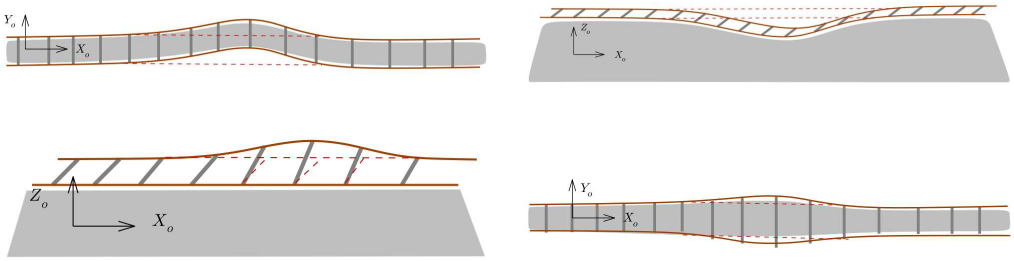

Figure 1.1: Track irregularities: lateral offset x_1 (top left), vertical offset x_2 (top right), cross level x_3 (bottom left) and gauge irregularity x_4 (bottom right).

Figure 1.2: High-speed train IRIS 320 for the tracks inspection.

measurements of the track geometry provided by IRIS 320 constitutes a big data base that can be exploited for a better knowledge of the track irregularities. The measured track irregularities are compared to certain limits that depend on the train speed. Three threshold levels are actually in use in France for the track irregularities monitoring:

- Alert Value, which refers to the value that necessitates monitoring or taking maintenance actions as part of regularly-planned maintenance operations,
- Intervention Value, which refers to the value that requires short term maintenance action,
- Slow-down Value, which refers to the value above which the speed limit for the trains is lowered to guarantee the comfort and the safety in the trains.

To compare the track measurements with the threshold levels and start off the maintenance operations, the four track irregularities are considered independently (although it could not be denied that the four track irregularities are dependent).

When a threshold level is reached for a track irregularity, a maintenance operation of

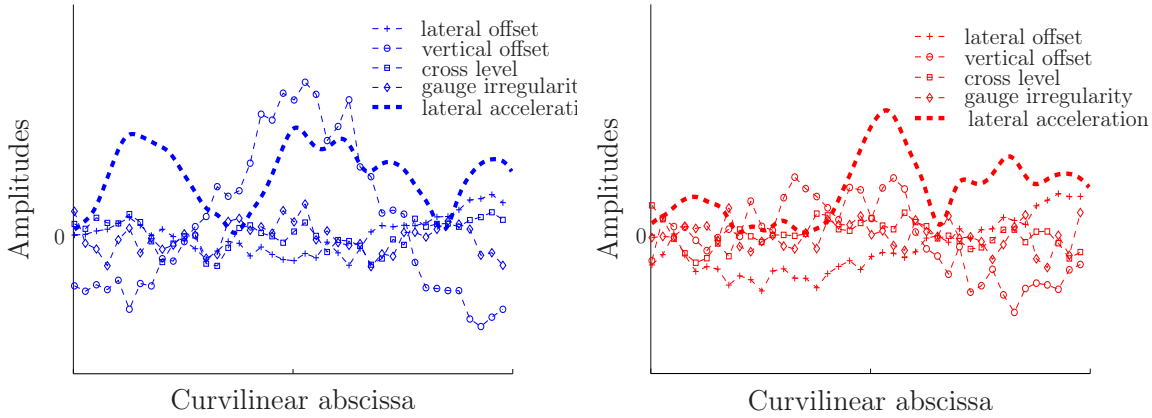

Figure 1.3: Nonlinearity of the train-track coupling: high amplitudes for track irregularities (left) produce lower lateral acceleration than smaller track irregularities (right).

the track is undertaken by the railway companies in order to correct the track irregularities. There are various types of maintenance operations, but the tamping is usually used to correct the track irregularities. The tamping may be carried out on a few meters (it is thus a localized maintenance) or on hundreds of meters (it is denoted heavy tamping). For the railway companies, the maintenance operations are very costly: it is considered that maintenance costs for rail-track subsystem may represent 55% of total maintenance costs in the case of the high-speed line system [1]. That is why many railway companies wish to optimize the scheduling of their maintenance operations, planning as well as possible the track stretches to be maintained and the moments for the maintenance works. Going further, it would be of great interest to be able to predict when the maintenance operations would be needed, before reaching the track irregularities threshold levels. The prediction of the maintenance operations would reduce the maintenance costs and improve the asset management as well as the comfort conditions in the train. In that case we talk about predictive maintenance.

It has to be noticed that the track geometry is strongly coupled to the dynamic response of the train. A better understanding of the train-track interaction would then be helpful to characterize the evolution of the track irregularities for a stretch of the railway track. This interaction has been studied in [2] and appears to be nonlinear: several small irregularities may have a bigger influence on the dynamic response of the train than a big irregularity. Figure 1.3 illustrates this nonlinearity: the lateral acceleration of a train bogie is plotted as a function of the curvilinear abscissa of the track, with the corresponding track irregularities, for two different sequences of irregularities. It can be observed that the amplitude of the lateral acceleration in the train is higher with smaller track irregularities.

1.2 Industrial objectives

The anticipation of the maintenance operations requires the ability to predict the long-term evolution of the train-track system for a given stretch of the railway track. The considerations presented in the previous section have three main consequences relatively to the long-term evolution of the train-track system:

- It confirms that the four track irregularities have to be considered altogether and not independently.
- This leads to look after, not only the track irregularities, but also the dynamic response of the train, and to start off the maintenance in function of accelerations in the train or forces applied to the train.
- Finally, it promotes the study of the track irregularities, not on a given point of the track anymore, but on a whole stretch of the railway track, in order to consider the succession of track irregularities.

Consequently, the first objective of this thesis is to construct a long-term evolution model of the dynamic response of the train for a given stretch of the railway track with respect to the degradation of the track geometry. The four track irregularities will be considered dependently on the given stretch of the railway track, and the long-term evolution of the dynamic response of the train will be observed at a given point of this stretch of the track. Criteria on the dynamic response of the train have to be introduce that allow the assessment of the train dynamics with respect to the track irregularities. The dynamic response of the train can be known either through experimental measurements performed by sensors embedded in the train, or through numerical simulation. For complex systems, the numerical dynamic simulation has encountered big improvements in recent years, allowing for simulating the behavior of a whole train on a track stretch. However, the dynamic simulation has to be very representative of the physical behavior of the system. The models of the trains, of the railway track, and of the wheel-rail contact have to be validated and the simulations have to be raised on realistic and representative sets of excitations. The use of stochastic processes allows for increasing the representativeness of the encountered conditions by taking into account the parameters and model uncertainties. It has also been shown in [3, 4] that the representation of the system uncertainties by stochastic processes increases the robustness of the modeling.

Thus, the second objective of this thesis is to take into account the track measurements for identifying the stochastic model of the track irregularities for a given stretch of the railway track, and for identifying the model uncertainties in the computational model of the train dynamics induced by modeling errors.

Thanks to the identification of the physical parameters of the computational model of the train (the French high-speed train TGV Duplex) by Kraft [5] and to the stochastic modeling of the track irregularities by Perrin (see for instance [6]), we have scientific and computational tools to construct a stochastic model for the long-term evolution of the dynamic response of the train with respect to the long-term evolution of the track irregularities. The proposed stochastic model of the dynamic response of the train has to

predict the long-term evolution of the dynamic response of the train for a given stretch of the railway track, allowing railway companies to anticipate the maintenance operations. In the following, the distinction will be done between the long time (of the order of the week), which is the time of degradation of the track geometry for a given stretch of the railway track, and the time of the dynamic response of the train (of the order of the second).

1.3 Scientific objectives

Modeling the variabilities and the uncertainties of the train-track system implies scientific challenges that are inherent to the railway context. From a scientific point of view, the track irregularities can be considered as a random field, which is neither stationary (non-homogeneous) nor Gaussian. For a given stretch of the railway track, a local stochastic model of the track irregularities has to be constructed taking into account these probabilistic properties. This local stochastic model is identified by using a statistical inverse method with experimental measurements of the track irregularities for the given stretch of the track. The variability of the track irregularities is then propagated in the train dynamics computational model, giving in output a random field for the dynamic response of the train. The Monte-Carlo method is used to propagate the variability and the uncertainties into the train dynamics simulation, as it is frequently done in order to compute the response of dynamic systems to random excitations (see for example [7]). The model uncertainties in the computational model of the train dynamics are also analyzed and identified in this work. For identifying the statistical properties of nonstationary and non-Gaussian random fields from a finite set of experimental data, experimental measurements of the dynamic response of the train and statistical inverse methods have to be used.

The presence of nonlinearities in the train dynamics computational model (due to contact forces and suspensions) prevents us from directly deducing the long-term evolution of the dynamic response of the train from the long-term evolution of the track irregularities. A few consequences of nonlinearities and methods to detect them can be found in [8]. The prediction of the long-term evolution of the dynamic response of the train requires to construct a stochastic predictive model for the dynamic response of the train, knowing the past and present time evolution of the dynamic response of the train. The dynamic response of the train is thus considered as a time series, which is non-Gaussian and nonstationary. Taking into account these probabilistic properties of the train dynamic reponse, methods for its long-term prediction will be analyzed in this work and a stochastic predictive model will be developed. Finally, since the number of long times for which measurements are performed is small (between 10 and 15), the choice of a long-term stochastic prediction model of the dynamic response of the train is relatively restricted, and consequently, an adapted nonstationary and non-Gaussian Kalman-filter type model has been chosen.

1.4 State of the art

The developments and applications presented in this thesis appeal to several fields of recent scientific advances that are summed up hereinafter. First, signal processing and data processing classic tools (an overview can be found in [9, 10, 11]) are used for the post-processing of the experimental measurements of the track irregularities and of the dynamic responses of the train.

Several track-irregularities modeling methods have been recently developed thanks to the improvements in computational resources, which allows the development of more complex modelings. An overview of these modeling methods is presented in Section 1.4.1. The degradation of the track geometry has also been studied using statistical tools, for which examples are given in Section 1.4.2. Recent advances in inverse problems allows for assessing the track quality through the dynamic response of the train, taking into account the nonlinear coupling between the track geometry and the dynamic response of the train, as presented in Section 1.4.3.

1.4.1 Modeling the track irregularities

The observation of track irregularities drove engineers to construct mathematical models for the track irregularities. First models are deterministic and use spectral representations or wavelet transforms of the measured track irregularities. Because these models are not able to take into account the variability of the track geometry, more advanced modelings have recently been developed, which consist in stochastic models whose statistical properties are identified by using statistical inverse methods with experimental measurements of the track irregularities. In a first approach, Iyengar and Jaiswal [12] describe the cross level as a stationary Gaussian random field, which is characterized by its power spectral density function. The same authors propose also a stationary non-Gaussian model for the track irregularities [13] and show that the non-Gaussian model is consistently better than the Gaussian one. The proof is given in analyzing the statistics of the number of crossings and of peaks for the cross level of a railway line. A stochastic model of the track irregularities, based on the use of the classical spectral representation for stationary Gaussian random processes and the corresponding random generator of track irregularities, has been proposed by Lei [14]. This representation allows for generating track irregularities in order to compute the dynamic response of the train with respect to the track irregularities. Track stretches of a length of 200 m are generated with the stochastic model, as recommended by Esveld [15], for an optimal use of the information and control of maintenance and renewal processes.

The statistical dependencies between the track irregularities are highlighted by Hamid [16], who intents to sum up the four track irregularities in establishing a track quality index as a function of the standard deviation of the four track irregularities. El-Sibaie and Zhang [17] improve the definition of the track quality index by introducing the train speed in its definition.

Another approach is proposed in [18] by introducing a representation of the track irregularities based on a discrete Fourier transform. More recently, the Perrin works [19, 6, 20] consider the four track irregularities as a nonstationary and non-Gaussian vector-valued random field, whose spatial discretization is a non-Gaussian random vector that is decomposed by the principal component analysis, and for which the dependent projections are represented by using a polynomial chaos expansion in high dimension. In addition, the experimental estimation of the correlation matrix of this random vector is enriched, by using a new technique related to stationary tools, in order to increase the rank of the estimated correlation matrix. The polynomial Gaussian chaos can represent non-Gaussian second-order random variables as the sum of polynomials of Gaussian random variables [21, 22]. Consequently, the model proposed in [19, 6, 20] enables to generate track irregularities for any track stretch of the studied high-speed line, while being representative of the whole studied high-speed line. This approach allows for propagating the variability of the track irregularities in the train dynamics computational model in order to simulate numerically the dynamic response of the train. However, it does not enable to observe the degradation of the track irregularities of a given local track stretch, because the specifity of each given track stretch is not preserved in such a global stochastic model.

1.4.2 Modeling the degradation of the track irregularities

In order to improve the track maintenance strategies and to predict the need for maintenance operations, railways engineers are interested in modeling the long-term evolution of the track irregularities. With the emergence of big data coming from the track measurements, the idea came progressively to use the track history to predict future states of track irregularities. Most of the existing degradation models are global models used for the asset management, but some local models for the degradation of a stretch of the railway track start being proposed.

In the case of global models, Hamid and Gross [16] developed an empirical degradation model for the track quality index through linear autoregressive techniques. A significant contribution has been brought by Bing and Gross [23], introducing a degradation model taking into account the train traffic, the track structure, the type of maintenance and the quality of ballast. A detailed study has been undertaken by Esveld [24], trying to understand the deterioration mechanism of the track. The results show that the degradation should be modeled at the scale of a track stretch and that the degradation model parameters should be identified using experimental data. Likewise, Zhang *et al.* [25] observed the relationship between several components of the tracks (subgrade, ballast, sleepers, rails), introducing a degradation model of the track quality index as a function of the track components and of the maintenance parameters.

The following research works focus on optimizing ballast tamping and renewal actions from a life-cycle cost perspective (see [26]). Other models have been developed by Patra *et al.* [27] and by Andrade *et al.* [28], introducing variability in the degradation model parameters. The former considers a linear degradation law of the standard deviation of the lateral offset, of which parameters are functions of the train speed and the tonnage (the sum of all axle loads of all trains that have run on the considered track stretch). The

model parameters are random variables whose probability distributions are identified by using the Bayes method. The model is improved in [29] by taking into account the number of tamping operations on the studied track stretch, and considering the dependency between the vertical offset and the lateral offset. The joint probability distribution for both irregularities gives better results than the independent case.

Another approach consists in modeling indicators on the track irregularities by introducing stochastic processes indexed by long time. For instance, a bivariate Gamma process with independent increments has been fitted to experimental data of the track geometry degradation and applied to the maintenance scheduling [30] and to the optimization of the maintenance planning [31]. The parameters of the probability distribution are identified by the maximum-likelihood method. Here again, it is noticed that considering the dependency between track irregularities increases the relevance of the model. The Dagum process has also been applied to fit the degradation of the longitudinal offset of the Portuguese railway Northern line [32]. Similarly, the standard deviation of the vertical offset is considered, at each long time, as a random variable following a Weibull distribution [33]. This work also shows that traffic speed and maintenance history have an impact on the track irregularities degradation. Then, prediction techniques, such as neural networks [34], stochastic state space methods [35], and Petri net models [36] have been applied to the long-term evolution of the track irregularities. The Petri net model introduces a framework for performing Monte Carlo simulations, in order to compare the effects of several asset management strategies. Markov models of a stretch of the railway track were developed and are simpler than the Petri net model. They allow the asset management of a single stretch of the railway track to be investigated [37, 38]. These techniques define discrete states of the track irregularities and model the long-term evolution from one state to another one. For instance, [38] distinguishes four states: good condition, maintenance requested, speed restriction required, and line closure required. Compared to the linear degradation laws, these approaches take into account the nonlinearity of the degradation and the previous states of the track irregularities, even though they are not directly related to the train behavior and to the train traffic on the considered track stretch.

After having looked at some asset management models, we will now focus on degradation models of local track stretches, allowing the prediction of maintenance operations for these track stretches. A first development consists in finding in the past the most possible similar track irregularity and in applying its long-term evolution to the studied track irregularity [39]. The same approach leads to a multi-stage linear model for the evolution of the track irregularities [40, 41], considering each track irregularity as an independent time series. New opportunities, such as linear autoregressive (AR) models, Kalman filter and artificial neural networks are explored in [42], considering the track irregularities of a given stretch of the railway track, represented by a track quality index, as a time series. Artificial neural networks give the best results because they have better durability, highly nonlinear and strong self-adapting learning ability.

The interaction between the degradation of the track and the train traffic has been studied, but mostly by focusing on the ballast degradation and very few on the track

irregularities. To this extent, the dynamic response of the track to the train traffic has been studied, for example in [43, 44]. The computations of the track dynamics rely on numerical models using finite elements that allow the infrastructure vibrations induced by the train traffic to be simulated, such as those developed in [45, 46, 47]. The measurement of the track response to the passage of trains (as in [48]) allows the models to be experimentally validated. Taking into account the variability in the ground vibration predictions reduces the distance between predicted and measured ground vibrations (see [49]). A relationship between the track settlements and the number of load cycles due to the train traffic has been established in [50]. Furthermore, a model for the prediction of the track settlement has been developed in [51] taking into account the train traffic thanks to the numerical dynamic simulation of the train behavior. The influence of the vehicle suspensions on the track settlements has been studied in [52].

The presented overview of prediction techniques for the degradation of the track irregularities shows the recent advances for modeling the long-term evolution of track irregularities. These advances make use of stochastic processes and of the history of a track stretch using experimental data. Nevertheless, the relationship between the track irregularities and the dynamic response of the train has to be deeply explored. Taking into account the advances presented before, the present work considers a stochastic model of the track irregularities for a given track stretch (and not only a track quality index or the track irregularity at a given point) on which the dynamic response of the train is simulated to take into account the complexity of the track irregularities. The long-term evolution of the given track stretch is observed through a vector-valued indicator on the dynamic response of the train.

1.4.3 Assessment of the track irregularities through the dynamic response of the train

Taking into account the mechanical coupling between the track irregularities and the train dynamics, engineers have observed the train behavior as a function of the track irregularities. Using computational models to predict the dynamic response of the train on the track, they detected the track stretches that have to be maintained. The nonlinear character of the train-track coupling is highlighted in [2, 53]. As a basic model for the train-track coupling, the cross level was first related to a ride comfort indicator via transfer functions [54]. Using a simple inverse method, this approach allows limits on the cross level to be set as a function of the ride comfort indicator. Then, the correlation between the derivatives of the track irregularities and the train-track forces has been observed in [55]. Thanks to the improvements of computational models, the dynamic response of the train can be precisely and rapidly predicted, which allows the model uncertainties to be taken into account in the simulation [56].

Other approaches try to determine criteria on the dynamic response of the train, which correspond to the required limits for the track irregularities. This is more feasible for vertical track irregularities (vertical offset), which are strongly related to the train vertical acceleration, whereas the relationship between other irregularities and the dynamic response of the train is more difficult to characterize, because of the small difference

between the track gauge and the wheels gauge and because of the nonlinearity in the wheel-rail contact. Thus a limit value on the vertical acceleration has been defined in [57] that corresponds to the limit value on the vertical offset. The vertical irregularities can be detected by observing the dynamic response of the train through experimental measurements [58, 59]. Going further, the dynamic response of the train is simulated on randomly generated track irregularities and the vertical accelerations are analyzed using the wavelet tranforms, in order to identify the damaged stretches of the track [60]. A model is then proposed to estimate the track irregularities by using inverse problems and measurements of the lateral and vertical accelerations of the train [61].

Thanks to the development of numerical tools (data processing and simulation) and of mathematical tools (statistical inverse problems in high dimension), the dynamic response of the train can be connected with the track irregularities. This allows criteria and threshold levels on the dynamic response of the train to be defined in order to observe the long-term evolution of the dynamic response of the train.

1.5 Adopted approach in the thesis

1.5.1 Choice of the adopted approach

- The goal of this thesis is to build a model of long-term evolution, that is based on experimental measurements of the track geometry and of the train dynamics. Thus, the goal is not to analyze the long-term evolution of some physical parameters of the track and of its underlying structure, as well as the long-term evolution of some mechanical and geometric parameters of the train and of the wheel-rail contact.

- This choice is guided by the fact that the railway network is spatially extremely heterogeneous for a same railway line. Moreover, the long-term evolution of the track depends on the considered stretch of the track and is related to the weather conditions and to the various types of trains that run on the line. Thus, a parametric approach is not feasible.

- This is why a global stochastic model of the track irregularities for the French railway network has been constructed and adapted for all considered stretches of the track using measurements of these stretches, which experimentally validate the constructed stochastic model.

- Furthermore, the train is used as a tool to characterize the impacts of the track irregularities on the comfort and the security of the train. In these conditions, it is important to take into account the modeling error in the train computational model, which is identified using simultaneous experimental measurements of the track geometry and of the corresponding responses of the train. Such an approach replaces a parameterized model of the train dynamics and of the vehicle-track interaction, for which the construction is not feasible.

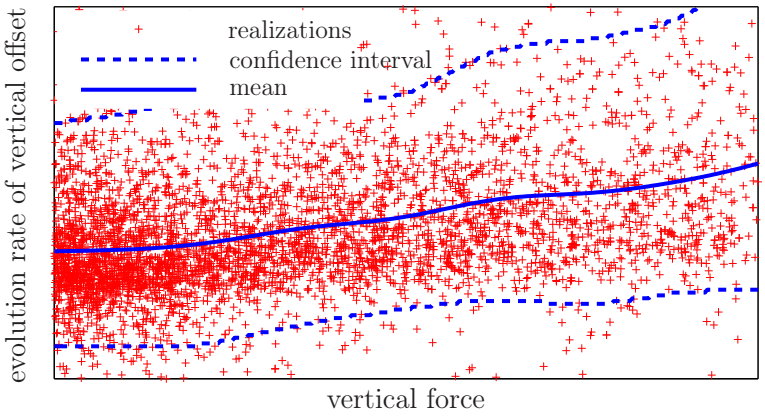

Figure 1.4: Evolution of the vertical offset as a function of the vertical force for the track stretches of the studied high-speed line.

1.5.2 Statistical approach

Given the previous research about the track irregularities modeling, about the degradation of the track irregularities, and about the train-track coupling, the present work aims at identifying a stochastic predictive model for the long-term degradation of a track stretch. In this thesis, we consider a track stretch belonging to a given high-speed line of the French railway network, typically the high-speed line between Paris and Marseille. The predictive model, which predicts the evolution of a given stretch of the railway track for future long time, allows for determining the best moment to start off the next maintenance operation. The long-term evolution of the track irregularities for the given track stretch is thus studied between two successive maintenance operations. To be more representative of the train safety and of the comfort in the train, maintenance operations should be scheduled according to criteria on the train dynamic reponse. The track irregularities of the given track stretch are experimentally measured at long times $\tau_1, \tau_2, \ldots, \tau_K$ by the measuring train IRIS 320: τ_1 is the first discrete long time of a track measurement after a maintenance operation, and τ_K is the last measurement time for the track stretch before the next maintenance operation. The time step between two measurements is not constant and depends on the considered stretch of the railway track.

As explained in Section 1.4, the long-term evolution of the track irregularities and its consequences on the dynamic response of the train depend a lot on the studied stretch of the railway track. For example, Figure 1.4 shows that the vertical force at the wheel-rail contact is hardly correlated to the evolution of the track vertical offset and thus depends a lot on the considered stretch of the railway track. It is thus necessary to study locally the long-term evolution of each stretch of the railway track and to develop a predictive model adapted to each track stretch. In the following, the high-speed track is divided into track stretches of constant length S. For a given stretch of the railway track, a local stochastic model of the track irregularities is constructed using an experimental measurement of the track irregularities and based on the global stochastic modeling developed in [19, 6, 20]. The global modeling considers track irregularities as a nonstationary and

non-Gaussian random field, and is able to generate realizations of the track irregularities for any stretch of the railway track of the studied high-speed line. Such a global stochastic model has to be adapted to take into account the specificities of the given track stretch, while preserving the statistical properties defined in the global stochastic model. The adapted model allows for reducing the statistical fluctuations for the given track stretch, with respect to the global stochastic model.

A first possible approach would be to characterize and to model the long-term evolution of the track irregularities. Then, the simulation of the dynamic response of the train for such predicted track irregularities would allow for predicting the degradation of the running conditions for the train, and thus for anticipating the maintenance operations. Unfortunately, two main drawbacks prevent us from using such a possible approach.

- The long-term evolution of the track-irregularities model is difficult to characterize because of the high dimension of the model. The model developed in [19, 6, 20] is chosen with $2,000$ components in order to get a small projection error. The observation of the long-term evolution of these $2,000$ components did not give any conclusive results.

- Criteria to start off the maintenance operations have to be defined for the dynamic response of the train. Unfortunately, the nonlinear coupling between the track irregularities and the dynamic response of the train implies that an evolution in the track irregularities is not directly related with an evolution of the dynamic response of the train. Therefore, the parameters of the track-irregularities model that influence the dynamic response of the train (and whose long-term evolution could be modeled) are unknown and consequently, their identification is an ill-posed problem.

Therefore, it has been chosen to characterize and to model the long-term evolution of the dynamic response of the train on a given track stretch. After validating the computational model of the train dynamics, the dynamic response of the train on the measured track stretch is simulated with the Monte-Carlo method, using in input realizations of the local stochastic model of the track irregularities. The simulation is performed with a multi-body software. An accurate modeling of the dynamic response of the train implies to take into account the model uncertainties in the train dynamics computational model. A vector-valued random indicator on the dynamic response of the train, which is representative of the train comfort, has to be defined, so that its long-term evolution can be analyzed and modeled. This random indicator, denoted by $\mathbf{C}(\tau_1), \ldots, \mathbf{C}(\tau_K)$, will be computed at each long time $\tau_1, \ldots, \tau_K$ using the numerical stochastic simulation of the train dynamics. To start off the maintenance operations, threshold levels on the random indicator have to be defined according to a given maintenance strategy.

Finally, a stochastic predictive model is proposed for predicting the statistical quantities of the random indicator. Since the long-term evolution of the train-track system is strongly nonstationary and non-Gaussian, it is assumed that the random indicators $\mathbf{C}(\tau_1), \ldots, \mathbf{C}(\tau_K)$ can be represented by a nonhomogeneous and non-Gaussian discrete time series. The stochastic predictive model is constructed using the stochastic results

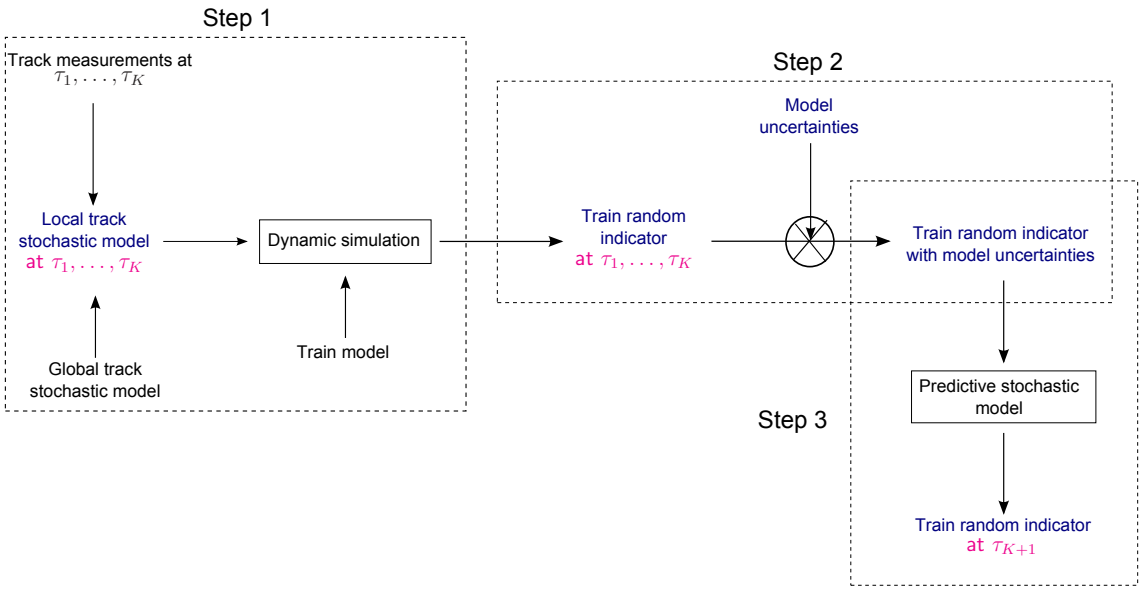

Figure 1.5: Proposed approach.

of the train dynamics simulation and is based on a nonstationary model of Kalman-filter type with a non-Gaussian initial condition. The model coefficients depend on the long time and have to be identified using the known realizations of the vector-valued random indicators $\mathbf{C}(\tau_1), \ldots, \mathbf{C}(\tau_K)$. Using the stochastic predictive model, the realization of the random indicator $\mathbf{C}(\tau_{K+1})$ is predicted for future long time τ_{K+1}, which allows for anticipating the need for track maintenance. The proposed model is validated using experimental data for the French railway network for the high-speed trains.

The adopted approach can be summarized in three steps, as presented by the diagram in Figure 1.5:

1. Construction of the local stochastic model of the track irregularities for a given stretch of the railway track.

2. Construction of the vector-valued random indicator for the dynamic response of the train and construction of the model uncertainties induced by modeling errors in the computational model of the train dynamics.

3. Construction of the predictive stochastic model for the random indicator.

1.6 Outline of the thesis

Given the adopted approach explained before, the thesis is organized as follows.

Chapter 2 is devoted to the construction of the local stochastic model of the track irregularities for a given stretch of the railway track. The modeling developed in [19, 6, 20] is briefly summarized, and the local stochastic model for a given stretch of the railway track is identified.

Chapter 3 adresses the computational nonlinear model of the high-speed train in presence of model uncertainties induced by modeling errors in the train dynamics computational model. In this chapter, the numerical simulation of the dynamic response of the train is validated using experimental measurements. The vector-valued random indicator on the dynamic response of the train is defined and the model uncertainties of the train dynamics computational model are characterized.

Chapter 4 deals with the construction of the stochastic predictive model for the long-term evolution of the random indicator.

Chapter 5 is devoted to the application of the model developed in the previous chapters for a given stretch of the railway track of the studied high-speed line. In particular, it will be shown how the adopted approach would allow for scheduling the track maintenance operations taking into account criteria for the train comfort.

1.7 Main scientific and industrial contributions

1.7.1 Scientific contributions

The main scientific contributions are:

1. The first one consists in developing advanced stochastic models in high stochastic dimension adapted to an industrial problem. These stochastic models are identified by solving statistical inverse problems on the basis of experimental measurements and by using advanced stochastic methods such as the multivariate maximum likelihood and the polynomial chaos expansion for the spatial discretization of nonstationary and non-Gaussian random fields and for non-Gaussian random vectors.

2. The second one consists in developing a stochastic predictive model for a nonstationary and non-Gaussian discrete time series for which only few data are available, preventing the use of all the classical Bayesian filterings. The stochastic predictive model is then based on a nonstationary model of Kalman-filter type with a non-Gaussian initial condition.

1.7.2 Industrial contributions

The adopted approach of the thesis emphasizes several results which are useful for the railway companies. The modeling of the dynamic response of the high-speed train for

a measured track stretch gives a better knowledge of the train-track coupling, thanks to the local stochastic model of the track irregularities and to the introduction of the model uncertainties in the computational model of the train dynamics. Such a stochastic model actually makes the prediction of the dynamic response of the train more robust.

Using the expertise and the current railway norms, a vector-valued random indicator on the dynamic response of the train is proposed to monitor the long-term evolution of the train safety and the comfort in the high-speed trains. A threshold level on this indicator is introduced in order to start off the maintenance operations when the threshold is exceeded. The threshold level is fixed according to the current maintenance policy but could be adjusted when changing the maintenance strategy. Thanks to the probabilistic model of the indicator for the dynamic response of the high-speed train, which is proposed, the maintenance operations can be scheduled in a way that takes into account the train safety and the comfort conditions in the high-speed train.

Finally, the stochastic predictive model developed in this thesis enables to predict the long-term evolution of the dynamic response of the train. This will help the railway network managers to anticipate the maintenance works and can lead to introduce a predictive maintenance.

1.8 Notations

This section aims at summarizing the main notations that are used in this document.

- $\mathbb{R}$ is the set of real numbers.
- $\mathbb{N}$ denotes the set of positive integers.
- $\Omega \subset \mathbb{R}$ refers to a subset of $\mathbb{R}$.
- $(\Theta, \mathcal{F}, \mathcal{P})$ is a probability space.
- For $N \in \mathbb{N}^*$, $\mathbb{M}_N(\mathbb{R})$ denotes the set of the $(N \times N)$ real matrices.
- a, b correspond to constants in $\mathbb{R}$.
- $\boldsymbol{a}$, $\boldsymbol{b}$ refer to vectors with values in $\mathbb{R}^Q$, $Q \geq 1$.
- $\boldsymbol{a}^T$ is the transpose of $\boldsymbol{a}$.
- $\otimes$ is the tensorial product such that $\boldsymbol{a} \otimes \boldsymbol{b} = \boldsymbol{a}\boldsymbol{b}^T$.
- A, B correspond to random variables with values in $\mathbb{R}$.
- $\boldsymbol{A}$, $\boldsymbol{B}$ denote random vectors with values in $\mathbb{R}^Q$, $Q \geq 1$.
- $[A]$, $[B]$ refer to real matrices.
- $\det\{[A]\}$ is the determinant of real matrix $[A]$.

- $E\{\cdot\}$ denotes the mathematical expectation.
- $\mathcal{P}^{(Q)}([0,S])$, where $S < +\infty$, is the space of all the second-order $\mathbb{R}^Q$-valued random fields, indexed by the compact interval $[0,S]$.
- For $Q \geq 1$, $\boldsymbol{X} = (X_1, \ldots, X_Q) = \{(X_1(s), \ldots, X_Q(s)),\ s \in [0,S]\}$ is in $\mathcal{P}^{(Q)}([0,S])$.
- δ_{mp} is the kronecker symbol that is equal to 1 if $m = p$ and 0 otherwise.
- $\mathrm{Tr}(\cdot)$ is the trace operator for square matrices.
- $\|\cdot\|_F$ is the Frobenius norm of matrices.
- $P_{\boldsymbol{A}}$ and $p_{\boldsymbol{A}}$ denote respectively the multidimensional probability distribution and the multidimensional Probability Density Function (PDF) of random vector $\boldsymbol{A}$.
- If random vector $\boldsymbol{A}$ is of second order, we denote by $\underline{\boldsymbol{A}}$ and $[C_{\boldsymbol{A}}]$ the mean and the covariance matrix of $\boldsymbol{A}$ respectively.

Chapter 2

Stochastic modeling of track irregularities using experimental measurements

2.1 Introduction

To observe the long-term evolution of the track irregularities and start off the track maintenance operations, track irregularities are regularly measured by railway companies. Planning the maintenance operations forces to consider the track as a succession of local track stretches which are observed and maintained. Moreover, as it has been explained in the previous chapter, the characteristics and the long-term evolution of the track irregularities vary greatly from one stretch of the track to another one. This partition of the track into track stretches must therefore be conserved for the modeling of the track irregularities.

In this thesis, it has been chosen to analyze each stretch of the track individually and to develop a local stochastic model for the track irregularities specific to each track stretch. To take into account the variability of the track irregularities (and possibly additional small measurement errors), the track irregularities of the track stretch that is measured are modeled in a stochastic framework. The construction of a nonstationary and non-Gaussian local stochastic model is based on the global stochastic model for the track irregularities that has been proposed in [20]. It is recalled that the global stochastic model is representative of the track irregularities for the whole high-speed line and has the capacity to generate the track irregularities for any given track stretch belonging to the studied high-speed line (this identification has been performed using a large experimental data base obtained by track measurements and is thus very robust with respect to the variability encountered in the whole railway network). Since the global stochastic model represents the whole railway network, the dispersion is relatively significant. This is the reason why a local stochastic model of the track irregularities is constructed and identified for a given track stretch in order to reduce the dispersion.

For the construction of the local stochastic model of the track irregularities, the measured track irregularities are first projected on the vector basis of the discretized global

stochastic model. This step enables to reduce the dimension of the vector representing the track irregularities. The next step consists in adding to this projection a random vector (called "additive noise") whose probability model has to be constructed and identified, and which has to verify some constraints imposed by the discretized global stochastic model. The probabilistic model of this additive noise depends on a hyperparameter that allows for controlling the intensity of the statistical fluctuations, and that is identified using the first measurement of the given track stretch. Such a local stochastic model preserves the spatial and statistical properties of the track irregularities.

In this chapter, the track measurements and the discretization of the track irregularities are introduced in Sections 2.2 and 2.3. Then, in Section 2.4, in order to simplify the reading, we give a short summary of the global stochastic modeling presented in [20] whose details can be found in [62, 63, 6, 64, 65]. The local stochastic model is constructed in Section 2.5.

2.2 Track measurements

The terminology "track geometry" means both the "track design" and the "track irregularities".

2.2.1 Description of the track geometry

A two-scale description is usually used to characterize the track geometry.

- The track design corresponds to the theoretical track (as it was planned before the construction) and can be decomposed into the horizontal track design and the vertical one. The horizontal track design is made up of tangent track, curved track and track transition curves (between a curved and a tangent track stretch or between two curved track stretches with different radii), and is described by the horizontal curvature c_H, the cant c_L, and the track gauge E. The characteristic length of the track design (for curved and straight stretches of track) is several hundreds of meters for a high-speed line. The vertical track design is composed of gradients and transition zones between two gradients, and is described by the vertical curvature c_V. The track design remains constant over time.

- The track irregularities arise during the track life cycle and are added to the track design. They are induced by the track degradation when the trains run, by the environnement (rain, frost), and by the behavior of the track substructure. They change over long time τ. In this thesis, we consider track irregularities along the track, for which the wavelengths are between 3 and 150 m, and for which the order of magnitude of the amplitude is one milimeter to a dozen of milimeters. Thus, the length scales of the track irregularities are separated from the length scales of the track design.

For the French high-speed lines, the track design and the track irregularities are defined as a function of the curvilinear abscissa along the track s.

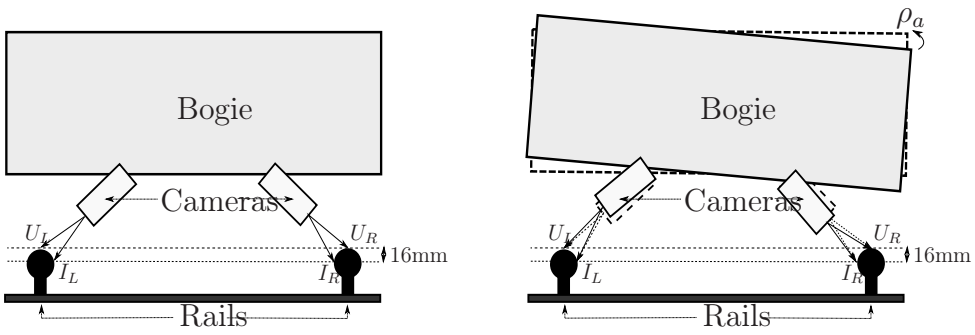

Figure 2.1: Experimental protocol.

2.2.2 Measurement of the track irregularities

The track irregularities are measured by a special high-speed train, called IRIS 320, equipped with measuring instruments, and owned by SNCF company (thus the measurements are performed under load). In order to measure the track irregularities, IRIS 320 measures the distance between a bogie of the train and four particular points of the rails [66, 67]. The distances are measured using two cameras fixed under the bogie, while the rails are enlightened by lasers (see Figure 2.1). However, the movements of the bogie introduce a bias in the measurements of the track geometry. To correct this bias, the measures of the track irregularities are post-processed. The post-processing consists in removing the translations and rotations due to the movements of the bogie, which are measured by accelerometers and a gyroscope. The incorrect measurements due to dysfunctions in the signal-acquisition equipments are removed. The curvilinear abscissa of the track is measured by an odometric wheel. Due to the variations of the rolling radius of the odometric wheel between two successive measurements, the curvilinear abscissa can vary from a track measurement to another one, and has to be rectified (see Appendix A). The measures from IRIS 320 give, for the curvilinear abscissa s,

- the lateral positions of the left rail $e_L(s)$ and of the right rail $e_R(s)$
- the vertical positions of the left rail $h_L(s)$ and of the right rail $h_R(s)$

Four track irregularities are computed from the track measurements (see Figure 2.2):

- the lateral offset: $x_1 = (e_L + e_R)/2$,
- the vertical offset: $x_2 = (h_L + h_R)/2$,
- the cross level: $x_3 = (h_L - h_R)/2$,
- the gauge irregularity : $x_4 = (e_L - e_R)/2$.

The distance between two successive measurements along the track is 0.25 m, which ensures a correct estimation of the considered track irregularities, since their smallest observed wavelength is 3 m. The track irregularities have been measured very frequently since 2007, providing a rich data base. For a stretch of the track, the four track irregularities are displayed in Figure 2.3.

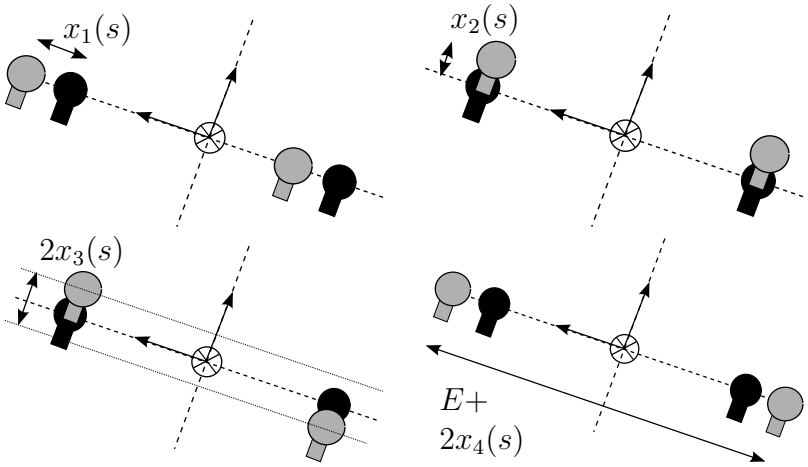

Figure 2.2: Parametrization of the track irregularities in the reference frame of the track (for each rail, the initial track design is represented in black, whereas the true position is in grey).

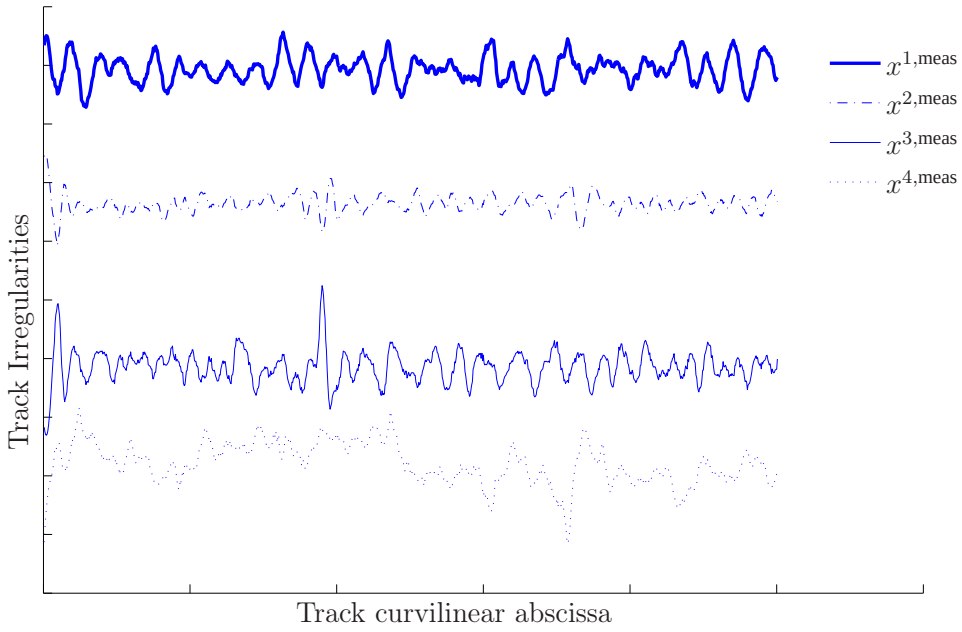

Figure 2.3: Track irregularities for a stretch of the railway track.

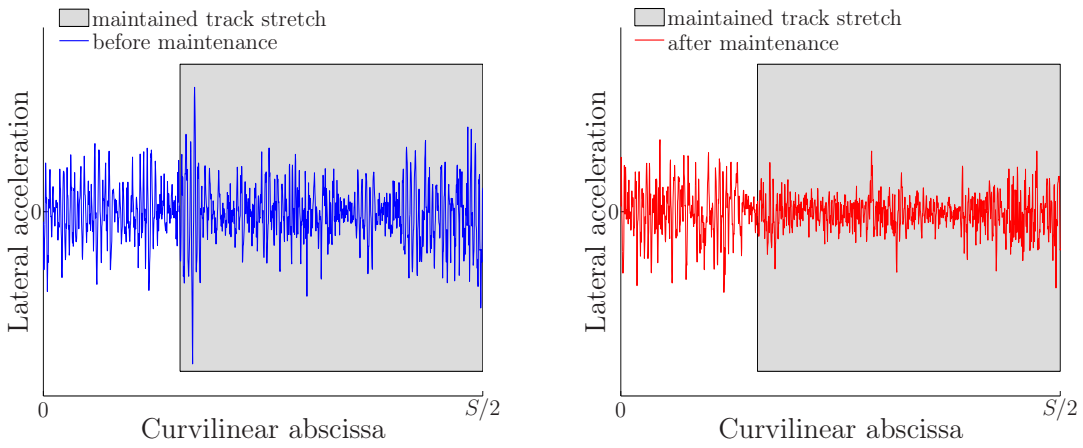

Figure 2.4: Comparison of the lateral acceleration in the first bogie of a TGV before a maintenance operation (left figure) and after the maintenance operation (right figure).

2.2.3 Analysis of the measured track irregularities and influence of the maintenance operations

The level of track irregularities increases with long time τ. To guarantee a good quality of running conditions of the train, track irregularities are frequently corrected by maintenance operations (tamping) of the track. For instance, the effects of a maintenance operation on the movements of a bogie can be seen in Figure 2.4, which compares the lateral acceleration in the first bogie of a high-speed train (TGV) before and after a maintenance operation. A maintenance operation may deeply modify the track geometry, and therefore the track irregularities before and after a maintenance are very different. For example, the cross level before and after a maintenance operation is displayed in Figure 2.5: the maintenance reduces the peaks amplitudes, especially for the small wavelengths (of the order of magnitude of $S/10$).

In the following, the long-term evolution of track irregularities is analyzed only between two successive maintenance operations. For instance, the vertical offset of a track stretch is represented in Figure 2.6 for the first measurement after a maintenance operation (at time τ_1), and the last measurement before the next maintenance (at time τ_K). For this track stretch, the long-term evolution is visible and localized at some peaks of the track irregularities.

2.3 Spatial sampling of the track for the measurements and for the stochastic modeling

2.3.1 Partitioning the track into track stretches

As explained in Section 2.1, the track has to be partitioned into track stretches in order to model the track irregularities for a given stretch of the track, because the statistical fluctuations of the track irregularities change from a track stretch to another one. Moreover,

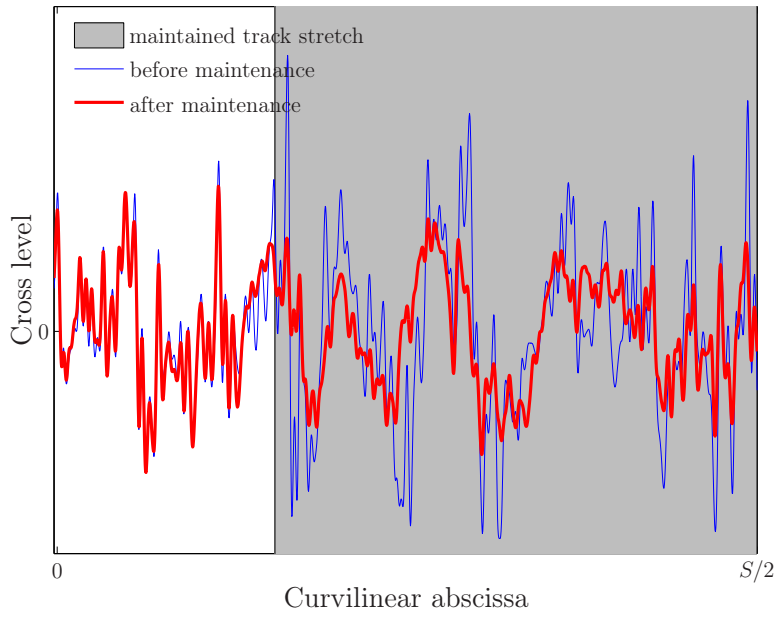

Figure 2.5: Comparison of the cross level of the track before a maintenance operation (thin line) and after the maintenance operation (thick line).

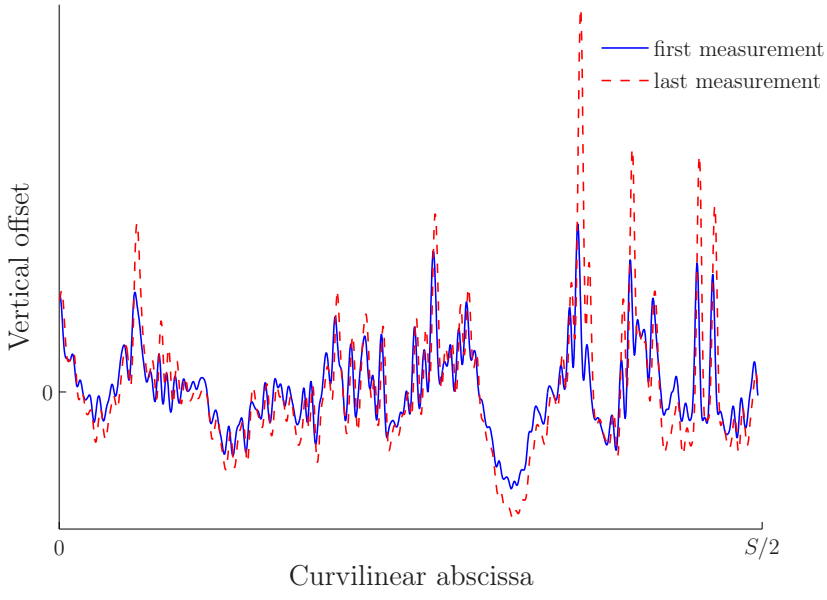

Figure 2.6: Evolution of the vertical offset of a track stretch between two successive maintenance operations: first measurement after a maintenance operation (solid blue line), last measurement before the next maintenance operation (dashed red line).

it can be noticed that the track irregularities strongly depend on the track curvature. Four types of curvature are considered:

- tangent track, for which the horizontal curvature is zero,
- curve entrance (transition curve approaching to a circular curve), for which the absolute value of the horizontal curvature is linearly increasing,
- curved track, for which the horizontal curvature is constant and non zero,
- curve exit (transition curve receding from a circular curve), for which the absolute value of the horizontal curvature is linearly decreasing.

The types of curvature have to be respected when partitioning the track into track stretches. This implies to localize the positions of the beginnings and the ends of the four curvature types. Then, for each curvature type, a series of measurements of same length S is extracted from the experimental data base. The lengths of the curve entrances and curve exits are generally lower than S.

2.3.2 Spatial sampling for the stochastic modeling of a track stretch for a given curvature type

For a given track stretch with a given curvature type, the track irregularities are represented by the centered vector-valued random field $\{\mathbf{X}(s),\, s \in [0,S]\}$, with values in $\mathbb{R}^4$ which is such that

$$\mathbf{X}(s) = (X^1(s), X^2(s), X^3(s), X^4(s))\,, \tag{2.1}$$

in which the real-valued random fields $\{X^\kappa(s), s \in [0,S]\}$, for $\kappa = 1,\ldots,4$, represent the lateral offset, the vertical offset, the cross level, and the gauge irregularity. The track is composed of ν_p track stretches of length S, indexed by ℓ, for which the track irregularities are measured by a measuring train. For a given track stretch ℓ, the track irregularities are sampled at N_s+1 sampling points $s_0 < s_1 < \ldots < s_{N_s}$ of the curvilinear abscissa of the track stretch, such that $s_0 = 0$ and $s_{N_s} = S$. For a given curvature type and for a given track stretch ℓ, the measurements of the track irregularities are represented by the vector $\mathbf{x}^{\text{meas},\ell} \in \mathbb{R}^{4(N_s+1)}$ whose components are $x^{1,\text{meas},\ell}(s_n), x^{2,\text{meas},\ell}(s_n), x^{3,\text{meas},\ell}(s_n), x^{4,\text{meas},\ell}(s_n)$, $n = 0,\ldots,N_s$. The measurements are performed at several discrete long time τ_k for $k = 1,\ldots,K$ between two successive maintenance operations. Long time τ_1 corresponds to the first measurement after a maintenance operation, and τ_K is the time of the last measurement for this track stretch before the next maintenance operation.

For the given track stretch ℓ with a given curvature type, the measured track irregularities at long time τ_k are then represented by the vector $\mathbf{x}^{\text{meas},\ell}(\tau_k)$ in $\mathbb{R}^{4(N_s+1)}$.

In all the following of the manuscript, we introduce the random vector $\mathbf{X} = (\mathbf{X}^1, \mathbf{X}^2, \mathbf{X}^3, \mathbf{X}^4)$ with values in $\mathbb{R}^{4(N_s+1)}$ corresponding to the spatial discretization of the random field $\{\mathbf{X}(s),\, s \in [0,S]\}$.

2.3.3 Construction of an optimal value for the length of the stretches

The railway track is considered as a concatenation of track stretches of same length S. The value of S has to be carefully chosen because it plays a key-role in the stochastic modeling of the track irregularities of a track stretch. Thus, to obtain a robust statistical description of a track stretch, S has to be chosen in order to obtain good statistical properties of the stochastic modeling of a track stretch. For instance (but not only), length S must be longer than the correlation length of the track irregularities.

The optimal value of S is constructed using the three following criteria quantified by introducing three error functions.

- Random vector $\mathbf{X}$ that models the track irregularities for two successive track stretches must be independent. In practice, this required statistical independence is replaced by a non-correlation property that is quantified by an error function (denoted by $err^2_{\text{cov}}(S)$), which measures a relative distance between covariance functions.

- A possible artificial periodicity must be avoided in order not to degrade the low-frequency part of the spectrum of the track irregularities in the stochastic model of the track stretch. Such a spectral error is quantified by the function denoted by $err^2_{\text{spect}}(S)$.

- The number of independent realizations of a random vector $\mathbf{X}$ for a given stretch of the track, which are extracted from the data base of track irregularities, must be sufficiently large in order to obtain a reasonnable convergence of the statistical estimators of the probabilistic quantities related to $\mathbf{X}$. This estimation error is quantified by the function denoted by $err^2_{\text{est}}(S)$.

The details of the construction of these three error functions can be found in [6]. For the chosen railway line, errors $err^2_{\text{cov}}(S)$, $err^2_{\text{spect}}(S)$ and $err^2_{\text{est}}(S)$ are represented in Figure 2.7. When S increases, it can be verified that $err^2_{\text{cov}}(S)$ and $err^2_{\text{spect}}(S)$ decrease whereas $err^2_{\text{est}}(S)$ increases. Length S has thus to be chosen as the right balance between these three error functions.

For confidentiality reasons, the exact value of S (which is several hundreds of meters) is however not given in this thesis and, in the following, all the spatial quantities are normalized with respect to length S.

2.4 Summary of the global stochastic model of track irregularities

In this section, we give a short summary of the global stochastic model of track irregularities for any track stretch with a same curvature type belonging to the French railway network of high-speed lines. This global stochastic model has been constructed and identified in [20], whose details can be found in [62, 6, 63, 64, 65].

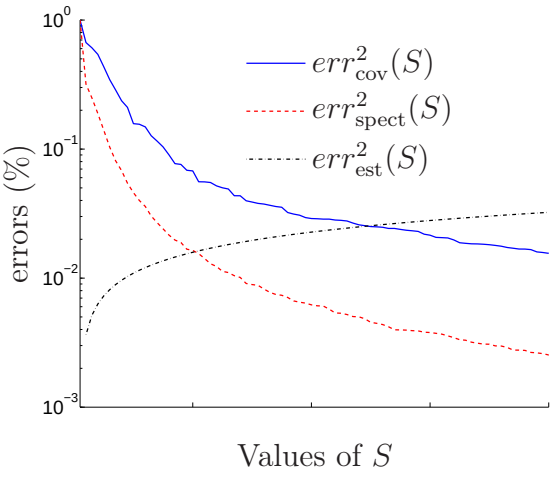

Figure 2.7: Graphs of errors $err^2_{\rm cov}(S)$, $err^2_{\rm spect}(S)$ and $err^2_{\rm est}(S)$ for the computation of the length S (figure extracted from [6], pp 103-104).

The global stochastic model of the track irregularities is constructed for any track stretch with the same curvature type and is thus independent of long time τ. The vector-valued random field $\mathbf{X} = (\mathbf{X}^1, \mathbf{X}^2, \mathbf{X}^3, \mathbf{X}^4)$, defined on the probability space $(\Theta, \mathcal{F}, \mathcal{P})$, with values in $\mathbb{R}^{4(N_s+1)}$, models the track irregularities of any track stretch with the same curvature, for which ν_p independent realizations $\mathbf{x}^{\text{meas},\ell} = (\mathbf{x}^{1,\text{meas},\ell}, \mathbf{x}^{2,\text{meas},\ell}, \mathbf{x}^{3,\text{meas},\ell}, \mathbf{x}^{4,\text{meas},\ell})$, with $\ell = 1, \ldots, \nu_p$, are known and correspond to measurements of track irregularities for the ν_p track stretches with a given curvature type (the independence property is induced by the identification of the optimal value of S). Random vector $\mathbf{X}$ with values in $\mathbb{R}^{4(N_s+1)}$, which corresponds to the spatial discretization of the random field $\{\mathbf{X}(s), s \in [0, S]\}$, is non-Gaussian, non-homogeneous (nonstationary), and centered. The construction of a representation of random vector $\mathbf{X}$ and its experimental identification is summarized in the two next sections.

2.4.1 Statistical reduced representation based on a principal component analysis

The first step of the construction consists in introducing a scaling related to the four types of irregularities and then in constructing a statistical reduced representation of random vector $\mathbf{X}$ using a principal component analysis. The scaling consists in replacing random vector $\mathbf{X}$ with values in $\mathbb{R}^{4(N_s+1)}$ by a scaled random vector $\boldsymbol{\chi}$ with values in $\mathbb{R}^{4(N_s+1)}$ such that,

$$\boldsymbol{\chi} = [\text{Diag}(\mathbf{O})]\mathbf{X}\,, \tag{2.2}$$

in which $[\text{Diag}(\mathbf{O})]$ is a diagonal matrix introduced for the scaling and detailed in [20]. Using the principal component analysis of random vector $\boldsymbol{\chi}$, the following statistical reduced representation $\boldsymbol{\chi}^{(M)}$ of order $M \ll 4(N_s+1)$ is introduced,

$$\boldsymbol{\chi}^{(M)} = \sum_{m=1}^{M} \sqrt{\lambda_m}\, \mathbf{k}^m\, \eta_m\,, \tag{2.3}$$

in which $\mathbf{k}^1, \ldots, \mathbf{k}^M$ is the orthonormal family of the eigenvectors of the covariance matrix of random vector $\boldsymbol{\chi}$, associated with the first M largest eigenvalues $\lambda_1, \ldots, \lambda_M$. The coordinates $\eta_1, \ldots, \eta_M$ are M second-order, centered, non-correlated, dependent, and normalized non-Gaussian random variables such that

$$\eta_m = \frac{1}{\sqrt{\lambda_m}} \boldsymbol{\chi}^T \mathbf{k}^m \quad , \quad 1 \leq m \leq M \, . \tag{2.4}$$

The corresponding statistical reduced representation $\mathbf{X}^{(M)}$ of order $M \ll 4(N_s + 1)$ is then written as

$$\mathbf{X}^{(M)} = \sum_{m=1}^{M} [\mathrm{Diag}(\mathbf{O})]^{-1} \, \mathbf{k}^m \, \sqrt{\lambda_m} \, \eta_m \, . \tag{2.5}$$

Introducing the $(4(N_s + 1) \times M)$ real matrix $[U]$ defined by

$$[U] = \left[\mathbf{k}^1 \ldots \mathbf{k}^M \right] \quad , \quad [U]^T \, [U] = [I_M] \, , \tag{2.6}$$

in which $[I_M]$ is the identity matrix, the diagonal matrix $[\lambda]$ whose diagonal entries are $\lambda_1, \ldots, \lambda_M$, and the random vector $\boldsymbol{\eta}$ such that

$$\boldsymbol{\eta} = (\eta_1, \ldots, \eta_M) \, , \tag{2.7}$$

the random vector $\mathbf{X}^{(M)}$ can be rewritten as

$$\mathbf{X}^{(M)} = [\mathrm{Diag}(\mathbf{O})]^{-1} \, [U] \, [\lambda]^{1/2} \, \boldsymbol{\eta} \, . \tag{2.8}$$

Random vector $\boldsymbol{\eta}$ is such that

$$E\{\boldsymbol{\eta} \, \boldsymbol{\eta}^T\} = [I_M] \, , \tag{2.9}$$

in which $E\{\cdot\}$ is the mathematical expectation. Introducing the $(M \times M)$ real matrix $[Q]$ such as

$$[Q] = [\mathrm{Diag}(\mathbf{O})]^{-1} \, [U] \, [\lambda]^{1/2} \, , \tag{2.10}$$

Eq. (2.8) can be rewritten as

$$\mathbf{X}^{(M)} = [Q] \, \boldsymbol{\eta} \, . \tag{2.11}$$

A convergence analysis has been carried out in order to define the value of M, which is $M = 2,000$ for a relative L^2-error of about 1.2%.

2.4.2 Polynomial chaos expansion

The second step consists in constructing a representation of the non-Gaussian second-order random vector $\boldsymbol{\eta}$ whose non-correlated components are statistically dependent. The chosen method is the Gaussian polynomial chaos expansion (PCE) method (see [68, 69, 70]).

The Gaussian PCE is based on a direct projection of the second-order random vector $\boldsymbol{\eta}$ on the Hilbertian basis $\mathcal{B}_{\mathrm{orth}} = \{\psi_j(\xi), 0 \leq j\}$ made up of the normalized multivariate Hermite polynomials, whose finite truncated representation, at order N, is written as

$$\boldsymbol{\eta} \simeq \boldsymbol{\eta}^{\mathrm{chaos}}(N) = \sum_{j=0}^{N} \mathbf{y}^{(j)} \psi_{\boldsymbol{\alpha}^{(j)}}(\boldsymbol{\xi}) \, , \tag{2.12}$$

in which $\boldsymbol{\xi} = (\xi_1, \ldots, \xi_{N_g})$ is a normalized Gaussian random vector with dimension $N_g \leq M$. The components $\xi_1, \ldots, \xi_{N_g}$ are independent normalized Gaussian real-valued random variables, and $\psi_{\boldsymbol{\alpha}^{(0)}}(\boldsymbol{\xi}), \ldots, \psi_{\boldsymbol{\alpha}^{(N)}}(\boldsymbol{\xi})$ are the multivariate orthonormal normalized Hermite polynomials (the Gaussian polynomial chaos), and where N, N_g, and the vectors $\mathbf{y}^{(0)}, \ldots, \mathbf{y}^{(N)}$ in $\mathbb{R}^M$ have to be identified. For $j = 0, \ldots, N$, the multi-index $\boldsymbol{\alpha}^{(j)}$ is defined by $\boldsymbol{\alpha}^{(j)} = (\alpha_1^j, \ldots, \alpha_{N_g}^j) \in \mathbb{N}^{N_g}$. If p denotes the maximal degree of the polynomials, we have $0 \leq \alpha_1^j + \ldots + \alpha_{N_g}^j \leq p$, and integer N is written as

$$N = \frac{(N_g + p)!}{(N_g!\, p!)} \,. \tag{2.13}$$

The polynomial chaos $\psi_{\boldsymbol{\alpha}^{(j)}}(\boldsymbol{\xi})$ are such that

$$\psi_{\boldsymbol{\alpha}^{(j)}}(\boldsymbol{\xi}) = \psi_{\alpha_1{}^{(j)}}(\xi_1) \times \ldots \times \psi_{\alpha_{N_g}{}^{(j)}}(\xi_{N_g}) \quad , \quad j = 1, \ldots, N \,, \tag{2.14}$$

with $\psi_{\boldsymbol{\alpha}^{(0)}}(\boldsymbol{\xi}) = 1$, and satisfy the orthonormal property,

$$E\{\psi_{\boldsymbol{\alpha}^{(j)}}(\boldsymbol{\xi})\psi_{\boldsymbol{\alpha}^{(k)}}(\boldsymbol{\xi})\} = \delta_{jk} \,. \tag{2.15}$$

As $\boldsymbol{\eta}$ is a centered random vector, the first coefficient $\mathbf{y}^{(0)} = \mathbf{0}$. The identification of the $(M \times N)$ real matrix $[y] = [\mathbf{y}^{(1)} \ldots \mathbf{y}^{(N)}]$ is performed by solving a statistical inverse problem using the ν_p independent experimental realizations $\eta^{\exp,\ell}, \ell = 1, \ldots, \nu_p$, of η such that

$$\eta_m^{\exp,\ell} = \frac{1}{\sqrt{\lambda_m}} (\mathbf{x}^{\mathrm{meas},\ell})^T [\mathrm{Diag}(\mathbf{O})]\, \mathbf{k}^m \quad , \quad 1 \leq m \leq M \,, \tag{2.16}$$

in which $\mathbf{x}^{\mathrm{meas},\ell}$, $\ell = 1, \ldots, \nu_p$ are the track irregularities measurements introduced in Section 2.3.2. The identification of matrix $[y]$ of the coefficients of the PCE is carried out by the maximum-likelihood method that is summarized hereinafter.

Let $\mathbf{h} \mapsto p_{\boldsymbol{\eta}}(\mathbf{h}; [y])$ be the probability density function of random vector $\boldsymbol{\eta}$ whose representation is given by Eq. (2.12) and depending on matrix $[y]$ that belongs to the set $\mathbb{M}_{M,N}$ of all the $(M \times N)$ real matrices that verify the constraints $[y]\,[y]^T = [I_M]$. Consequently, $[y]$ must be identified in the admissible set defined by

$$\mathcal{C}_{[y]} = \big\{ [y] \in \mathbb{M}_{M,N} \quad \text{such that} \quad [y]\,[y]^T = [I_M] \big\} \,. \tag{2.17}$$

For each fixed $[y]$ and fixed $\mathbf{h}$, $p_{\boldsymbol{\eta}}(\mathbf{h}; [y])$ is estimated by using samples calculated with Eq. (2.12) and the Gaussian kernel estimation method. Matrix $[y]$ is identified by the method described in [65, 6], which is briefly summarized hereinafter.

For integers N_g and p fixed, the optimal value $[y^{\mathrm{opt}}(N_g, p)]$ of $[y]$ is calculated by solving the optimization problem (maximum log-likelihood method),

$$[y^{\mathrm{opt}}(N_g, p)] = \arg \max_{[y] \in \mathcal{C}_{[y]}} \sum_{\ell=1}^{\nu_p} \ln(p_{\boldsymbol{\eta}}(\boldsymbol{\eta}^{\exp,\ell}; [y])) \,. \tag{2.18}$$

The optimal values of integers N_g and p are calculated in order to minimize the value of N defined by Eq. (2.13). Since the constraint $[y]\,[y]^T = [I_M]$ imposes $M(M+1)/2$ conditions on $[y]$, the set $\mathcal{Q}$ of the admissible values for p and N_g is written as

$$\mathcal{Q} = \big\{ (p, N_g) \in \mathbb{N}^2 \mid N_g \leq M,\ N = (N_g + p)!/(N_g!\, p!) \geq (M+1)/2 \big\} \,. \tag{2.19}$$

The truncation error is quantified by the following error function:

$$\mathrm{err}(N_g, p) = \sum_{j=1}^{M} \int_{\mathrm{BI}_j} |\log_{10}(p_{\eta_j^{\mathrm{exp}}}(h_j)) - \log_{10}(p_{\eta_j}(h_j; [y^{\mathrm{opt}}(N_g, p)]))|\, dh_j\,, \tag{2.20}$$

in which $p_{\eta_j^{\mathrm{exp}}}$ is the probability density function estimated by using the Gaussian kernel estimation method and the realizations $\eta_j^{\mathrm{exp},\ell}$, $\ell = 1, \ldots, \nu_p$, and where BI_j is the interval on which the probability density function of η_j^{exp} is higher than $1/\nu_p$,

$$\mathrm{BI}_j = \{h_j \,|\, p_{\eta_j^{\mathrm{exp}}}(h_j) \geq 1/\nu_p\} \quad , \quad j = 1, \ldots, M\,. \tag{2.21}$$

The optimal value $(N_g^{\mathrm{opt}}, p^{\mathrm{opt}})$ of (N_g, p) are thus calculated as

$$(N_g^{\mathrm{opt}}, p^{\mathrm{opt}}) = \arg \min_{(N_g,p)\in\mathcal{Q}} \mathrm{err}(N_g, p)\,. \tag{2.22}$$

Using Eqs. (2.11) and (2.12), random vector $\mathbf{X}^{(M)}$ is written as

$$\mathbf{X}^{(M)} = [Q]\, [y^{\mathrm{opt}}(N^{\mathrm{opt}}, p^{\mathrm{opt}})]\, \boldsymbol{\Psi}(\boldsymbol{\xi})\,, \tag{2.23}$$

in which $\boldsymbol{\Psi}(\boldsymbol{\xi}) = (\psi_{\alpha^{(1)}}(\boldsymbol{\xi}), \ldots, \psi_{\alpha^{(N)}}(\boldsymbol{\xi}))$ is a $\mathbb{R}^N$-valued random vector.

2.5 Local stochastic modeling

2.5.1 Construction of the local stochastic model

For a given stretch of the track with a given curvature type, the first measurement of the track irregularities at long time τ_1 is denoted by $\mathbf{x}_{\tau_1}^{\mathrm{meas}} = (\mathbf{x}_{\tau_1}^{1,\mathrm{meas}}, \mathbf{x}_{\tau_1}^{2,\mathrm{meas}}, \mathbf{x}_{\tau_1}^{3,\mathrm{meas}}, \mathbf{x}_{\tau_1}^{4,\mathrm{meas}})$. As explained in Section 2.1, we are interested in constructing a local stochastic model adapted to this given track stretch using only the local measurement $\mathbf{x}_{\tau_1}^{\mathrm{meas}}$. As previously mentionned, the objective of this local stochastic model is to take into account (i) the local variability of the given track stretch in order to decrease the "statistical distance" between the global stochastic model and the local measurements and (ii) a possible presence of measurement noise.

The local stochastic modeling is constructed in adapting the global stochastic model of the track irregularities recalled in Section 2.3 to the given track stretch. The method proposed for constructing such a local stochastic model consists in introducing a random field noise for which the spatial properties are driven by the global stochastic model. The intensity of the statistical fluctuations of this random field noise has to be identified using measurement $\mathbf{x}_{\tau_1}^{\mathrm{meas}}$.

For $\kappa = 1, \ldots, 4$, the statistical reduced representation of the random vector $\mathbf{X}^{\kappa}$ with values in $\mathbb{R}^{(N_s+1)}$ (at order M, and which represents a type of track irregularities for a given stretch of the track), deduced from Eq. (2.11), is written (in removing notation (M)) as

$$\mathbf{X}^{\kappa} = [Q^{\kappa}]\, \boldsymbol{\eta}\,, \tag{2.24}$$

in which $[Q^\kappa]$ is a $((N_s+1)\times M)$ real matrix that is deduced from matrix $[Q]$ introduced in Eq. (2.10). The proposed local stochastic model is written as

$$\widetilde{\mathbf{X}}^\kappa(\boldsymbol{\delta}) = \mathbf{X}^\kappa + \mathbf{B}^\kappa(\boldsymbol{\delta})\,, \tag{2.25}$$

in which $\mathbf{B}^\kappa(\boldsymbol{\delta})$ is a random vector with values in $\mathbb{R}^{(N_s+1)}$, which depends on a vector-valued hyperparameter $\boldsymbol{\delta} = (\delta^1, \delta^2, \delta^3, \delta^4)$ that allows for controlling the level of statistical fluctuations, and which has to be identified. In order to preserve the statistical properties of the track irregularities, random vector $\mathbf{B}^\kappa(\boldsymbol{\delta})$ is written as

$$\mathbf{B}^\kappa(\boldsymbol{\delta}) = \delta^\kappa\,[Q^\kappa]\,\mathbf{G}^\kappa\,, \tag{2.26}$$

in which $\mathbf{G}^\kappa$ is a $\mathbb{R}^M$-valued Gaussian second-order centered random vector, defined on the probability space $(\Theta', \mathcal{F}', \mathcal{P}')$, for which the covariance matrix is the identity matrix. The random vectors $\mathbf{G}^1, \mathbf{G}^2, \mathbf{G}^3, \mathbf{G}^4$ are statistically independent. The optimal value $\boldsymbol{\delta}^{\text{opt}}$ of the vector-valued hyperparameter $\boldsymbol{\delta} = (\delta^1, \delta^2, \delta^3, \delta^4)$ has to be identified for the given track stretch using local measurement $\mathbf{x}_{\tau_1}^{\text{meas}}$. Combining Eqs. (2.24) and (2.25) yields the local stochastic model of the track irregularities that is written as,

$$\widetilde{\mathbf{X}}^\kappa(\boldsymbol{\delta}) = [Q^\kappa]\;(\boldsymbol{\eta} + \delta^\kappa\,\mathbf{G}^\kappa) \quad , \quad \kappa = 1, 2, 3, 4\,. \tag{2.27}$$

It should be noted that the proposed local stochastic model allows for analyzing the long-term evolution of each type of irregularities.

2.5.2 Identification of hyperparameter $\boldsymbol{\delta}$

The optimal value $\boldsymbol{\delta}^{\text{opt}} = (\delta^{1,\text{opt}}, \delta^{2,\text{opt}}, \delta^{3,\text{opt}}, \delta^{4,\text{opt}})$ of hyperparameter $\boldsymbol{\delta}$ is estimated by using the multivariate maximum log-likelihood method for the random observation vector $\mathbf{W}(\boldsymbol{\delta}) = (W^1(\boldsymbol{\delta}), W^2(\boldsymbol{\delta}), W^3(\boldsymbol{\delta}), W^4(\boldsymbol{\delta}))$ such that

$$W^\kappa(\boldsymbol{\delta}) = \frac{\|\widetilde{\mathbf{X}}^\kappa(\boldsymbol{\delta})\|}{E\{\|\mathbf{X}^\kappa\|\}}\,, \tag{2.28}$$

where $\mathbf{X}^\kappa$ is generated with the global stochastic model (Eq. (2.24)), and where $\|\cdot\|$ is the Euclidean norm. The experimental observation vector $\mathbf{w}_{\tau_1}^{\text{meas}} = (w_{\tau_1}^{1,\text{meas}}, w_{\tau_1}^{2,\text{meas}}, w_{\tau_1}^{3,\text{meas}}, w_{\tau_1}^{4,\text{meas}})$ that corresponds to the experimental measurement of $\mathbf{W}(\boldsymbol{\delta})$ at long time τ_1 is such that

$$w^{\kappa,\text{meas}} = \frac{\|\mathbf{x}_{\tau_1}^{\kappa,\text{meas}}\|}{E\{\|\mathbf{X}^\kappa\|\}},\;\; 1 \le \kappa \le 4\,. \tag{2.29}$$

Let $\mathcal{L}_{\mathbf{W}}(\mathbf{w}_{\tau_1}^{\text{meas}}; \boldsymbol{\delta}) = \ln p_{\mathbf{W}}(\mathbf{w}_{\tau_1}^{\text{meas}}; \boldsymbol{\delta})$ be the log-likelihood function in which $p_{\mathbf{W}}(\mathbf{w}_{\tau_1}^{\text{meas}}; \boldsymbol{\delta})$ is the value of the probability density function $\mathbf{w} \mapsto p_{\mathbf{W}}(\mathbf{w}; \boldsymbol{\delta})$ of random vector $\mathbf{W}$ at $\mathbf{w} = \mathbf{w}_{\tau_1}^{\text{meas}}$. The optimal value $\boldsymbol{\delta}^{\text{opt}}$ is then identified solving the following optimization problem:

$$\boldsymbol{\delta}^{\text{opt}} = \arg\max_{\boldsymbol{\delta}} \{\mathcal{L}_{\mathbf{W}}(\mathbf{w}_{\tau_1}^{\text{meas}}; \boldsymbol{\delta})\}\,. \tag{2.30}$$

The quantity $p_{\mathbf{W}}(\mathbf{w}_{\tau_1}^{\text{meas}}; \boldsymbol{\delta})$ is estimated using independent realizations of $\mathbf{W}(\boldsymbol{\delta})$, and multivariate Gaussian kernel method (see for instance [71, 72]).

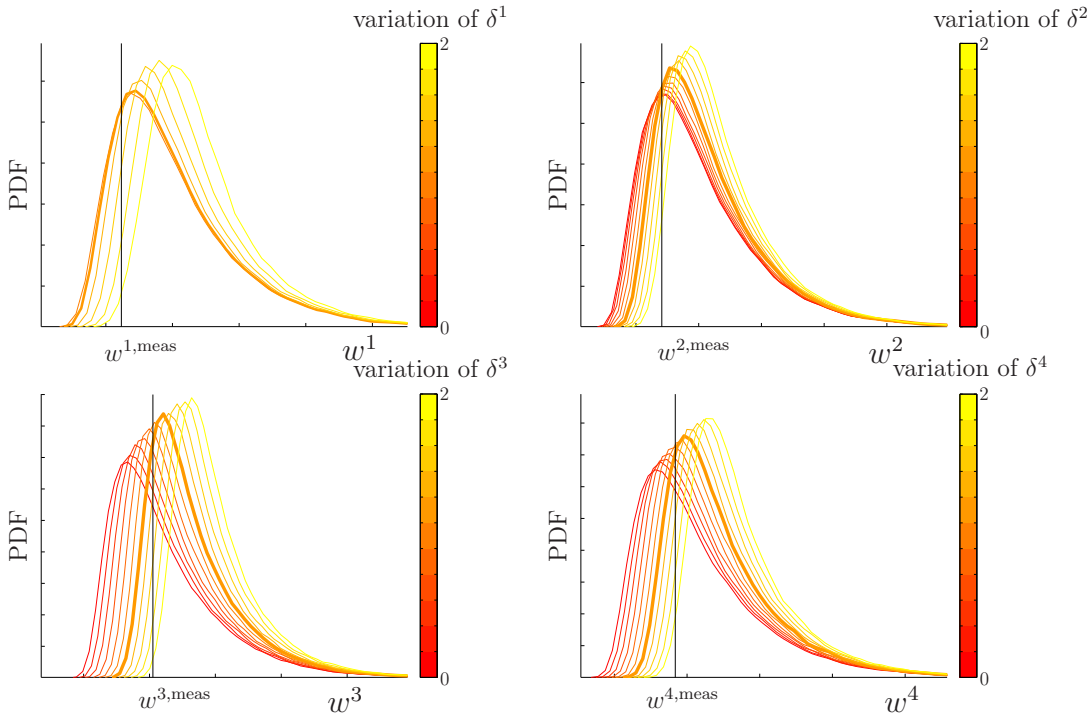

Figure 2.8: Graphs of the PDF, $w^\kappa \mapsto p_{W^\kappa(\delta^\kappa)}(w^\kappa;\delta^\kappa)$, as a function of δ^κ (the bold line is obtained for $\delta^\kappa = \delta^{\kappa,\text{opt}}$), for $\kappa = 1,2,3,4$.

The admissible set for $\boldsymbol{\delta}$ is defined as the domain $[0,2]^4$ of $\mathbb{R}^4$. Since the dimension of the admissible set of parameter $\boldsymbol{\delta}$ is small, and since each component δ^κ belongs to a given finite interval, a deterministic algorithm can be used for solving the optimization problem defined by Eq. (2.30). The identification of $\boldsymbol{\delta}^{\text{opt}}$ is made in two steps. First, the admissible set is partitioned in 20^4 meshes corresponding to a constant step of 0.1 for each coordinate. For each value of $\boldsymbol{\delta}$ corresponding to a node of the mesh, the log-likelihood is computed with $10,000$ realizations of $\mathbf{W}(\boldsymbol{\delta})$. This stage allows the identification of the node of the mesh corresponding to the maximum of the log-likelihood. This node is then denoted by $\boldsymbol{\delta}_1 = (\delta_1^1, \delta_1^2, \delta_1^3, \delta_1^4)$. Then, the subdomain $\Pi_{\kappa=1}^4[\delta_1^\kappa - 0.25, \delta_1^\kappa + 0.25]$ is explored for $\boldsymbol{\delta}$ with a precision of 0.05 for each coordinate (10^4 nodes for the subdomain). The log-likelihood is computed with $100,000$ realizations for $\mathbf{W}(\boldsymbol{\delta})$. For $\kappa = 1,\ldots,4$, the graphs of the marginal probability density function (PDF) $w^\kappa \mapsto p_{W^\kappa(\boldsymbol{\delta})}(w^\kappa;\delta^\kappa)$ of random variable $W^\kappa(\boldsymbol{\delta})$ are featured in Figure 2.8 as a function of δ^κ (the other components of $\boldsymbol{\delta}$ being fixed to their optimal values). In 1-D, the maximum likelihood is obtained when the PDF of $W^\kappa(\delta^\kappa)$ is maximal at $w^\kappa = w_{\tau_1}^{\kappa,\text{meas}}$. Here, the bold curve indicates the PDF corresponding to the optimal value of δ^κ. It can be noticed that the bold curve is not always the curve for which the PDF of $W^\kappa(\delta^\kappa)$ is maximal at $w^\kappa = w_{\tau_1}^{\kappa,\text{meas}}$, because the four components are simultaneously taken into account to identify the maximum likelihood. The values obtained for each coordinate of $\boldsymbol{\delta}^{\text{opt}}$ can be deduced from Figure 2.9, which displays the sections (following each coordinate δ^κ of $\boldsymbol{\delta}$) of the hypersurface defined by the graph $\boldsymbol{\delta} \mapsto \mathcal{L}_{\mathbf{W}}(\mathbf{w}_{\tau_1}^{\text{meas}}, \boldsymbol{\delta})$ of the multidimensional log-likelihood function.

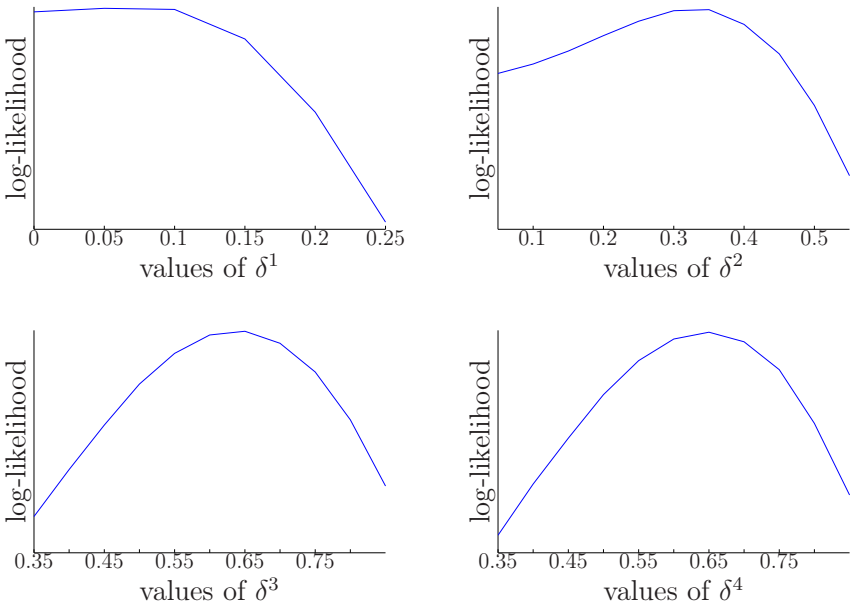

Figure 2.9: Graphs of the sections of the log-likelihood $\mathcal{L}_{\mathbf{W}}(\mathbf{w}_{\tau_1}^{\text{meas}}; \boldsymbol{\delta})$.

2.5.3 Local stochastic modeling for the long-term evolution of a given stretch of the track with a given curvature type

The local stochastic model of the track irregularities for a given stretch of the track with a given curvature type at long time τ_k, $k = 1, \ldots, K$, is constructed as follows. For fixed long time τ_k, the measurement of the track stretch is $\mathbf{x}_{\tau_k}^{\text{meas}} = (\mathbf{x}_{\tau_k}^{1,\text{meas}}, \mathbf{x}_{\tau_k}^{2,\text{meas}}, \mathbf{x}_{\tau_k}^{3,\text{meas}}, \mathbf{x}_{\tau_k}^{4,\text{meas}})$. After identifying the optimal value $\boldsymbol{\delta}^{\text{opt}}$ of the hyperparameter $\boldsymbol{\delta}$ (see Section 2.5.2), we have to compute the realization $\boldsymbol{\eta}_{\tau_k}^{\text{meas}}$ of random vector $\boldsymbol{\eta}$ on the generalized coordinates of the global stochastic model defined by Eq. (2.11). This realization $\boldsymbol{\eta}_{\tau_k}^{\text{meas}}$ is deduced from Eqs. (2.6) to (2.11) as the projection of the measurement $\mathbf{x}_{\tau_k}^{\text{meas}}$ on the global stochastic model, which yields

$$\boldsymbol{\eta}_{\tau_k}^{\text{meas}} = [\lambda]^{-1} [Q]^T [\text{Diag}(\mathbf{O})]^2 \mathbf{x}_{\tau_k}^{\text{meas}} . \tag{2.31}$$

For fixed long time τ_k, the local stochastic model is then defined by

$$\widetilde{\mathbf{X}}_{\tau_k}^{\kappa}(\boldsymbol{\delta}^{\text{opt}}) = [Q^{\kappa}] \left(\boldsymbol{\eta}_{\tau_k}^{\text{meas}} + \delta^{\kappa,\text{opt}} \mathbf{G}^{\kappa} \right) \quad , \quad \kappa = 1, 2, 3, 4 . \tag{2.32}$$

As an illustration of the local stochastic model for the track irregularities, the measured vertical offset, as well as a realization of $\widetilde{\mathbf{X}}_{\tau_1}^2(\boldsymbol{\delta}^{\text{opt}})$ and the confidence region at 90% are displayed in Figure 2.10. This figure shows that the vertical offset generated with the local stochastic model keeps the geometrical and statistical properties of the measured vertical offset, and that the confidence region at 90% is satisfactory, because it is not too large and it keeps the statistical properties of the track irregularities. In order to validate the local stochastic model with respect to the amplitude of the track irregularities, the upcrossings for the four track irregularities are featured in Figure 2.11 (the upcrossings refers to the number of times for which the observed signal crosses a given amplitude in ascending direction). It can be seen that the number of upcrossings respects the

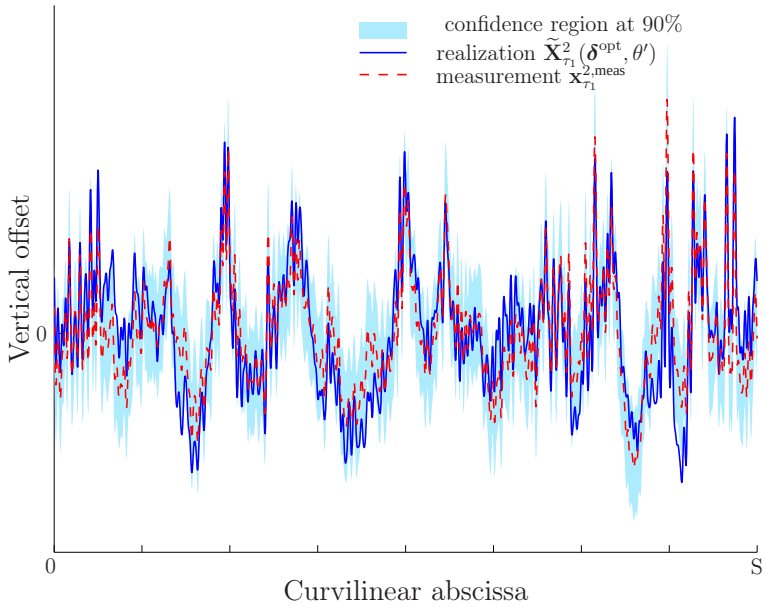

Figure 2.10: Local stochastic model for the vertical offset of a track stretch.

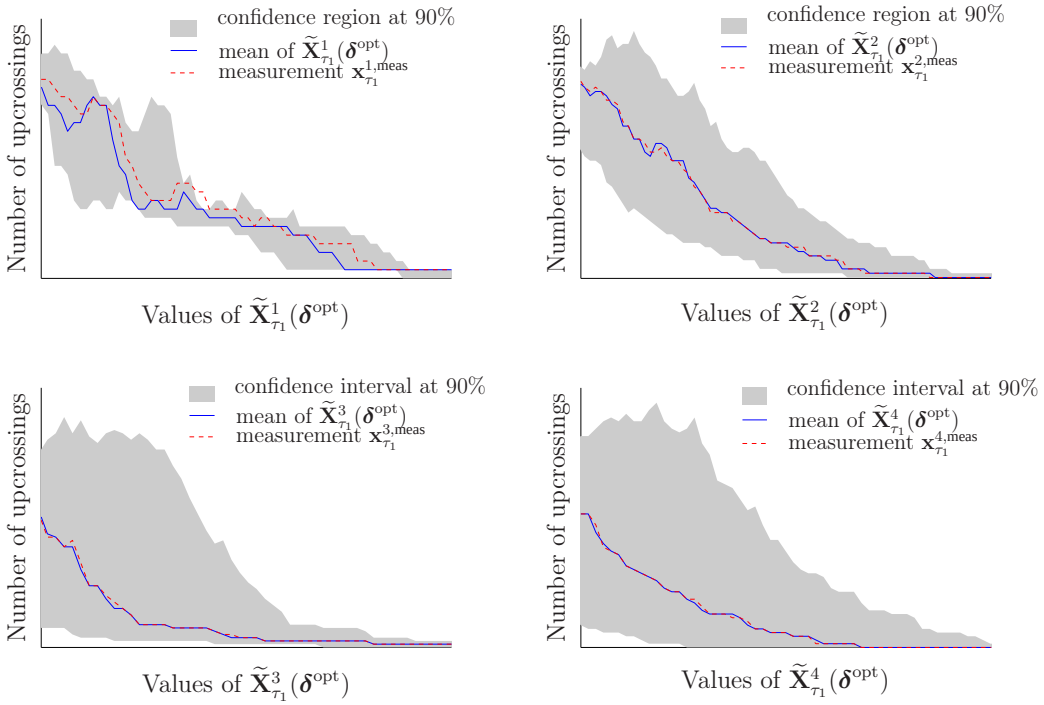

Figure 2.11: Statistical validation of the local stochastic modeling of the track irregularities.

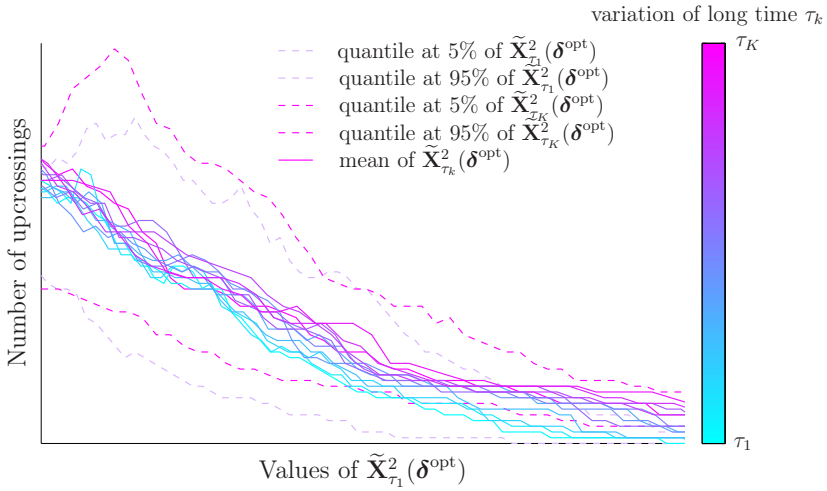

Figure 2.12: Long-term evolution of the number of upcrossings for the vertical offset $\widetilde{\mathbf{X}}^2_{\tau}(\boldsymbol{\delta}^{\mathrm{opt}})$.

statistical properties of the track irregularities. For different long times, the observation of the upcrossings displayed in Figure 2.12 shows that the local stochastic model allows for observing a significant long-term evolution of the track irregularities. In this figure, it can be seen that the number of upcrossings increases with long time τ, which confirms the degradation of the track irregularities. The local stochastic model is validated by Figures 2.10, 2.11, and 2.12, because it preserves the statistical properties of the track irregularities and is sensitive to their long-term degradation.

2.6 Conclusion

In this chapter, the track irregularities for a given stretch of the track with a given curvature type and their long-term evolution have been observed and processed to construct a local stochastic model for the track irregularities, which has been identified. This local stochastic model is adapted to the given track stretch, it preserves the statistical properties of the track irregularities and allows the observation of their long-term evolution.

Chapter 3

Computational nonlinear model of the high-speed train dynamics in presence of model uncertainties

3.1 Introduction

This chapter is devoted to the numerical simulation of dynamic response of the high-speed train (TGV) on a given track stretch, and to the identification of the model uncertainties induced by the modeling errors in the computational model of the train dynamics. The dynamic model of the train is performed in the framework of multibody dynamics. The computational model is the one identified in [5] using experimental identification of the model parameters, and updating of these parameters using the experimental dynamic response of the train. We will validate this computational model for a TGV Duplex (the double-decker french high-speed train), using experimental measurements of the dynamic response of the train on a high-speed line.

An indicator related to the dynamic responses of the train is defined, in order to assess the train safety and the comfort in the train. The maintenance operations will be scheduled by observing this indicator that is computed from dynamic quantities (accelerations and forces) in the train. The comparison between the indicator computed by the numerical simulation and the corresponding one that is experimentally measured, highlights modeling errors. The distinction has to be done between the model-parameter uncertainties (parameters of the computational model) and the model uncertainties induced by modeling errors in the computational model of the train dynamics. The model uncertainties may be induced, for example, by the model of the nonlinearities in the train suspensions and by the nonlinear model of the wheel-rail contact. In order to increase the robustness of the prediction of the proposed indicator, the model uncertainties in the computational model of the train dynamics are taken into account by introducing a multiplicative random vector in the output of the computational model. Hence, this random vector will take into account both the model-parameter uncertainties and the model uncertainties in the computational model of the train dynamics. This multiplicative random vector is constructed by using a reduced statistical representation coupled with a polynomial chaos expansion, whose coefficients are identified by comparing the experi-

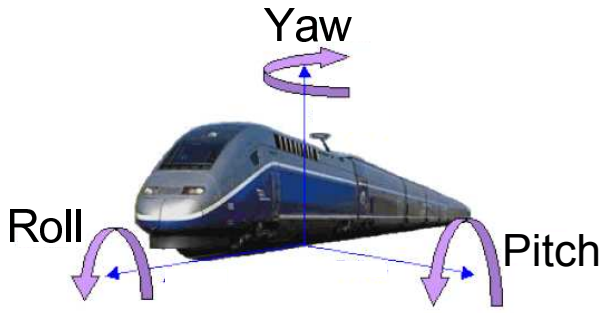

Figure 3.1: Degrees of freedom of a rigid body.

mental measurements and the predictions with the computational model for the indicator.

The computational model of the TGV dynamics is presented in Section 3.2. In Section 3.3, numerical results of the dynamic responses of the train (accelerations and contact forces) are compared with experimental measurements, which allow for checking the accuracy of the computational model predictions. Section 3.4 deals with the definition of the vector-valued indicator and with the comparison between experimentally measured indicators and those predicted by the computational model. The multiplicative random vector in the output is introduced and is characterized in Section 3.5.

3.2 Computational model of the TGV

The computational model of the train dynamics is classically constructed using a rigid body modeling of the train and has been developed with the commercial software *Vampire*. It should be noted that *Vampire* is a blackbox that does not allow for implementing modeling errors but only model-parameter uncertainties. In the considered computational model of the train dynamics, the track and the subgrade are modeled by damping elastic media.

The coaches, the bogies, and the wheelsets of the train are considered as rigid bodies, which are linked by suspensions. Each rigid body is characterized by the position of its center of mass, its mass, and its tensor of inertia. Each suspension is characterized by a rheological model composed of linear and nonlinear springs and dampers. Each rigid body has three degrees of freedom in translation (longitudinal, lateral and vertical) and three degrees of freedom in rotation (roll around the longitudinal axis, pitch around the lateral axis, and yaw around the vertical axis (see Figure 3.1)). In the computational model, the pitch and yaw angles are assumed to be small. The mechanical model of the track is composed of springs and dampers positioned under each wheel of the train, for which the stiffness and the damping are assumed to be constant along the track.

In the computational model, the values of some vehicle parameters are given by the train manufacturer and the values of the other parameters have been identified using experimental measurements achieved on the French high-speed lines (see [5]). In this

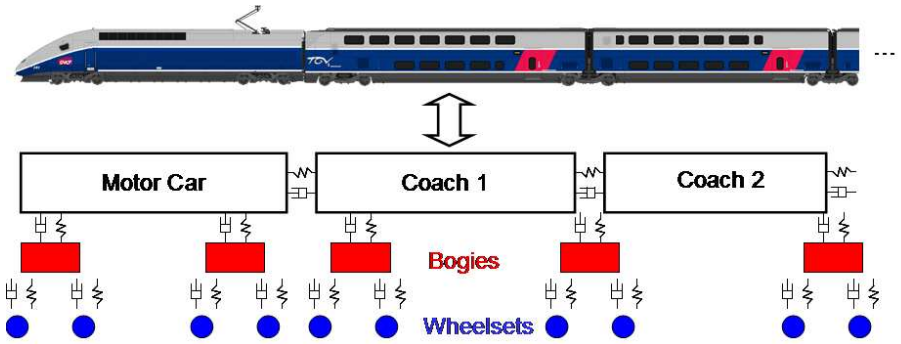

Figure 3.2: Description of a multibody model of a TGV.

work, the high-speed train ("TGV Duplex") is made up of two locomotives, eight coaches, 13 bogies, and 26 wheelsets. Figure 3.2 displays a schematic representation of the TGV Duplex model. The number of degrees of freedom of the vehicle is denoted by $N_{DoF} = 294$.

The vehicle speed on the railway track is given and can be non constant. The excitation of the train is induced by the track geometry (track design and track irregularities), which is detailed in Chapter 2, through the wheel-rail contact forces.

The wheel-rail contact model is pre-processed using the geometrical description of the wheel and the rail profiles. A Hertzian contact model is used in the vertical direction. The wheel and rail profiles allow for computing the wheel-rail contact forces using the Kalker theory [73, 74] in the lateral and longitudinal directions. In this work, the wheel and the rail profiles are assumed to be perfect (the wear effect is analyzed in [75]).

It should be noted that there are strong nonlinearities in the computational model due to the wheel-rail contact forces, to the nonlinear suspensions in the train (for example the airsprings between the bogies and the coaches), and to the bumpstops in the train. The nonlinear dynamic matrix equations are solved with an explicit scheme. The spatial sampling of the track is 0.25 m and is transformed in terms of time. The time step is chosen small enough with respect to the time sampling of the track, in order to obtain a stability of the numerical scheme and a required accuracy for the predicted time responses. A convergence analysis has been performed for identifying an optimal value of this time step that has been found equal to 5.10^{-4}s for the largest speed of the train (300 km/h).

The time observations of the computational model are the accelerations, speeds, and displacements of the rigid bodies (coaches, bogies, and wheelsets), and the wheel-rail contact forces (taking into account both quasi-static and dynamic loads). Since the coaches and locomotives are modeled by rigid bodies (the elasticity is not taken into account), the frequency domain of analysis is restricted to the frequency band $[0, 20]$ Hz for the reasons explained hereinafter.

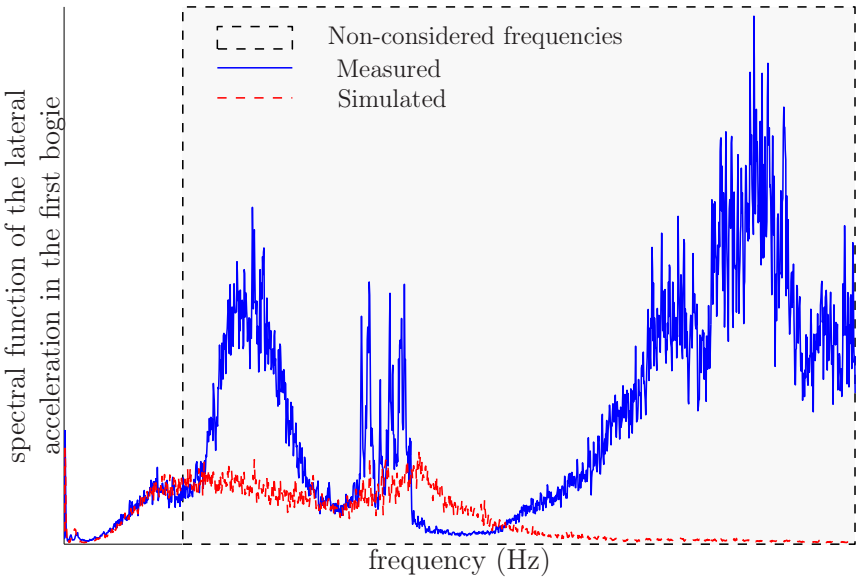

Figure 3.3: Frequency analysis of the lateral acceleration of the first bogie of a TGV. See Figure 3.8 for a zoom of the useful low-frequency band.

As the elastic modes of the coaches, the bogies, and the wheelsets cannot be predicted with the computational model due to the use of a multibody dynamic modeling, the responses, which are experimentally measured and which are used for the comparisons with the computational model predictions, must be filtered to remove the contributions in the frequency band that contains the elastic modes. The corresponding cut-off frequency, which has to be defined, will also be used for filtering the responses predicted with the computational model (the contributions predicted by the computational model above this cut-off frequency are not due to the elastic modes, which do not exist in the computational model, but are due to the transport of the vibrational energy induced by the nonlinearities). In order to find this cut-off frequency, a spectral function is introduced as explained in Appendix B. The comparison between these spectral functions for the measured accelerations and for the simulated accelerations gives the cut-off frequency, as shown in Figure 3.3, which compares the spectral functions of the measured and simulated lateral accelerations of the first bogie. Frequencies under 0.4 Hz also have to be filtered in order to remove the quasi-static rigid body movements (movements induced by the spatial evolution of the track design). For the accelerations, a band-pass filter (with a gradient of -24 dB per octave) is thus applied to the measurements and to the responses predicted with the computational model. For the forces, a low-pass filter with a cut-off frequency of 20 Hz is applied to the measurements and to the responses predicted with the computational model. It is verified that the frequency range $[0.4, 20]$ Hz for the dynamic response of the train is excited by the considered track irregularities (with a wavelength between 3 and 150 m) when the TGV runs between 220 and 300 km/h.

3.3 Experimental measurements and updating of the computational model

3.3.1 Experimental measurements used for the updating

In order to update the deterministic computational model of the dynamic response of the train, the outputs of the numerical simulation are compared with experimental measurements. Five measurement campaigns have been performed by SNCF for the TGV Duplex running on a French high-speed line. The quantities that have been simultaneously measured are:

- accelerations in the bogies and in the coaches of the train;
- wheel-rail contact forces that are deduced from the strain gauges attached on the wheels; the lateral forces are denoted by Y_i^L and Y_i^R and the vertical forces are denoted by Q_i^L and Q_i^R, where $i = 1, \ldots, 26$ denotes the indices for wheelsets, index L stands for "left wheel" and index R for "right wheel";
- the train speed (which is not constant)is between 280 and 300 km/h.

The longitudinal direction is the (Ox)-axis and corresponds to the track axis. The lateral direction is the (Oy)-axis and corresponds to the direction that is horizontal and perpendicular to (Ox). The vertical direction is the (Oz)-axis and is oriented upwards. The measurements are performed with a sampling frequency $f_s = 400$ Hz, which is also used in the computational model. The total number ν_p of track stretches of length S that are measured during the five measurement campaigns is $\nu_p = 937$. For the updating procedure, the dynamic responses of the train are computed for these ν_p track stretches in order to construct the five updated computational models corresponding to the five experimental campaigns.

3.3.2 Updating the computational model

For the updating of the computational model of the TGV, the dynamic response of the train is simulated for the configurations that are as close as possible to the experimental conditions. The track irregularities have been measured by the recording train IRIS 320 at a long time, which is very close (a few days) to the moment for which the experimental campaigns are carried out. These measurements of the track irregularities are used in input of the computational model of the train dynamics. The train speed that has been measured during the experimental campaigns is used for the numerical simulation.

For the experimental campaigns, the mass of the second coach of the TGV Duplex that is used is different and unkown for each measurement campaign, and consequently, is slightly different from the computational model described in Section 3.2, which has therefore to be updated. A quick optimization loop has then been implemented to find the appropriate mass m_2 for the second coach. The computational observation is the total static vertical force $Q_{\text{obs}}^{\text{sim}}$ applied to the first bogie of the second coach (the fifth bogie of the

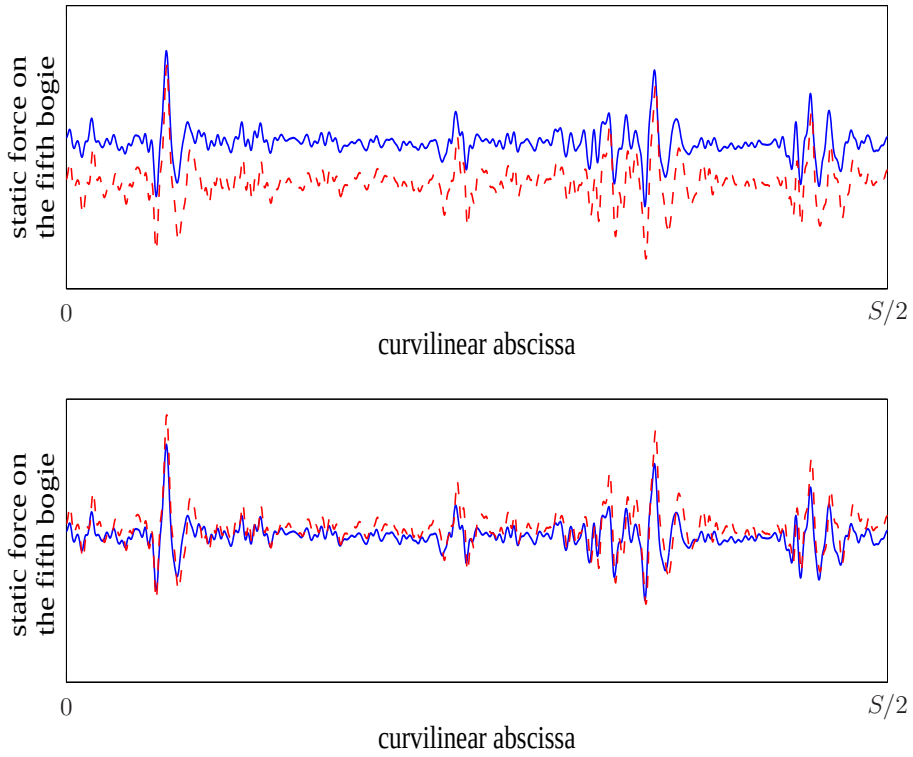

Figure 3.4: For one of the five experimental campaigns, comparison of the experimental static force $Q_{\text{obs}}^{\text{exp}}$ (solid blue line) with the simulated static force $Q_{\text{obs}}^{\text{sim}}$ (dashed red line), before the updating (up figure) and after the updating (down figure).

train). The corresponding experimental observation is denoted by $Q_{\text{obs}}^{\text{exp}}$. The updated value m_2^{up} of m_2 is obtained by solving the following optimization problem:

$$m_2^{\text{up}} = \arg \min_{m_2 \in \mathbb{R}^+} \{m_2 \,,\, |Q_{\text{obs}}^{\text{exp}} - Q_{\text{obs}}^{\text{sim}}| \leq \varepsilon_m\} \,, \tag{3.1}$$

in which ε_m is a given tolerance. This updating procedure leads us to construct five computational models that are updated with respect to the five experimental campaigns. For one of the five experimental campaigns, Figure 3.4 shows the comparison of the experimental static force $Q_{\text{obs}}^{\text{exp}}$ with the simulated static force $Q_{\text{obs}}^{\text{sim}}$, before and after the updating.

3.3.3 Evaluation of the accuracy of the updated computational model

The validation of the computational model is performed in the time and the frequency domains for most of the available measured forces and accelerations. Because of the lack of precision in the localization of the measuring train with respect to the track design (the localization is performed with an odometric wheel), the curvilinear abscissa of the measured quantities has to be corrected by introducing a spatial shift before the

post-processing, as explained in Appendix C. Figure 3.5 represents the measured and simulated vertical forces on the first wheelset for the measured track. It can be noticed that the measured vertical forces are well reproduced by the simulation concerning their amplitude. .

The vertical and lateral accelerations are displayed in Figure 3.6. The accelerations in the bogies are very similar in the simulation and in the measurements. The acceleration in the second coach is different in the simulation and in the measurements (probably because of the nonlinear suspensions between bogies and coaches), but the appearance is globally reproduced, which is enough to start off the maintenance operations. The vertical accelerations and forces are better modeled than the lateral ones, because the nonlinearities are more important in the lateral direction than in the vertical one. The spectral function defined in Appendix B of the vertical forces in the first wheelset is featured in Figure 3.7. The spectral functions of the lateral acceleration in the first and in the fifth bogie, of the lateral acceleration in the second coach, and of the vertical acceleration in the first bogie are displayed in Figure 3.8. These figures allow for comparing the measurements with the simulations concerning their frequency spectra, and show a good similarity between both. It is deduced from these observations that the updated computational model of the train dynamics is satisfactory for the observed criteria (forces and accelerations in output of the simulation): the wheel-rail contact, the suspensions, the masses and the inertia tensors of the rigid bodies are sufficiently well modeled.

3.4 Introduction of a vector-valued indicator for quantifying the dynamic response of the train

3.4.1 Definition of the vector-valued indicator

The dynamic response of the high-speed train is usually assessed by comfort and safety criteria. Safety criteria are based on the analysis on wheel-rail contact forces and are described in the UIC (International Union of Railways) Leaflet 518 [76] for the vehicles certification. One often-used safety criteria is the Nadal criteria which gives a threshold value for the quotient between lateral and vertical wheel-rail contact forces: $Y/Q \leq 0.8$. Figure 3.9 provides an illustration of these forces. The UIC Leaflet 518 [76] also gives comfort criteria, which are based on accelerations in the wheelsets or in the coaches. Due to the coupling between the track and the dynamic response of the train, safety and comfort criteria characterize not only the vehicle state, but also the track stretch on which the train runs. Actually, criteria on the dynamic response of the train can be used to characterize the long-term evolution of the track irregularities for a given stretch of the railway track. These criteria are usually defined by taking the maximum of the quantities of interest related to the dynamic response of the train for a given stretch of the railway track. To assess the track irregularities and start off the maintenance, some threshold values, which are phenomenologically defined (see [59] for example), can be assigned to those criteria.

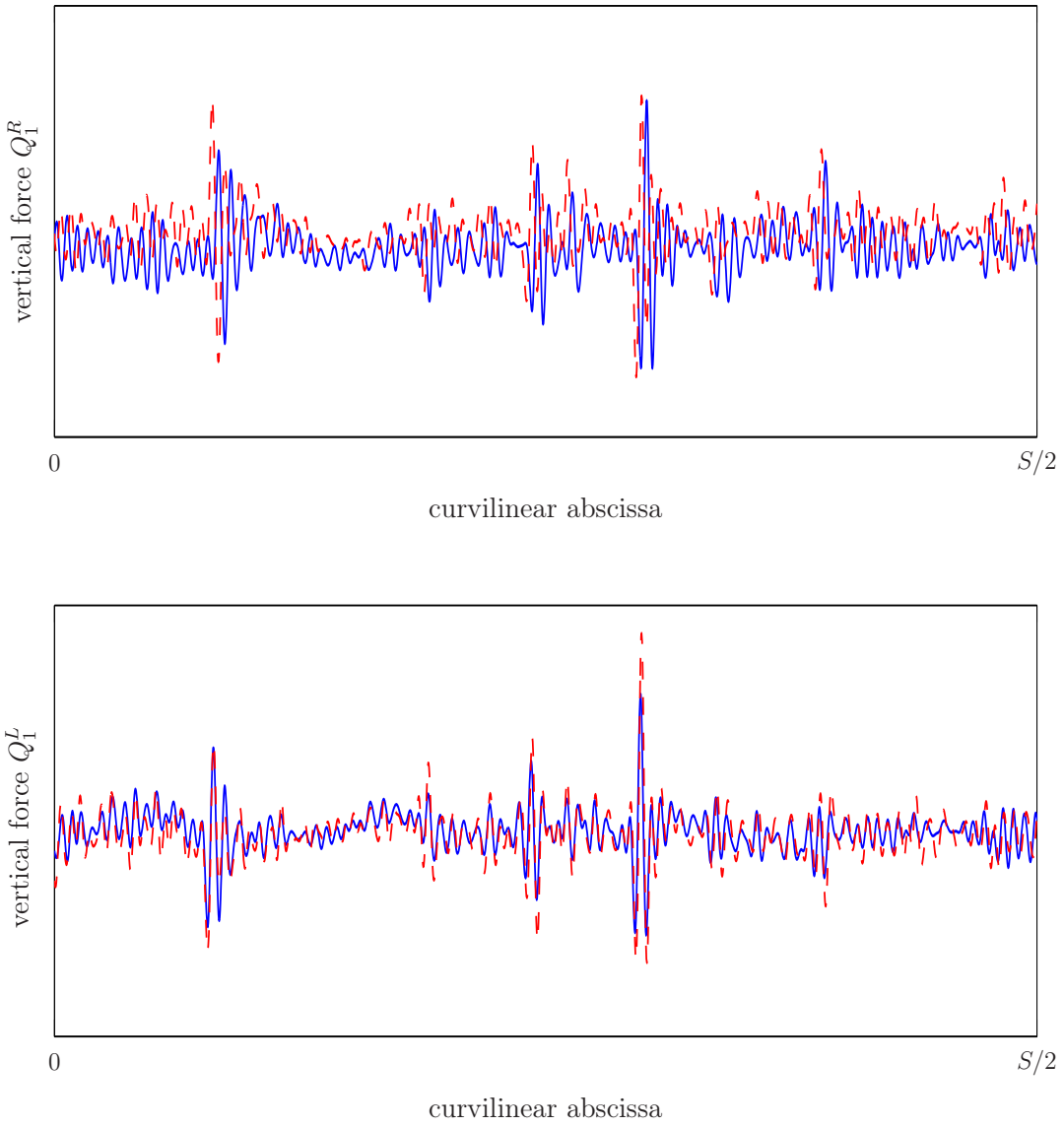

Figure 3.5: Vertical forces on the first wheelset as a function of the curvilinear abscissa. Comparison of the measured forces (solid blue line) with the simulated forces (dashed red line).

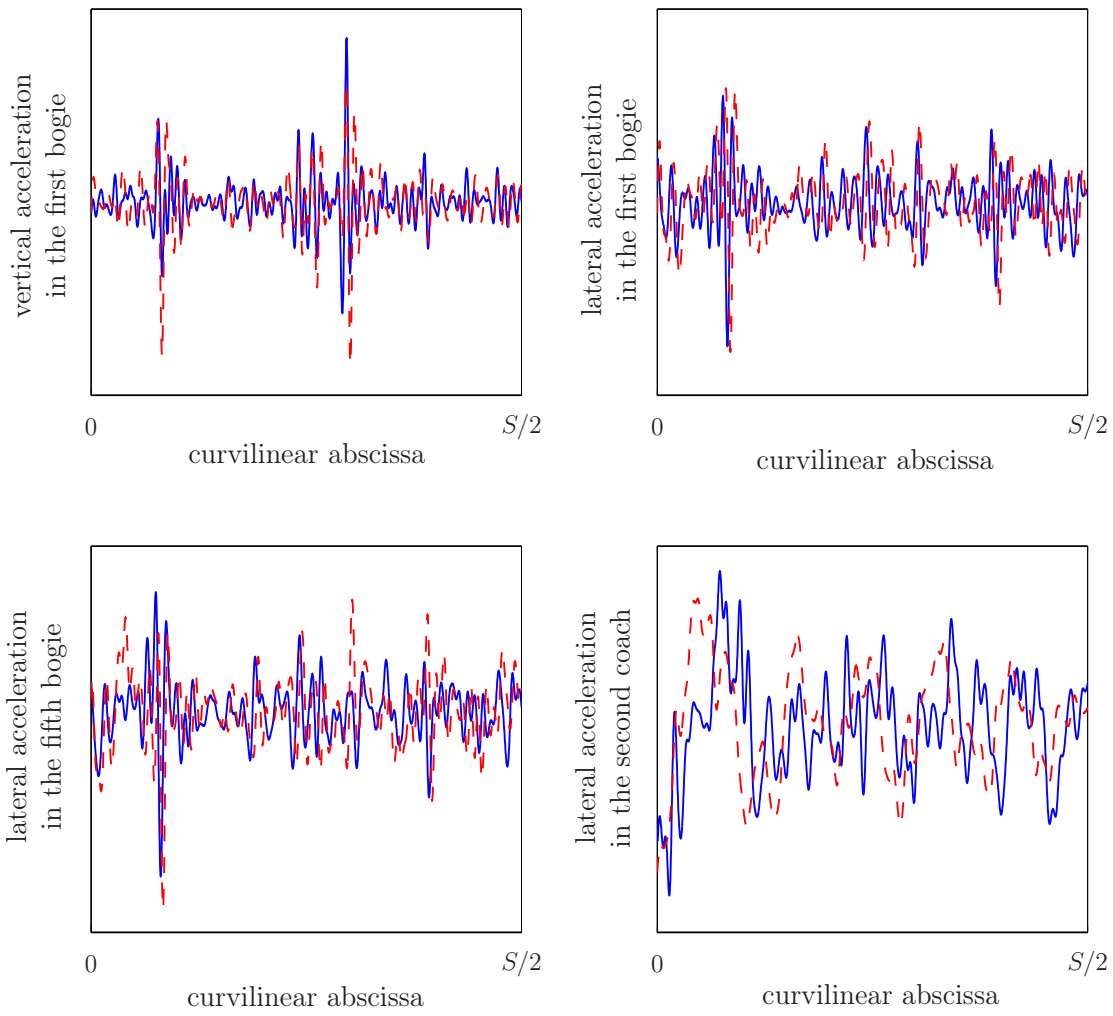

Figure 3.6: Acceleration response as a function of the curvilinear abscissa. Comparison of the measured acceleration (solid blue line) with the simulated acceleration (dashed red line).

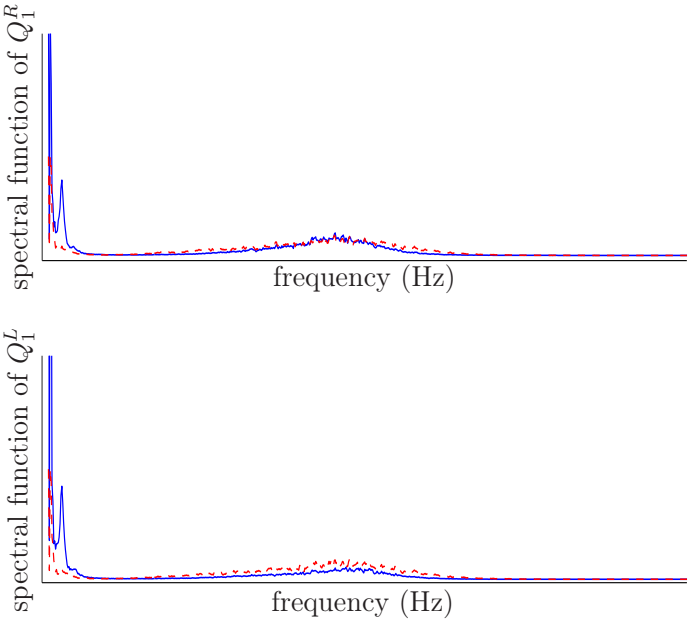

Figure 3.7: Validation for the vertical forces of the first wheelset in the frequency domain. Comparison of the measured forces (solid blue line) with the simulated forces (dashed red line).

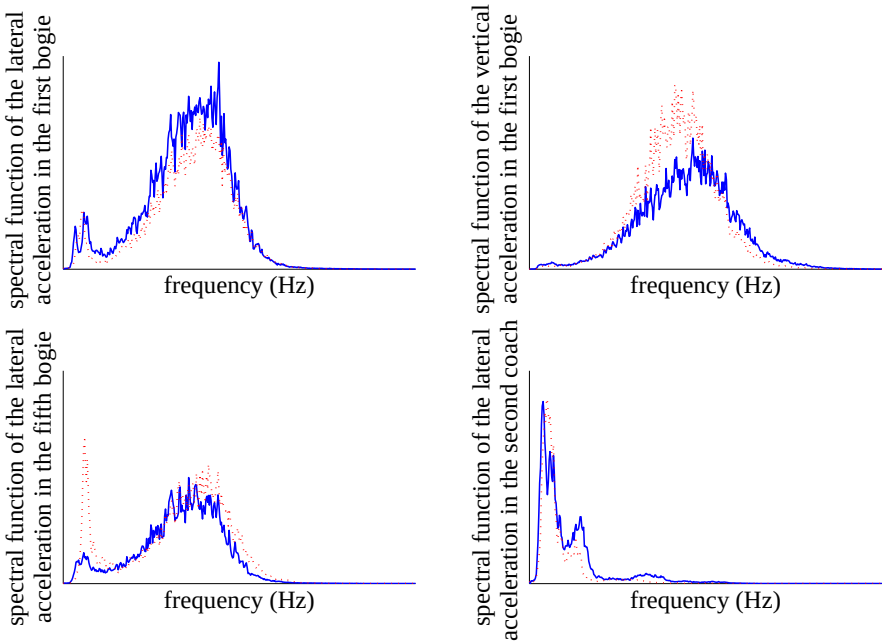

Figure 3.8: Validation for acceleration responses in the frequency domain. Comparison of the measured accelerations (solid blue line) with the simulated accelerations (dashed red line).

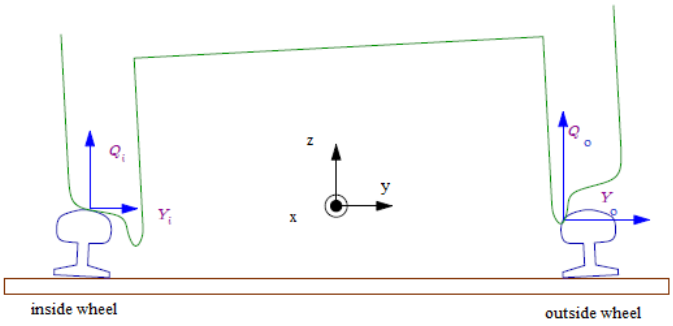

Figure 3.9: Lateral and vertical forces at the wheel-rail contact.

In this thesis, a vector-valued indicator on the dynamic response of the train is introduced in order to observe the long-term evolution of the track irregularities for a given stretch of the railway track. This indicator is constructed from N_c quantities of interest related to the dynamic response of the high-speed train, and which are described in UIC Leaflet 518 [76]. The components of the indicator are also chosen depending on the dynamic quantities measured by the measuring TGV Duplex, in order to compare measured and simulated indicators. Those quantities of interest are defined as a function of forces and accelerations at different locations in the train, for a given stretch of the railway track, and for which measurements are available. Some experimental and numerical results for the quantities of interest are featured in Figures 3.6 (for the accelerations) and 3.10 (for the forces), and allow for selecting the $N_c = 9$ most sensitive components for the vector-valued indicator.

For s belonging to $[0, S]$, the nine quantities of interest are the following:

- the lateral acceleration of the first bogie of the train, denoted by $Z_1(s)$,
- the vertical acceleration of the first bogie of the train, denoted by $Z_2(s)$,
- the lateral acceleration of the third bogie of the train, denoted by $Z_3(s)$,
- the lateral acceleration of the second coach of the train, denoted by $Z_4(s)$.
- the sum of lateral forces on the ninth wheelset, defined by $Z_5(s) = Y_9^R(s) + Y_9^L(s)$,
- the sum of vertical forces on the first wheelset, defined by $Z_6(s) = Q_1^R(s) + Q_1^L(s)$,
- the sum of vertical forces on the second wheelset, defined by $Z_7(s) = Q_2^R(s) + Q_2^L(s)$,
- the sum of vertical forces on the tenth wheelset, defined by $Z_8(s) = Q_{10}^R(s) + Q_{10}^L(s)$,
- the difference between right-wheel and left-wheel vertical forces on the tenth wheelset, defined by $Z_9(s) = Q_{10}^R(s) - Q_{10}^L(s)$.

As explained before, the dynamic quantities of interest are filtered as follows. For the accelerations Z_1, Z_2, Z_3 and Z_4, the fourth-order band-pass linear filter defined in Section 3.2 is used. For the forces Z_5, Z_6, Z_7, Z_8 and Z_9, the filter is a fourth-order low-pass

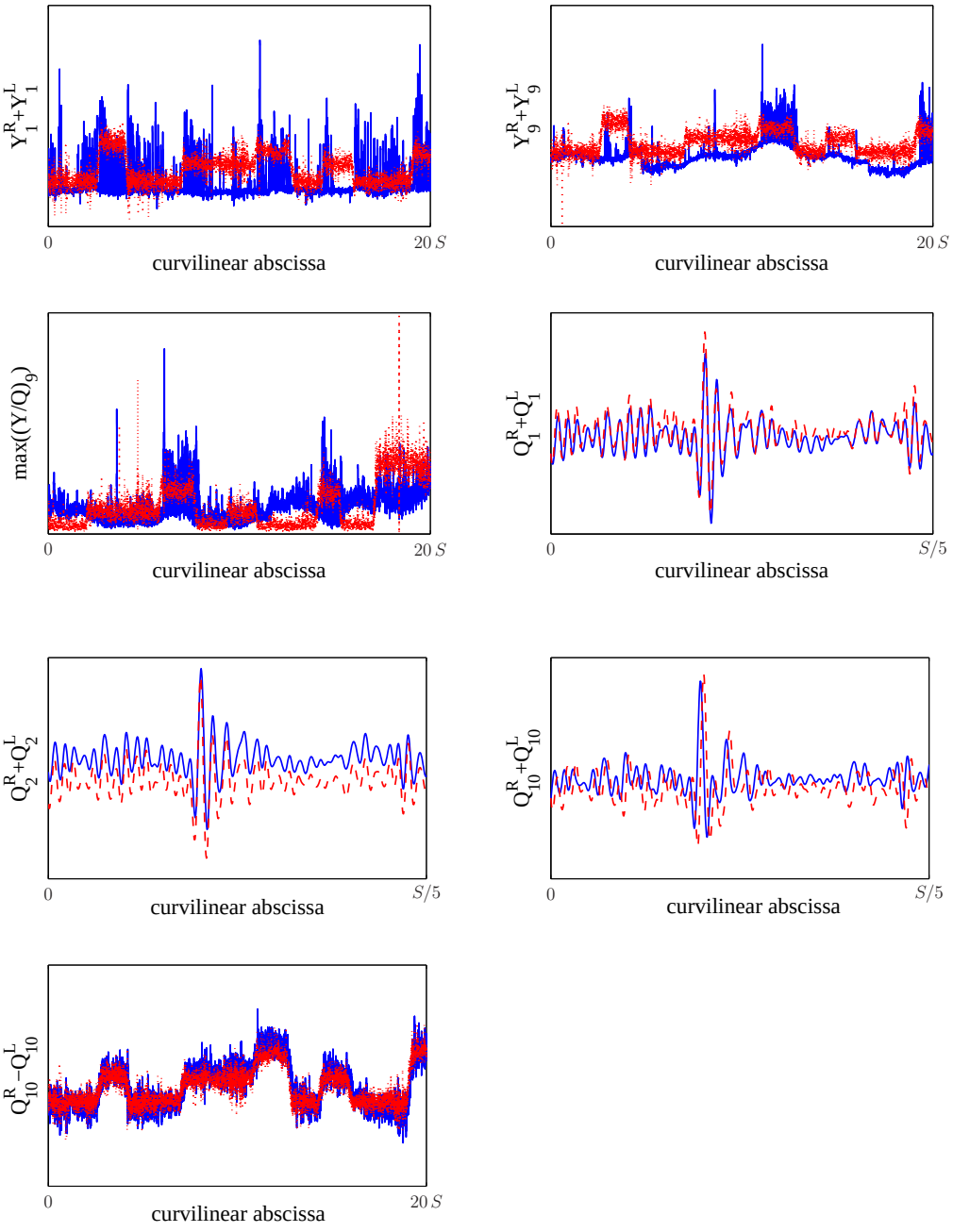

Figure 3.10: Examples of dynamic criteria related to the wheel-rail contact forces. Comparison of the measured forces (solid blue line) with the simulated forces (dashed red line).

linear filter with cut-off frequency at 20 Hz. The components of the indicator vector $\mathbf{c} = (c_1, \ldots, c_{N_c})$ are defined by

$$c_j = \max_{s \in [0,S]} |Z_j(s)| \quad , \quad j = 1, \ldots, N_c \, . \tag{3.2}$$

3.4.2 Calculation of the indicators for the experimental measurements and for the numerical simulation

In order to characterize the model uncertainties in the computational model of the train dynamics, we need to compare, for each stretch of the track, the indicator vector $\mathbf{c}^{\text{sim}} = (c_1^{\text{sim}}, \ldots, c_{N_c}^{\text{sim}})$ obtained by simulation with the experimental indicator vector $\mathbf{c}^{\text{exp}} = (c_1^{\text{exp}}, \ldots, c_{N_c}^{\text{exp}})$.

The experimental indicator vector $\mathbf{c}^{\text{exp}}$ is calculated using the measurements of the dynamic response of the train described in Section 3.3. The measurements of the accelerations and forces are performed for ν_p track stretches of length S (taking into account the five measurement campaigns) and post-processed to obtain the indicators $\mathbf{c}^{\text{exp},\ell}$, $\ell \in \{1, \ldots, \nu_p\}$. It is assumed that $\mathbf{c}^{\text{exp},1}, \ldots, \mathbf{c}^{\text{exp},\nu_p}$ are ν_p independent realizations of a vector-valued random indicator denoted by $\mathbf{C}^{\text{exp}}$. For a given measurement campaign, the dynamic responses of the train for two different stretches of the track are considered as independent. The five measurement campaigns are also considered as independent (due, in particular, to the change of the train speed between two campaigns).

For each stretch of the railway track, the dynamic response of the train on the track is then numerically simulated using the computational model. The track geometry used in input of the simulation is the deterministic track geometry $\mathbf{x}^{\text{exp},1}, \ldots, \mathbf{x}^{\text{exp},\nu_p}$ measured during the measurement campaigns (without using the adapted stochastic model of Chapter 2). The speed depending on time is recorded by the measuring TGV Duplex and is used as a parameter of the computational model, which is the one identified in [5], and for which the mass of the second coach has been updated in Section 3.3.2.

The quantities of interest related to the accelerations, which can be estimated with the experimental measurements, cannot directly be calculated with the computational model, and consequently, have to be constructed as described hereinafter. The computed accelerations have to take into account the momentum due to the off-centering of the accelerometers. For the lateral accelerations, the quantities of interest $Z_1^{\text{sim}}(s), Z_3^{\text{sim}}(s)$, and $Z_4^{\text{sim}}(s)$ for the components of the indicator are constructed such as

$$Z_j^{\text{sim}}(s) = \ddot{y}_j(s) + \ddot{w}_j^z(s)\, l_j^x - \ddot{w}_j^x(s)\, l_j^z \quad , \quad s \in [0, S] \quad , \quad j = 1, 3, 4 \, , \tag{3.3}$$

where $\ddot{y}_j(s)$ is the lateral acceleration of the considered bodies, l_j^x and l_j^z are the distances between the center of mass of the bodies and the sensor in the longitudinal and vertical directions respectively, and where $\ddot{w}_j^x$ and $\ddot{w}_j^z$, are the angular accelerations about the longitudinal and vertical axes respectively. For the vertical acceleration, the quantity of interest $Z_2^{\text{sim}}(s)$ is constructed such that

$$Z_2^{\text{sim}}(s) = \ddot{z}_2(s) + \ddot{w}_2^x(s)\, l_2^y - \ddot{w}_2^y(s)\, l_2^x \quad , \quad s \in [0, S] \, , \tag{3.4}$$

in which $\ddot{z}_2(s)$ is the vertical acceleration of the first bogie, l_2^y is the distance between the center of mass of the bogie and the accelerometer in the lateral direction, and where $\ddot{w}_2^y$ is the angular acceleration about the lateral axis. Quantities $\mathbf{Z}^{\text{sim}}(s) = (Z_1^{\text{sim}}(s), \ldots, Z_{N_c}^{\text{sim}}(s))$ are then filtered and the indicator vectors $\mathbf{c}^{\text{sim},1}, \ldots, \mathbf{c}^{\text{sim},\nu_p}$ are computed as defined in Eq (3.2).

It is assumed that $\mathbf{c}^{\text{sim},1}, \ldots, \mathbf{c}^{\text{sim},\nu_p}$ are ν_p independent realizations of a random indicator vector denoted by $\mathbf{C}^{\text{sim}}$. Due to the local stochastic model introduced in Section 2.5, $\mathbf{C}^{\text{sim}}$ is a second-order random vector defined on the probability space $(\Theta', \mathcal{F}', \mathcal{P}')$ with values in $(\mathbb{R}^+)^{N_c}$. Any realization of random vector $\mathbf{C}^{\text{sim}}$ is denoted by $\mathbf{C}^{\text{sim}}(\theta')$ for $\theta' \in \Theta'$.

For a selection of 64 stretches among the $\nu_p = 898$ stretches of the track, the realizations of the $N_c = 9$ components of the vector-valued indicators $\mathbf{C}^{\text{exp}}$ and $\mathbf{C}^{\text{sim}}$ are featured in Figure 3.11. It can be noticed that the experimental realizations of the indicator are not exactly the same as the simulated realizations, which underlines the presence of modeling errors in the computational model of the train. Moreover, it should be noted that the modeling errors in the computational model of the train dynamics depend on the track curvature, because the train suspensions, which are modeled in the computational model of the train, are not solicited in the same way depending on the track curvature. Consequently, the modeling uncertainties induced by modeling errors have to be identified for each curvature type defined in Section 2.3.1. We have $\nu_A = 341$ straight stretches of the track, $\nu_C = 311$ curved stretches, $\nu_{EC} = 114$ stretches in curve entrance, and $\nu_{SC} = 132$ stretches in curve exit.

3.5 Model uncertainties induced by modeling errors

3.5.1 Stochastic modeling of model uncertainties

As explained in the previous section, the comparison of simulated and measured values of the indicator shows that there are modeling errors in the computational model of the train, which are taken into account by introducing model uncertainties. The model uncertainties induced by modeling errors have to be distinguished from the model-parameter uncertainties (as explained in [70]). One way to take into account the model uncertainties is the use of the nonparametric probabilistic approach (see [70] and some examples of application in [77, 78]). Nevertheless, since the *Vampire* software is a blackbox, such a nonparametric probabilistic approach of uncertainties cannot be implemented. We then propose to use the output-prediction-error method, which consists in introducing an additive or a multiplicative noise in the output of the computational model. Such a method allows for taking into account all the uncertainties in the computational model of the train dynamics: uncertainties due to the rigid bodies modeling, uncertainties in the parameters of the train model (due to the identification of the parameters or to the degradation of the train), uncertainties in the track and subgrade modeling, and numerical uncertainties. The stochastic computational model constructed hereinafter to take into account modeling errors is based on the introduction of a multiplicative output noise.

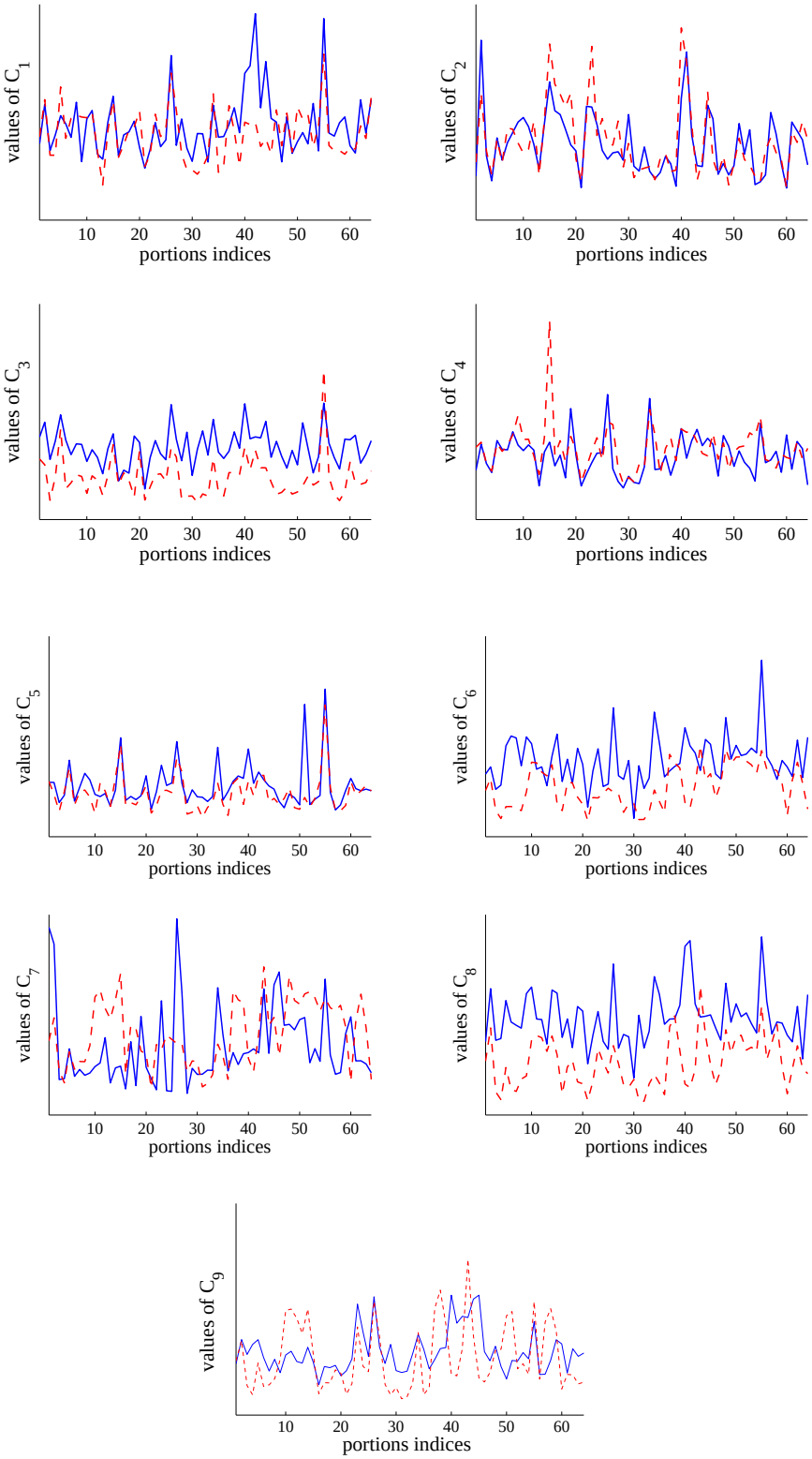

Figure 3.11: Comparison of the experimental indicator vector $\mathbf{C}^{\text{exp}}$ (solid blue line) with the simulated indicator vector $\mathbf{C}^{\text{sim}}$ (dashed red line) for 64 track stretches.

To characterize this multiplicative output noise, a random vector $\mathbf{B}^{\text{out}}$ is introduced, which is statistically independent of the simulated indicator $\mathbf{C}^{\text{sim}}$, and consequently has been defined on another probability space denoted by $(\Theta'', \mathcal{F}'', \mathcal{P}'')$. The random indicator vector that includes model uncertainties is denoted by $\mathbf{C}^{\text{mod}} = (C_1^{\text{mod}}, \ldots, C_{N_c}^{\text{mod}})$, and is constructed as a function of the simulated indicator vector $\mathbf{C}^{\text{sim}}$ and of the random vector $\mathbf{B}^{\text{out}}$. Random vector $\mathbf{B}^{\text{out}} = (B_1^{\text{out}}, \ldots, B_{N_c}^{\text{out}})$ is defined as a non-Gaussian second-order $\mathbb{R}^{N_c}$-valued random vector, which has to be identified using measurements. By construction, the vector-valued indicator $\mathbf{C}^{\text{sim}}$ is a non-Gaussian second-order random vector with values in $(\mathbb{R}^+)^{N_c}$. Consequently, the random vector $\mathbf{C}^{\text{mod}}$ is defined on the product of the probability space $(\Theta', \mathcal{F}', \mathcal{P}')$ and $(\Theta'', \mathcal{F}'', \mathcal{P}'')$, and is a non-Gaussian second-order $(\mathbb{R}^+)^{N_c}$-valued random vector, which is written as

$$C_j^{\text{mod}}(\theta', \theta'') = C_j^{\text{sim}}(\theta') \, \exp(B_j^{\text{out}}(\theta'')) \ , \ j = 1, \ldots, N_c \ , \ \theta' \in \Theta' \ , \ \theta'' \in \Theta'' \, . \tag{3.5}$$

Random vector $\mathbf{B}^{\text{out}}$ has to be identified in comparing the random indicator vector $\mathbf{C}^{\text{mod}}$ with the corresponding experimental random indicator vector $\mathbf{C}^{\text{exp}}$ for which measurements have been carried out for the ν_p track stretches previously used. Since random vector $\mathbf{B}^{\text{out}}$ is non-Gaussian, its representation on the Gaussian polynomial chaos is used. For that, a principal component analysis of $\mathbf{B}^{\text{out}}$ is performed, and the non-Gaussian centered and non-correlated coordinates are developed using the Gaussian polynomial chaos expansion. Consequently, random vector $\mathbf{B}^{\text{out}}$ is written as

$$\mathbf{B}^{\text{out}} = \underline{\mathbf{b}} + \sum_{j=1}^{N_c} \sqrt{\lambda_j} \, \eta_j \, \boldsymbol{\varphi}^j \, , \tag{3.6}$$

in which $\underline{\mathbf{b}} = E\{\mathbf{B}^{\text{out}}\}$ is the mean value, and where $\lambda_1, \ldots, \lambda_{N_c}$ and $\boldsymbol{\varphi}^1, \ldots, \boldsymbol{\varphi}^{N_c}$ are the positive eigenvalues and the orthonormal eigenvectors of the covariance matrix $[C_{\mathbf{B}^{\text{out}}}] = E\{(\mathbf{B}^{\text{out}} - \underline{\mathbf{b}})(\mathbf{B}^{\text{out}} - \underline{\mathbf{b}})^T\}$ that has to be estimated with the measurements. The non-Gaussian random vector $\boldsymbol{\eta} = (\eta_1, \ldots, \eta_{N_c})$, for which the components are such that $\eta_j = \lambda_j^{-1/2}(\mathbf{B}^{\text{out}} - \underline{\mathbf{b}})^T(\boldsymbol{\varphi}^j)$, is such that $E\{\boldsymbol{\eta}\} = 0$ and $E\{\boldsymbol{\eta}\boldsymbol{\eta}^T\} = [I_{N_c}]$ (the identity matrix). In order to represent a family of parameterized probability distributions of the non-Gaussian random vector $\boldsymbol{\eta}$, the following finite polynomial chaos expansion (PCE) (see for instance [68, 69, 70]) is introduced,

$$\boldsymbol{\eta} = \sum_{i=0}^{N} \mathbf{y}^{(i)} \psi_{\boldsymbol{\alpha}^{(i)}}(\boldsymbol{\xi}) \, , \tag{3.7}$$

in which $\boldsymbol{\xi} = (\xi_1, \ldots, \xi_{N_g})$ is a normalized Gaussian random vector of dimension $N_g \leq N_c$, $\psi_{\boldsymbol{\alpha}^{(0)}}(\boldsymbol{\xi}), \ldots, \psi_{\boldsymbol{\alpha}^{(N)}}(\boldsymbol{\xi})$ are the multivariate orthonormal normalized Hermite polynomials (the polynomial chaos), and where N, N_g, and the vectors $\mathbf{y}^{(0)}, \ldots, \mathbf{y}^{(N)}$ in $\mathbb{R}^{N_c}$ have to be identified. For $i = 0, \ldots, N$, the multi-index $\boldsymbol{\alpha}^{(i)}$ is the vector of integers defined by $\boldsymbol{\alpha}^{(i)} = (\alpha_1^i, \ldots, \alpha_{N_g}^i) \in \mathbb{N}^{N_g}$. Since $\boldsymbol{\eta}$ is centered, and since $\psi_{\boldsymbol{\alpha}^{(0)}}(\boldsymbol{\xi}) = 1$, $\mathbf{y}^{(0)} = \mathbf{0}$.

3.5.2 Identification of the output noise $\mathbf{B}^{\text{out}}$

The output noise $\mathbf{B}^{\text{out}}$ is identified by solving a statistical inverse problem using experimental measurements $\mathbf{c}^{\text{exp}}$, which are considered as independent realizations of $\mathbf{C}^{\text{mod}}$,

and using realizations of $\mathbf{C}^{\text{sim}}$. As previously, we consider ν_p track stretches of index ℓ. Let $\mathbf{c}^{\text{exp},\ell}$ be the indicator of the response measured in the train excited by the track irregularities of the track stretch of index ℓ. Let $\mathbf{c}^{\text{sim},\ell}$ be the indicator of the response calculated with the computational model of the train excited by the same track irregularities of the track stretch of index ℓ. Taking into account the hypothesis concerning the statistical independence, for all $j = 1, \ldots, N_c$, the independent realizations $b_j^{\text{exp},\ell}$ for $\ell = 1, \ldots, \nu_p$ of the component B_j^{out} of random vector $\mathbf{B}^{\text{out}}$ are written (see Eq. (3.5)) as

$$b_j^{\text{exp},\ell} = \ln\left(\frac{c_j^{\text{exp},\ell}}{c_j^{\text{sim},\ell}}\right) \quad , \quad j = 1, \ldots, N_c \quad , \quad \ell = 1, \ldots, \nu_p \, . \tag{3.8}$$

For numerical conditioning reasons, for fixed ℓ, each component $b_j^{\text{exp},\ell}$ of vector $\mathbf{b}^{\text{exp},\ell} = (b_1^{\text{exp},\ell}, \ldots, b_{N_c}^{\text{exp},\ell})$ is normalized by $\max_{\ell=1,\ldots,\nu_p} |b_j^{\text{exp},\ell}|$. The following estimations of mean value $\underline{\mathbf{b}}$ and covariance matrix $[C_{\mathbf{B}^{\text{out}}}]$ (defined in Section 3.5.1) are written as

$$\underline{\mathbf{b}} \simeq \widehat{\underline{\mathbf{b}}} = \frac{1}{\nu_p} \sum_{\ell=1}^{\nu_p} \mathbf{b}^{\text{exp},\ell} \quad , \quad [C_{\mathbf{B}^{\text{out}}}] \simeq [\widehat{C}_{\mathbf{B}^{\text{out}}}] = \frac{1}{\nu_p - 1} \sum_{\ell=1}^{\nu_p} (\mathbf{b}^{\text{exp},\ell} - \underline{\mathbf{b}}^{\text{exp}})(\mathbf{b}^{\text{exp},\ell} - \underline{\mathbf{b}}^{\text{exp}})^T \, . \tag{3.9}$$

For $\ell = 1, \ldots, \nu_p$, the independent realizations $\boldsymbol{\eta}^{\text{exp},\ell} = (\eta_1^{\text{exp},\ell}, \ldots, \eta_{N_c}^{\text{exp},\ell})$ of random vector $\boldsymbol{\eta}$ are then calculated by $\eta_j^{\text{exp},\ell} = \lambda_j^{-1/2} (\mathbf{b}^{\text{exp},\ell} - \widehat{\underline{\mathbf{b}}}^{\text{exp}})^T (\boldsymbol{\varphi}^j)$.

Let $\mathbf{h} \mapsto p_{\boldsymbol{\eta}}(\mathbf{h}; [y])$ be the probability density function of random vector $\boldsymbol{\eta}$ defined by Eq. (3.7), which depends on the matrix $[y] = [\mathbf{y}^0, \ldots, \mathbf{y}^N]$ that belongs to the set $\mathbb{M}_{N_c,N}$ of all the real $(N_c \times N)$ matrices, and which must verify the constraint $[y]\,[y]^T = [I_{N_c}]$. Consequently, $[y]$ has to be identified in the admissible set defined by

$$\mathcal{C}_{[y]} = \left\{ [y] \in \mathbb{M}_{N_c,N} \quad \text{such that} \quad [y]\,[y]^T = [I_{N_c}] \right\} \, . \tag{3.10}$$

For each fixed $[y]$ and fixed $\mathbf{h}$, $p_{\boldsymbol{\eta}}(\mathbf{h}; [y])$ is estimated by using samples calculated with Eq. (3.7) and the Gaussian kernel estimation method. Matrix $[y]$ is identified by the method described in [6, 65], which has briefly been summarized in Section 2.4.2.

3.5.3 Results

Because the dynamic response of the train depends on the track curvature, the noise $\mathbf{B}^{\text{out}}$ is identified for each class of curvature: tangent track, curve entrance, curved track and curve exit. For instance, for the identification of $\mathbf{B}^{\text{out}}$ for the tangent track, we have $\nu_p = \nu_A = 341$ track stretches. The estimations of the marginal probability density functions (PDF) of the components of $\mathbf{B}^{\text{out}}$ for the tangent track are computed with the Gaussian kernel method. Figure 3.12 displays (i) the Gaussian PDFs centered on $\underline{\mathbf{b}} \approx \widehat{\underline{\mathbf{b}}}$ and with the standard deviation $[C_{\mathbf{B}^{\text{out}}}]_{ii} \approx [\widehat{C}_{\mathbf{B}^{\text{out}}}]_{ii}, i = 1, \ldots, 9$ computed on the same closed domain, (ii) the estimated marginal PDFs of $\mathbf{B}^{\text{out}}$ for a straight stretch of the track, and (iii) for a curved stretch of the track. This figure confirms that the output noise $\mathbf{B}^{\text{out}}$ is non-Gaussian and depends on the curvature class.

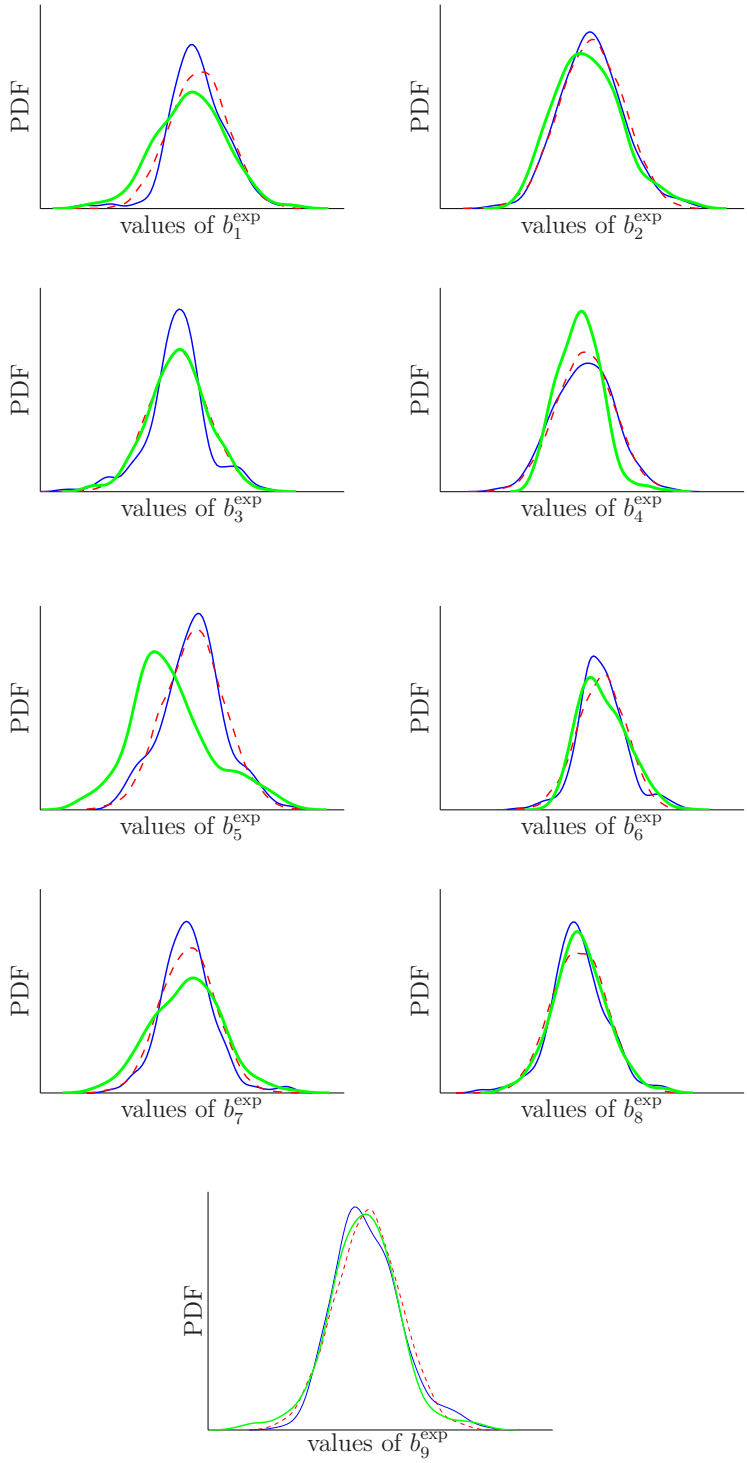

Figure 3.12: For each component B_j^{out} of random vector $\mathbf{B}^{\text{out}}$, comparison of the marginal PDF of B_j^{out} for an alignment (solid blue line), for a curve (bold green line), and for the Gaussian model (dashed red line), computed from the experimental realizations $\mathbf{b}^{\text{exp},\ell}$, $\ell = 1, \ldots, \nu_p$.

For each admissible couple (N_g, p), the optimal value $[y^{\text{opt}}(N_g, p)]$ of matrix $[y]$ is computed with the maximum log-likelihood method (see Eq. (2.18)) using $100,000$ realizations. Then, the error function $(N_g, p) \mapsto \text{err}(N_g, p)$ is computed according to Eq. (2.20). For example, for the straight stretches of the track, error function $(N_g, p) \mapsto \text{err}(N_g, p)$ is featured in Figure 3.13 as a function of N_g and p. It can be noticed that the minimum of the function is obtained for $(N_g^{\text{opt}}, p^{\text{opt}}) = (7, 2)$. The same result is obtained for the

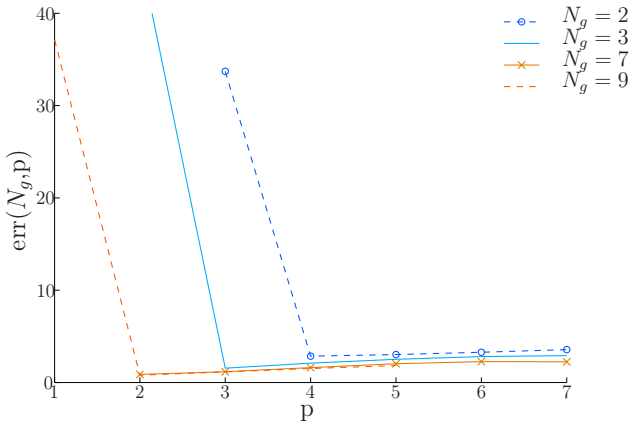

Figure 3.13: Error function $\text{err}(N_g, p)$ as function of N_g and p.

other classes of track stretches. For a given curvature class, once the polynomial chaos of $\mathbf{B}^{\text{out}}$ has been identified, matrix $[y^{\text{opt}}(N_g^{\text{opt}}, p^{\text{opt}})]$ is used to construct the output noise $\mathbf{B}^{\text{out}}$ such as

$$\mathbf{B}^{\text{out}} = \underline{\mathbf{b}} + \sum_{j=1}^{N_c} \sqrt{\lambda_j} \, (\sum_{i=0}^{N} y_j^{\text{opt},(i)}(N_g^{\text{opt}}, p^{\text{opt}}) \psi_{\boldsymbol{\alpha}^{(i)}}(\boldsymbol{\xi})) \, \boldsymbol{\varphi}^j \, . \tag{3.11}$$

For the components of $\mathbf{B}^{\text{out}}$, Figures 3.14 and 3.15 show the comparisons (in linear and log scales) between the marginal PDFs of the experimental values estimated by the nonparametric statistics with the marginal PDFs estimated using the stochastic representation defined by Eq. (3.11). For the track stretch $\ell = 1$, the joint probability density function of the random variables $C_1^{\text{mod},1}$ and $C_2^{\text{mod},1}$ (the first two components of $\mathbf{C}^{\text{mod},1}$) is plotted in Figure 3.16. In this figure, the two points corresponding to the experimental value $c_{1,2}^{\text{exp},1} = (c_1^{\text{exp},1}, c_2^{\text{exp},1})$ and to the simulated value $c_{1,2}^{\text{sim},1} = (c_1^{\text{sim},1}, c_2^{\text{sim},1})$ are displayed. This figure shows that the random indicators vector $\mathbf{C}^{\text{mod},1}$ (that takes into account the train dynamics modeling errors for a given track geometry) yields a better modeling of the experimental dynamic response of the train than $\mathbf{c}^{\text{sim},1}$.

3.6 Conclusion

In this chapter, the dynamic response of the train has been numerically simulated on a measured track for the French TGV Duplex. The simulation results have been compared with experimental measurements of the dynamic response of the train, which allows for

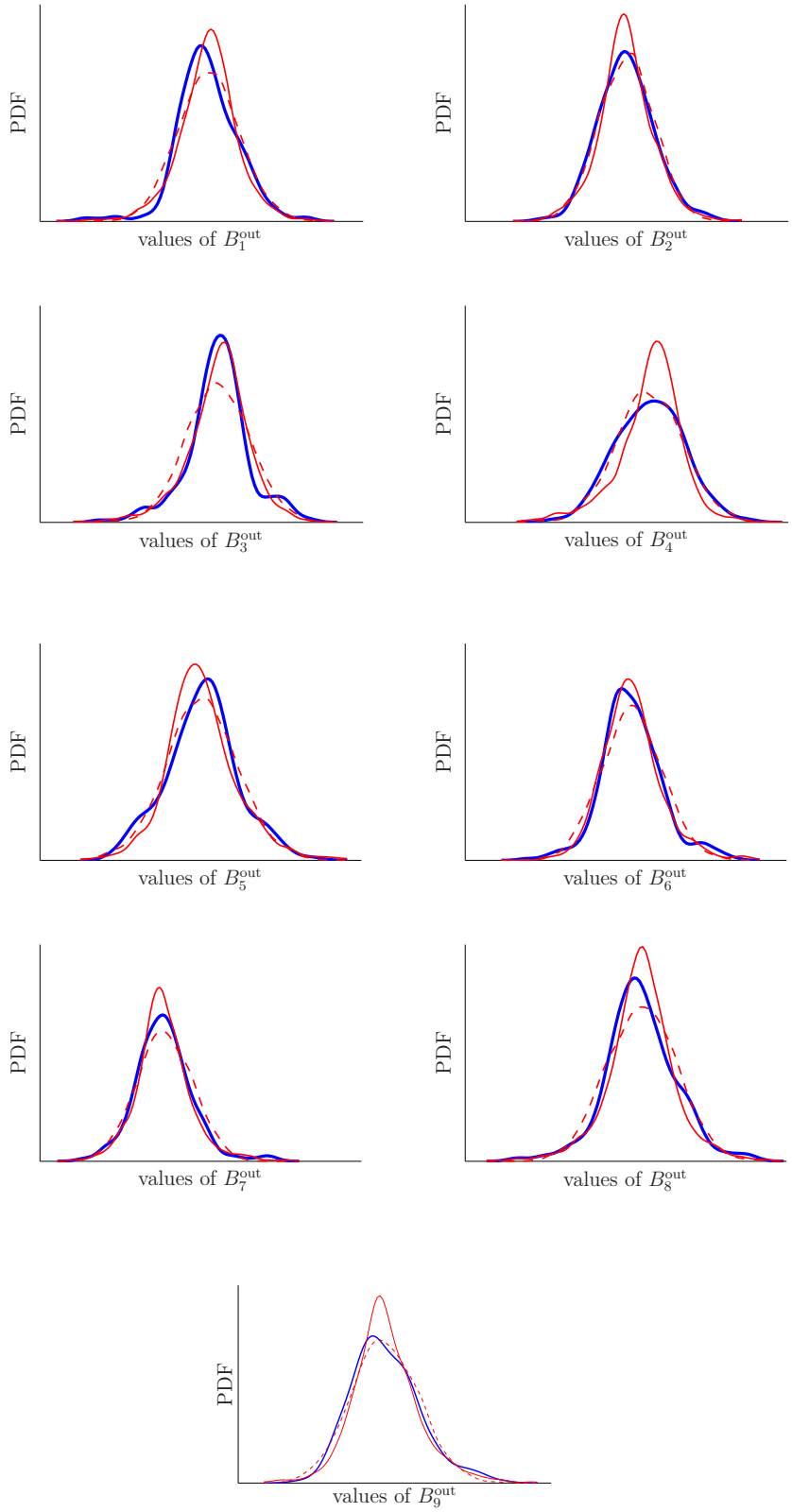

Figure 3.14: Comparison of the marginal PDFs in linear scale of the components of $\mathbf{B}^{\text{out}}$: experimental realizations $\mathbf{b}^{\text{exp}}$ (bold blue line), modeled $\mathbf{B}^{\text{out}}$ (solid red line), and Gaussian distributions (dashed red line).

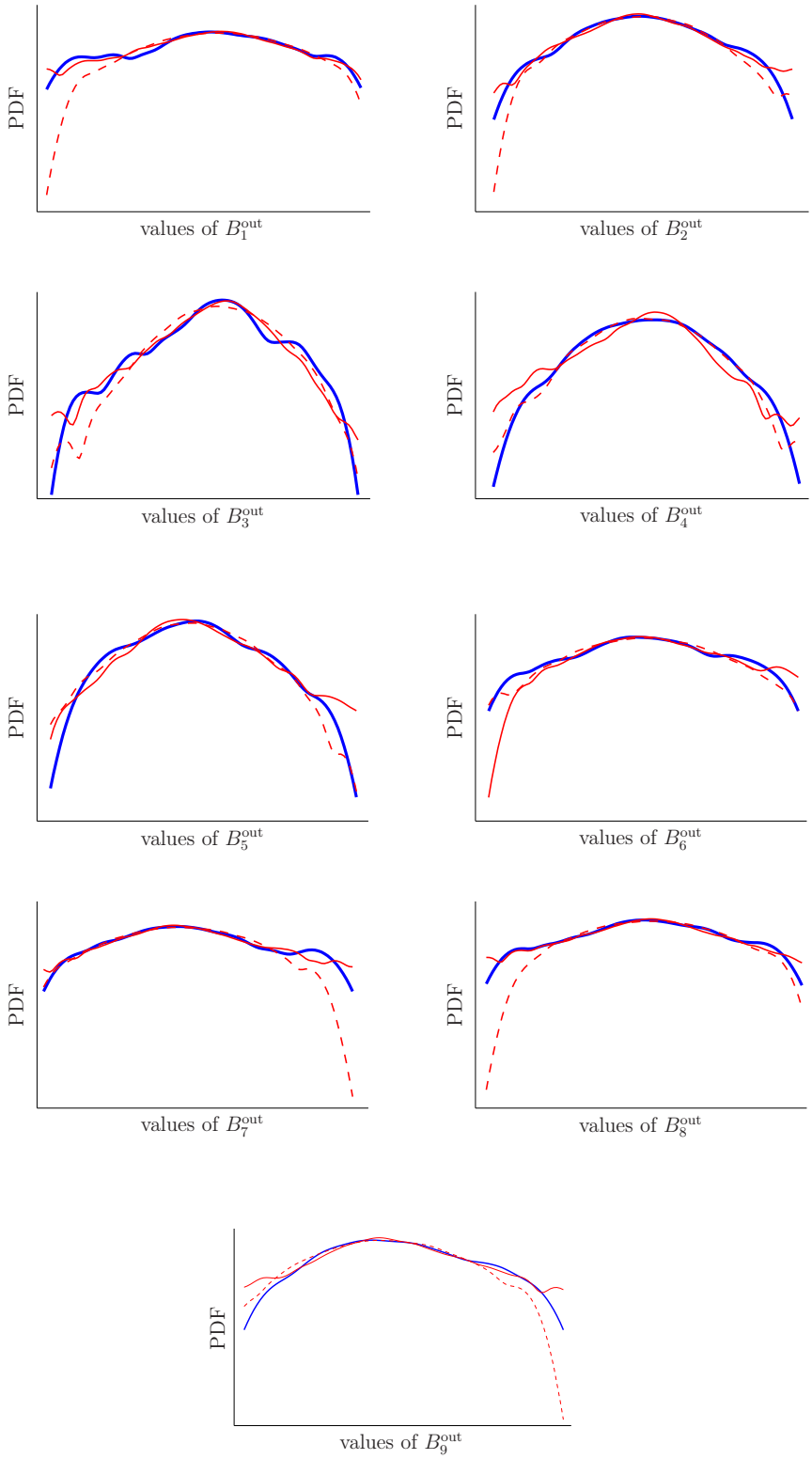

Figure 3.15: Comparison of the marginal PDFs in log scale of the components of $\mathbf{B}^{\text{out}}$: experimental realizations $\mathbf{b}^{\text{exp}}$ (bold blue line), modeled $\mathbf{B}^{\text{out}}$ (solid red line), and Gaussian distributions (dashed red line).

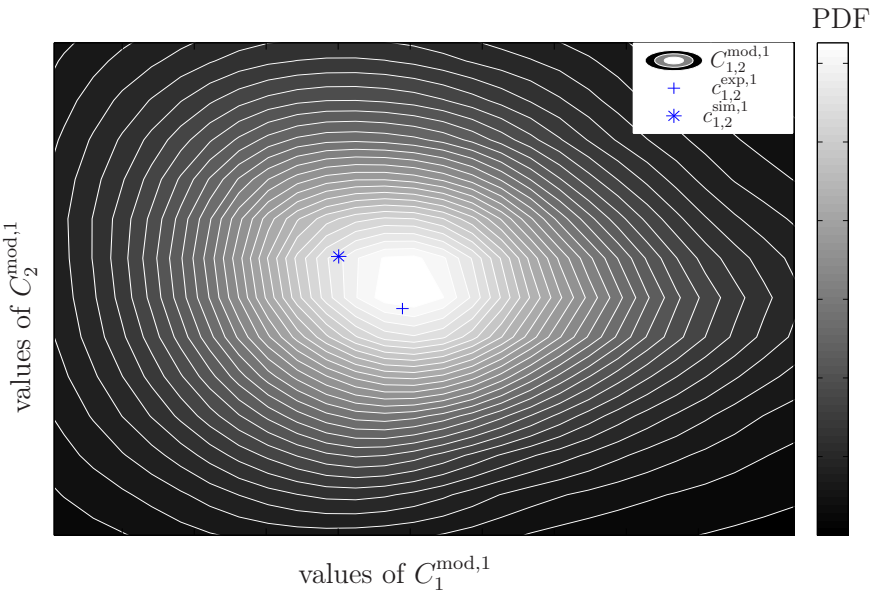

Figure 3.16: Position of the two points $c_{1,2}^{\mathrm{exp},1}$ and $c_{1,2}^{\mathrm{sim},1}$ into the 2D graph of the joint probability density function of random variables $C_1^{\mathrm{mod},1}$ and $C_2^{\mathrm{mod},1}$.

updating the computational model of the train and for validating the numerical results. A vector-valued random indicator has been defined in order to assess the dynamic response of the train on a given stretch of the track. The components of this indicator have been chosen according to the expertise and are constructed by post-processing the dynamic response of the train on the given track stretch. In order to take into account the model uncertainties of the computational model of the train dynamics, a multiplicative output noise has been introduced in the construction of the indicator. This output noise is a non-Gaussian random vector which has been identified by solving an inverse statistical problem using experimental realizations of the vector-valued indicator. Taking into account the model uncertainties increases the robustness of the indicator, and expands the possible running conditions which are taken into account in the simulation of the train dynamics.

Chapter 4

Modeling the long-time evolution of the train dynamic response

4.1 Introduction

In the previous chapter, a vector-valued random indicator has been introduced in order to characterize the dynamic response of the train on a given stretch of the railway track. The long-term evolution of this indicator allows for describing the long-term evolution of the dynamic response of the train on the given track stretch, giving information about the long-term evolution of the track irregularities. The track maintenance operations can then be started off using the observation of the vector-valued random indicator. In order to be able to plan in advance the track maintenance operations, we are interested in the prediction of the long-term evolution of the vector-valued random indicator. Several approaches have been proposed in [42, 30, 32, 36, 38] for predicting the long-term evolution of a given stretch of the track. But the proposed models were restrained to criteria on the track irregularities and took into account nor the dependence between the track irregularities neither the dynamic response of the train. The case described in this work focuses on the non-Gaussian 9-dimensional vector-valued random indicator, which characterizes the dynamic response of the train. Moreover the long-term evolution of the proposed indicator is nonstationary. The vector-valued random indicator is thus considered as a non-Gaussian and nonstationary time series whose long-term evolution has to be characterized.

Consequently, the goal of this chapter is to build and to identify a stochastic predictive model of long-term evolution of the vector-valued random indicator. The identification is performed using the known values of the random indicator that are generated at discrete long time $\{\tau_1, \tau_2, \ldots, \tau_K\}$. Their generation is performed by the numerical simulation of the dynamic response of the train using the stochastic computational model presented in the previous chapters for a given stretch of the track corresponding to a given curvature class. Such a stochastic predictive model must be able to predict the statistics of the vector-valued random indicator at following long time τ_{K+1}, providing information to start off the maintenance operation. The methodology proposed is presented in Section 4.2. Section 4.3 explains the construction of the stochastic predictive model, whose

parameters are identified in Section 4.4. Section 4.5 is devoted to the statistical prediction of the random indicator at long time τ_{K+1}.

4.2 Strategy of the methodology proposed

We present hereinafter a stochastic predictive model of the vector-valued random indicator to long-term evolution of track irregularities. For such a prediction, the following hypotheses are used:

- The prediction is performed for a given track stretch of length S, as defined in Section 2.3.3.
- Measurements of the track geometry of this stretch are carried out at discrete long time $\{\tau_1, \tau_2, \ldots, \tau_K\}$.
- The stochastic computational model of the high-speed train dynamics is used for estimating the statistics of random quantities of interest that are the vector-valued indicator represented by a $\mathbb{R}^{N_c}$-valued time series $\mathbf{C}^{\mathrm{mod}}(\tau_1), \ldots, \mathbf{C}^{\mathrm{mod}}(\tau_K)$. For the proposed construction of the stochastic computational model, the main steps are explained in Chapters 2 and 3 and are summarized hereinafter:
  - A local stochastic modeling of the track irregularities for the given track stretch is constructed using the experimental measurements of the track geometry (Chapter 2) and a global stochastic model of the track irregularities representative of the whole line.
  - A stochastic modeling of model uncertainties in the computational model of the train dynamics is constructed using simultaneously experimental measurements of the track geometry and experimental measurements of the train dynamics (Chapter 3).
- Using the statistics of the vector-valued random indicator $\mathbf{C}^{\mathrm{mod}}(\tau_1)$, ..., $\mathbf{C}^{\mathrm{mod}}(\tau_K)$, which have been calculated for long times $\tau_1, \ldots, \tau_K$, a stochastic predictive model of the vector-valued indicator to long-term evolution of track irregularities is constructed and then identified. The vector-valued random indicator that is predicted by the stochastic predictive model is represented by the $\mathbb{R}^{N_c}$-valued time series $\mathbf{C}^k$ (or by $\mathbf{C}(\tau_k)$). If the stochastic predictive model were perfect (no error), we would have $\mathbf{C}(\tau_k) = \mathbf{C}^{\mathrm{mod}}(\tau_k)$ for $k = 1, \ldots, K$ (which is not the case).
- Using the stochastic predictive model identified with $\mathbf{C}^{\mathrm{mod}}(\tau_1), \ldots, \mathbf{C}^{\mathrm{mod}}(\tau_K)$, the statistics of the vector-valued random indicator $\mathbf{C}^{K+1}$ are calculated for discrete long time τ_{K+1}. Such a prediction is obtained using the identified stochastic predictive model starting at initial condition $\mathbf{C}^K = \mathbf{C}^{\mathrm{mod}}(\tau_K)$.
  - The probability distribution of the vector-valued random indicator $\mathbf{C}^{K+1}$ is estimated.
  - An estimation of the error induced by the stochastic predictive model is given.

The construction and the identification of the stochastic predictive model of the vector-valued random indicator are relatively difficult for the following reasons:

- The long-term evolution is strongly nonstationary (and consequently statistics cannot be enriched by using time averaging estimators).
- The nonstationarity of the problem implies that only one experimental realization of the track irregularities of the given track stretch is available at each discrete time τ_k, which induces that the amount of experimental data is very limited.
- The number of discrete long times K used for predicting the statistics of the vector-valued random indicator at discrete long time τ_{K+1} is very low (typically K is of order 10).
- The vector-valued random indicator is a non-Gaussian random vector, in particular the initial value $\mathbf{C}^{\mathrm{mod}}(\tau_1)$ is non-Gaussian, which means that the time series $\mathbf{C}^{\mathrm{mod}}(\tau_1), \ldots, \mathbf{C}^{\mathrm{mod}}(\tau_K)$ is non-Gaussian.

Two steps are required for predicting the statistics of thevector-valued random indicator at long time. The first one is related to the choice and the construction of a stochastic predictive model, and the second one consists in identifying it by solving a statistical inverse problem.

4.3 Stochastic modeling of the long-term evolution for the vector-valued random indicator

4.3.1 Representing the random indicator by a time series

Since it is a discrete time stochastic process with values in $(\mathbb{R}^+)^{N_c}$, the sequence of vector-valued random indicators $\{\mathbf{C}(\tau_k), k \in \mathbb{N}^*\}$ is a time series. Time series have extensively been treated in the literature (see for instance [79, 80, 81, 82, 83, 84, 85]) and are used in many applications, such as astronomy [86], wheather forecast [87], biology [88], economy [89], and more generally in all the engineering sciences. In the following, the vector-valued random indicator will also be denoted by $\{\mathbf{C}^k,\, k \geq 1\}$.

The time series $\{\mathbf{C}^k,\, k \geq 1\}$ is non-Gaussian and nonstationary, with a non-Gaussian initial value $\mathbf{C}^1 = \mathbf{C}^{\mathrm{mod}}(\tau_1)$. For $k \geq 1$, the relationship between $\mathbf{C}^k$ and $\mathbf{C}^{k+1}$ is, *a priori*, nonlinear because of the nonlinear train-track coupling. Consequently the identification of a discrete time-evolution stochastic model for the time series $\mathbf{C}(\tau_1)$, ..., $\mathbf{C}(\tau_K)$ requires to solve a nonstationary statistical inverse problem using the time series $\mathbf{C}^{\mathrm{mod}}(\tau_1), \ldots, \mathbf{C}^{\mathrm{mod}}(\tau_K)$. Several methods have been tested for constructing and identifying the nonstationary stochastic predictive model. Below, we will present several approaches based on Bayesian filtering [90, 91] of Markov chain models.

- In Section 4.3.2, we consider the discrete time-evolution stochastic model as a non-homogeneous (nonstationary) Markov chain, whose transition probability has to

be identified. The method would consist in a direct identification of the transition probabilities family. Due to the nonstationarity properties and due to data limitation (small value of K), such an approach is not efficient and will not be used.

- In Section 4.3.3, we shortly summarize fundamental elements useful for constructing discrete time-evolution stochastic models, which can be viewed as an introduction of the proposed method that will be presented in Section 4.3.4.

4.3.2 Direct estimation of a transition probabilities family of a nonstationary one-order Markov chain

Since the long-term evolution of the track irregularities depends on the track history, it could be assumed that the vector-valued random indicator $\{\mathbf{C}^k, k \geq 1\}$ has the Markov property, as long as the train traffic remains the same. Such a hypothesis is supported by the fact that the track history contains the information allowing the prediction of the track irregularities. The proposed model does not directly take into account the number of running trains either infrastructure data, although they have an influence on the long-term evolution of the track irregularities.

Let $\mathcal{B}$ be the state space on which the Markov chain $\{\mathbf{C}^k, k \geq 1\}$ is defined. State space $\mathcal{B}$ is supposed to be finished, countable, and composed of n states $B_1, \ldots, B_n$ such that $\mathcal{B} = \bigcup_{i=1}^{n} B_i$ and $\bigcap_{i=1}^{n} B_i = \emptyset$. For $k \geq 1$, B and B' in $\mathcal{B}$, let $\mathsf{P}(k, B; k+1, B') = P\{\mathbf{C}^{k+1} \in B' \,|\, \mathbf{C}^k \in B\}$ be the conditionnal probability of the event $\{\mathbf{C}^{k+1} \in B'\}$ given $\mathbf{C}^k \in B$. For any finite $k \geq 2$, any collection of times $1, 2, \ldots, k-1, k, k+1$ and for all $B_1, \ldots, B_{k-1}, B, B'$ in $\mathcal{B}$, the Markov property for the random indicator can be written as

$$\begin{aligned} P\{\mathbf{C}^{k+1} \in B' \,|\, \mathbf{C}^1 \in B_1, \ldots, \mathbf{C}^{k-1} \in B_{k-1}, \mathbf{C}^k \in B\} &= P\{\mathbf{C}^{k+1} \in B' \,|\, \mathbf{C}^k \in B\} \\ &= \mathsf{P}(k, B; k+1, B')\,. \end{aligned} \tag{4.1}$$

Since the Markov chain is assumed to be nonstationary, the conditional probability depends on k. Then, for all $1 \leq k < k'' < k'$, for all B and B' in $\mathcal{B}$, the conditional probability $B' \mapsto \mathsf{P}(k, B; k', B)$ verifies the Chapman-Kolmogorov equation,

$$\mathsf{P}(k, B; k', B') = \sum_{i=1}^{n} \mathsf{P}(k, B; k'', B_i)\, \mathsf{P}(k'', B_i; k', B')\,. \tag{4.2}$$

For all $k \geq 1$, $B' \mapsto \mathsf{P}(k, B; k+1, B')$ is a system of transition probabilities from state B to state B'. Thus, the probability that $\mathbf{C}^{k+1}$ is in state B' at time $k+1$ is

$$P(\mathbf{C}^{k+1} \in B') = \sum_{i=1}^{n} \mathsf{P}(k, B_i; k+1, B')\, P(\mathbf{C}^k \in B_i)\,. \tag{4.3}$$

Hence, for all $k \geq 1$, the knowledge of the $\mathbb{M}_n(\mathbb{R})$-valued transition matrix $[\mathsf{P}(k, k+1)]$ defined by $[\mathsf{P}(k, k+1)]_{ij} = [\mathsf{P}(k, B_i; k+1, B_j)]$, with i and j in $\{1, \ldots, n\}$, determines the complete Markov chain with $\sum_{j=1}^{n} [\mathsf{P}(k, k+1)]_{ij} = 1$. Markov chain $\{\mathbf{C}^k, k \geq 1\}$ being nonstationary, its transition matrix depends on k. Moreover, since Markov chain

$\{\mathbf{C}^k, k \geq 1\}$ is known only by its realizations $\mathbf{C}^{\mathrm{mod}}(\tau_1), \ldots, \mathbf{C}^{\mathrm{mod}}(\tau_K)$, its transition matrix can only be estimated. The construction of the estimator $[\widehat{\mathsf{P}}(k, k+1)]$ of the transition matrix $[\mathsf{P}(k, k+1)]$ is performed as follows.

For $i \neq j$, let $M_{ij}(k, k+1)$ represent the number of B_i to B_j transitions from time k to $k+1$ for N independent realizations of the Markov chains $\{\mathbf{C}^k, k \geq 1\}$. Let $N_i(k)$ represent the number of observed chains in state B_i at time k. Finally, $R_i(k)$ denotes $1/N_i(k)$ if $N_i(k) > 0$, and 0 otherwise. For $k \geq 1$, the classical estimator $[\widehat{\mathsf{P}}(k, k+1)]_{ij}$ is given by

$$\begin{aligned} [\widehat{\mathsf{P}}(k, k+1)]_{ij} &= M_{ij}(k, k+1) R_i(k) \quad \text{if} \quad i \neq j \,, \\ [\widehat{\mathsf{P}}(k, k+1)]_{ii} &= 1 - \sum_{j \neq i} M_{ij}(k, k+1) R_i(k) \,. \end{aligned} \tag{4.4}$$

Fleming *et al.* have proven [92] that this estimator is the maximum-likelihood estimator for nonstationary Markov chains. Unfortunately, in our case, the identification of the coefficients of the transition matrix is limited by the lack of data. This would not be the case if the system were stationary. Therefore, the transition matrices are not used to model the long-term evolution of the vector-valued random indicator. In order to bypass this problem, we chose to linearize the long-term evolution of the vector-valued random indicator and to use linear filtering for the prediction (see below).

4.3.3 Summarizing fundamental elements useful for constructing discrete time-evolution stochastic models

In order to prepare the construction of the stochastic predictive model, which will be presented in Section 4.3.4, we briefly present below some fundamental elements concerning linear filtering.

ARMA models for time series

ARMA models with time-independent coefficients were first introduced by Whittle [79, 93] and popularized by Box and Jenkins [80], Priestley [82], and Hamilton [94]. Such ARMA models allow for describing a Gaussian stationary centered time series as a linear filtering of a discrete Gaussian white noise. Modeling a centered time series $\{\mathbf{C}^k, k \in \mathbb{Z}\}$ by an ARMA process of order (p, q) (with $p \in \mathbb{N}^*$ and $q \in \mathbb{N}^*$) means that $\{\mathbf{C}^k, k \in \mathbb{Z}\}$ is represented as the stationary solution of the stochastic recurrence equation:

$$\mathbf{C}^k + [A_1]\mathbf{C}^{k-1} + \ldots + [A_p]\mathbf{C}^{k-p} = \varepsilon(k) + [B_1]\varepsilon(k-1) + \ldots + [B_q]\varepsilon(k-q) \quad , \quad k \in \mathbb{Z} \,, \tag{4.5}$$

in which the time series $\{\varepsilon(k), k \in \mathbb{Z}\}$ is a discrete Gaussian white noise, and the $(N_c \times N_c)$ real matrices $[A_0], [A_1], \ldots, [A_p]$ and $[B_0], [B_1], \ldots, [B_q]$, with $[A_0] = [B_0] = [I_{N_c}]$ (the identity matrix), are such that all the zeros of $\det\{\sum_{k=0}^{p} [A_k] Z^{-k}\} = 0$ and of $\det\{\sum_{k=0}^{q} [B_k] Z^{-k}\} = 0$, with $|Z| > 0$, are located inside the unit circle centered at the origin of the complex Z plane. The identification of the model parameters $[A_1], \ldots, [A_p]$ and $[B_1], \ldots, [B_q]$ is performed with the Yule-Walker equations, which are obtained by

multiplying the two sides of Eq. (4.5) by $(\mathbf{C}^{k-m})^T$, for all m in $\{1,\ldots,k-1\}$, and by taking the mathematical expectation, which yields to

$$E\{\mathbf{C}^k(\mathbf{C}^{k-m})^T\} + [A_1]E\{\mathbf{C}^{k-1}(\mathbf{C}^{k-m})^T\} + \ldots + [A_p]E\{\mathbf{C}^{k-p}(\mathbf{C}^{k-m})^T\} \\ = E\{\varepsilon(k)(\mathbf{C}^{k-m})^T\} + [B_1]E\{\varepsilon(k-1)(\mathbf{C}^{k-m})^T\} + \ldots + [B_q]E\{\varepsilon(k-q)(\mathbf{C}^{k-m})^T\}\,. \tag{4.6}$$

Since $\varepsilon(k)$ is centered and independent of $\mathbf{C}^{k-1},\ldots,\mathbf{C}^{k-m}$, Eq. (4.6) yields

$$E\{\mathbf{C}^k(\mathbf{C}^{k-m})^T\} + [A_1]E\{\mathbf{C}^{k-1}(\mathbf{C}^{k-m})^T\} + \ldots + [A_p]E\{\mathbf{C}^{k-p}(\mathbf{C}^{k-m})^T\} = [0]\,. \tag{4.7}$$

For all $k \in \mathbb{Z}$ and $m < k$, the quantities $E\{\mathbf{C}^k(\mathbf{C}^{k-m})^T\},\ldots,E\{\mathbf{C}^{k-p}(\mathbf{C}^{k-m})^T\}$ can be estimated using the classical statistical estimators.

Such a stationary ARMA model cannot be used in the present case, because the vector-valued random indicator is nonstationary. Instead, a nonstationary ARMA model for $k \geq 1$ could be used, for which the matrices $[A_1],\ldots,[A_p]$ and $[B_1]$, ..., $[B_q]$ would depend on discrete time k, and with a given random initial condition $\mathbf{C}^1$ (for the ARMA modeling of nonstationary stochastic processes, one can refer to [83, 95, 96]). If we would consider such a nonstationary ARMA model with a minimum of parameters, we would choose $p = q = 1$, and consequently we would have to identify the sequence of matrices $[A_1]$ and $[B_1]$, which depend on discrete time k. As we have explained, due to the lack of experimental data, such an identification could not be performed. Consequently, this type of nonstationary ARMA models cannot be used.

Kalman filters

Another popular representation in linear filtering is the Kalman filter [97, 98, 99] (which can be viewed as a non-centered and nonstationary ARMA model) which, for the time series $\{\mathbf{C}^k, k \geq 1\}$, can be written as

$$\mathbf{C}^{k+1} = [A_k]\mathbf{C}^k + [B_k]\mathbf{u}_k + [G_k]\mathbf{w}_k \quad , \quad k \geq 1\,, \tag{4.8}$$

for which the initial condition $\mathbf{C}^1$ is a given random vector, where $\{\mathbf{u}_k, k \geq 1\}$ is a given deterministic sequence in $\mathbb{R}^{N_c}$ (which yields a non-centered time series $\{\mathbf{C}^k, k \geq 1\}$), and where $\{\mathbf{w}_k, k \geq 1\}$ is a Gaussian $\mathbb{R}^{N_c}$-valued white noise. The $(N_c \times N_c)$ real matrices $[A_k]$, $[B_k]$, and $[G_k]$ depend on discrete time k. In our case, $\mathbf{u}_k$, $[A_k]$, $[B_k]$, and $[G_k]$ can be viewed as parameters, which have to be identified from realizations of $\{\mathbf{C}^k, k \geq 1\}$. Moreover the vector-valued indicator is non-Gaussian. In such a case, an extended Kalman filter [90, 100, 101] should be used for reproducing the non-Gausian property of the vector-valued random indicator. Again, the nonstationary and non-Gaussian properties of the vector-valued indicator do not allow for using a general Kalman or extended Kalman filters due to the lack of data. Nevertheless, the representation of the vector-valued indicator presented in Section 4.3.4 will be a Kalman-filter type model.

Stochastic differential equation

The most general representation of a nonstationary and non-Gaussian vector-valued stochastic process indexed by an interval of $\mathbb{R}$, is given by nonlinear Itô stochastic differential equations (ARMA models and Kalman filters correspond to discrete version of particular cases of such a general representation). In this section, we briefly summarize some elements for a particular Itô stochastic differential equation, from which is derived the predictive model proposed in Section 4.3.4.

We consider the $\mathbb{R}^{N_c}$-valued stochastic process $\{\mathbf{C}(\tau), \tau \geq \tau_1\}$ indexed by $[\tau_1, +\infty[\subset \mathbb{R}$, with $\tau_1 \geq 0$, which is the solution of the Itô stochastic differential equation (see [102, 103, 104, 105]),

$$d\mathbf{C}(\tau) + [A]\mathbf{C}(\tau)d\tau = \mathbf{g}(\tau)d\tau + [h(\tau)]d\mathbf{W}(\tau) \quad , \quad \tau \geq \tau_1 \,, \tag{4.9}$$

with the given non-Gaussian initial condition

$$\mathbf{C}(\tau_1) = \mathbf{C}^{\mathrm{mod}}(\tau_1) \quad a.s \,, \tag{4.10}$$

in which $\tau \mapsto \mathbf{g}(\tau)$ is a given function defined on $[\tau_1, +\infty[$ with values in $\mathbb{R}^{N_c}$, $\tau \mapsto [h(\tau)]$ is a given function defined on $[\tau_1, +\infty[$ with values in $\mathbb{M}_{N_c}(\mathbb{R})$, where $[A]$ is a given $(N_c \times N_c)$ real matrix independent of time, and where $\mathbf{W}(\tau)$ is the $\mathbb{R}^{N_c}$-valued Wiener process on $\mathbb{R}^+$, such that

- $\mathbf{W}$ is a stochastic process with independent increments,
- $\mathbf{W}(0) = \mathbf{0}$ almost surely,
- for all $0 \leq s < t < +\infty$, increment $\Delta\mathbf{W}_{st} = \mathbf{W}(t) - \mathbf{W}(s)$ is a second-order $\mathbb{R}^{N_c}$-valued random variable which is Gaussian, centered and with a covariance matrix $[C_{st}]$ in $\mathbb{M}_{N_c}(\mathbb{R})$ such that

$$[C_{st}] = E\{\Delta\mathbf{W}_{st}\Delta\mathbf{W}_{st}^T\} = (t-s)[I_{N_c}] \,. \tag{4.11}$$

We assume that functions $\mathbf{g}$, $[h]$ and matrix $[A]$ are such that the problem defined by Eqs. (4.9) and (4.10) has a unique solution which is a non-Gaussian, nonstationary, second-order, non-centered, Markov, diffusion stochastic process.

The algebraic form of Eq. (4.9) highlights the role played by functions $\mathbf{g}$ and $[h]$ with respect to the long-term evolution of stochastic process $\{\mathbf{C}(\tau), \tau \geq \tau_1\}$:

- function $\mathbf{g}$ aims at controlling the mean value of $\{\mathbf{C}(\tau), \tau \geq \tau_1\}$ and at contributing to model the nonstationary property,
- function $[h]$ aims at controlling the tensor-valued correlation function of $\{\mathbf{C}(\tau), \tau \geq \tau_1\}$.

4.3.4 Constructing the stochastic predictive model as a Kalman-filter type model

Since long time τ takes only discrete values $\tau_1, \ldots, \tau_K$, the proposed stochastic predictive model is constructed in discretizing the problem defined by Eqs. (4.9) and (4.10), which yields

$$\mathbf{C}^k - \mathbf{C}^{k-1} + \Delta\tau_k \, [A] \, \mathbf{C}^{k-1} = \Delta\tau_k \, \mathbf{g}^k + [h^k] \, \Delta\mathbf{W}^k \quad , \quad k = 2, \ldots, K \, , \tag{4.12}$$

with the given non-Gaussian initial condition

$$\mathbf{C}^1 = \mathbf{C}^{\mathrm{mod}}(\tau_1) \, , \tag{4.13}$$

in which

- $[A]$ is a matrix in $\mathbb{M}_{N_c}(\mathbb{R})$, which has to be identified.
- $\Delta\tau_k = \tau_k - \tau_{k-1}$ are given time steps that depend on k.
- $\Delta\mathbf{W}^k = \sqrt{\Delta\tau_k}\,\boldsymbol{\mathcal{N}}^k$, in which $\boldsymbol{\mathcal{N}}^2, \ldots, \boldsymbol{\mathcal{N}}^K$ are independent Gaussian normalized random vectors defined on a new probability space $(\Theta^*, \mathcal{F}^*, \mathcal{P}^*)$, with values in $\mathbb{R}^{N_c}$ ($E\{\boldsymbol{\mathcal{N}}^k\} = 0$, $E\{\boldsymbol{\mathcal{N}}^k \, (\boldsymbol{\mathcal{N}}^k)^T\} = [I_{N_c}]$). Therefore, $E\{\Delta\mathbf{W}^k \otimes \Delta\mathbf{W}^k\} = \Delta\tau_k \, [I_{N_c}]$. The family of random vectors $\{\boldsymbol{\mathcal{N}}^k, k \geq 2\}$ is statistically independent of random vectors $\mathbf{G} = (\mathbf{G}^1, \mathbf{G}^2, \mathbf{G}^3, \mathbf{G}^4)$ defined in Section 2.5.1 and $\mathbf{B}^{\mathrm{out}}$ defined in Section 3.5, and consequently, is independent of $\mathbf{C}^{\mathrm{mod}}(\tau_1)$.
- $\{\mathbf{g}\} = \{\mathbf{g}^2, \ldots, \mathbf{g}^K\}$ is a family of $K-1$ vectors in $\mathbb{R}^{N_c}$, which has to be identified.
- $\{[h]\} = \{[h^2], \ldots, [h^K]\}$ is a family of $(K-1)$ real matrices in $\mathbb{M}_{N_c}(\mathbb{R})$, which has to be identified. For all k, since $[h^k]$ controls the diffusion term of $\mathbf{C}^k$, $[h^k]$ is chosen with positive diagonal entries.
- in the initial condition, $\mathbf{C}^{\mathrm{mod}}(\tau_1)$ is a non-Gaussian second-order $\mathbb{R}^{N_c}$-valued random variable whose probability distribution is known (estimated using the stochastic computational model of the high-speed train dynamics described in Chapters 2 and 3).

Eq. (4.12) can be rewritten as

$$\mathbf{C}^k = ([I_{N_c}] - \Delta\tau_k \, [A])\mathbf{C}^{k-1} + \Delta\tau_k \, \mathbf{g}^k + [h^k] \, \Delta\mathbf{W}^k \quad , \quad k = 2, \ldots, K \, . \tag{4.14}$$

It can be noticed that the model proposed for the prediction of $\mathbf{C}_k$, $k = 1, \ldots, K$ is a Kalman-filter type model, and that the non-Gaussian character of the stochastic process $\mathbf{C}_k$, $k = 1, \ldots, K$, is induced by the non-Gaussian initial condition $\mathbf{C}^{\mathrm{mod}}(\tau_1)$. In this model:

- The nonstationary property is induced by the coefficients $\mathbf{g}^k$ and $[h^k]$, which depend on discrete time τ_k, represented by index k.
- The matrix $[A]$ does not depend on discrete time k. It should be noted that, if matrix $[A]$ had been chosen as a function of k, the time series $[A^k]$, $\mathbf{g}^k$, and $[h^k]$ could not be identified by the lack of data.

- The matrix $[A]$ could be considered as a random matrix, whose distribution could be identified by Bayesian inference. Nevertheless, if matrix $[A]$ were random, $[A]$, $\mathbf{g}^k$, and $[h^k]$ could not be identified by the lack of data.

- The convergence condition on the spectral radius of $[I_{N_c}] - \Delta\tau_k\,[A]$ is not necessary because of the nonbounded property of the time series $\{\mathbf{C}_k, k \geq 1\}$ (any trajectory of the time series can increase).

- If the initial condition $\mathbf{C}^1 = \mathbf{C}^{\text{mod}}(\tau_1)$ were a deterministic vector or a Gaussian random vector, then the nonstationary time series $\mathbf{C}(\tau_k)$ would be Gaussian. Nevertheless, since random vector $\mathbf{C}^{\text{mod}}(\tau_1)$ is not Gaussian, the time series $\mathbf{C}(\tau_k)$ generated by the predictive model above is a non-Gaussian time series.

In the proposed stochastic predictive model, the prediction of the vector-valued random indicator $\mathbf{C}$ at long time τ_{K+1} must not depend on the measurement time scale. For this reason the discrete long times $\tau_1, \ldots, \tau_{K+1}$ are transformed in dimensionless discrete long times (named as dimensionless long time τ) as follows. A reference time-increment denoted by $\Delta\tau_{\text{ref}}$ is introduced such as

$$\Delta\tau_{\text{ref}} = \Delta\tau_{K+1} = \tau_{K+1} - \tau_K\,, \tag{4.15}$$

and the dimensionless long times are written as $\tau_k/\Delta\tau_{\text{ref}}$ for $k = 1, \ldots, K+1$. In the following, long time τ will be supposed to be dimensionless in order to lighten the notations.

4.4 Identification of the parameters of the stochastic model for the long-term evolution

For the identification of the model parameters $[A]$, $\{\mathbf{g}\}$ and $\{[h]\}$ of the stochastic model defined by Eq. (4.14), the classical least-squares method with weights is used. In analogy with the construction of the Yule-Walker equations Eq. (4.7), the identification is performed using the first- and second-order moments equations associated with Eq. (4.14). Due to the large number of parameters, three moments equations are needed, for which the first-order vector moment $E\{\mathbf{C}^k\}$, $k = 2, \ldots, K$, the second-order tensor moment $E\{\mathbf{C}^k \otimes \mathbf{C}^k\}$, $k = 2, \ldots, K$, and the second-order cross-tensor moment $E\{\mathbf{C}^k \otimes \mathbf{C}^{k-\mu}\}$, $k = 2, \ldots, K$ and $\mu = 1, \ldots, k-1$, are estimated using the random indicators $\mathbf{C}^{\text{mod}}(\tau_1), \ldots, \mathbf{C}^{\text{mod}}(\tau_K)$ of the high-speed train dynamics constructed in Chapter 3, for which the joint probability distribution is known (estimated). The cost function for the least-squares method is then constructed using the first-order vector moment equation, the second-order tensor moment equation, and the second-order cross-tensor moment equations.

4.4.1 First-order vector moment equation with weights used for constructing the cost function

Taking the mathematical expectation of Eq. (4.14) yields the following $K-1$ first-order vector moment equations,

$$\mathbf{f}^k([A],\{\mathbf{g}\}) = \mathbf{0}_{N_c} \quad , \quad k = 2,\dots,K\,, \tag{4.16}$$

in which, for all k fixed in $\{2,\dots,K\}$, the $\mathbb{R}^{N_c}$-valued function $\mathbf{f}^k$ is defined by

$$\mathbf{f}^k([A],\{\mathbf{g}\}) = [\mathbb{N}_f^k]\left(E\{\mathbf{C}^k\} - ([I_{N_c}] - \Delta\tau_k[A])\,E\{\mathbf{C}^{k-1}\} - \Delta\tau_k\,\mathbf{g}^k\right)\,, \tag{4.17}$$

in which, for all i and j in $\{1,\dots,N_c\}$, the weights $[\mathbb{N}_f^k]_{ij}$ are introduced for normalization reasons inside the cost function. The cost function must not be influenced by the values taken by the components of $\mathbf{C}^k$, but by its more or less strong long-term evolution: we should be able to give a more important weight α_j to certain components C_j^k of the vector-valued indicator $\mathbf{C}^k$ in the cost function. A more important weight is given to the components which have the most significant long-term evolution and whose long-term evolution has therefore to be better modeled. The matrix $[\mathbb{N}_f^k]$ of these weights is thus defined by

$$[\mathbb{N}_f^k]_{ij} = \frac{\alpha_i}{E\{C_i^k\}}\delta_{ij}\,, \tag{4.18}$$

in which δ_{ij} is the Kronecker symbol, where $C_1^k,\dots,C_{N_c}^k$ are the components of the random vector $\mathbf{C}^k$, and where $\{\alpha_1,\dots,\alpha_{N_c}\}$ is the family of weight coefficients that have to be arbitrarily chosen and that belong to the admissible set $\mathcal{C}_1$ defined by

$$\mathcal{C}_1 = \{\,\alpha_1 \geq 0,\dots,\alpha_{N_c} \geq 0\;,\;\sum_{j=1}^{N_c}\alpha_j = 1\,\}\,. \tag{4.19}$$

4.4.2 Second-order tensor moment equation with weights used for constructing the cost function

For each $k = 2,\dots,K$, Eq. (4.14) is right-tensorized by $\mathbf{C}^k$ and the mathematical expectation is applied, which yields the following second-order tensor moment equation,

$$\begin{aligned} E\{\mathbf{C}^k\otimes\mathbf{C}^k\} = ([I_{N_c}] - \Delta\tau_k[A])\,E\left\{\mathbf{C}^{k-1}\otimes\mathbf{C}^k\right\} + \Delta\tau_k\,\mathbf{g}^k\otimes E\{\mathbf{C}^k\} \\ + [h^k]\,E\{\Delta\mathbf{W}^k\otimes\mathbf{C}^k\}\,. \end{aligned} \tag{4.20}$$

As $\Delta\mathbf{W}^k$ and $\mathbf{C}^{k-1}$ are statistically independent, and as $\Delta\mathbf{W}^k$ is centered, the term $E\{\Delta\mathbf{W}^k\otimes\mathbf{C}^k\}$ can be expressed as

$$\begin{aligned} E\{\Delta\mathbf{W}^k\otimes\mathbf{C}^k\} &= E\{\Delta\mathbf{W}^k\otimes((([I_{N_c}] - \Delta\tau_k\,[A])\mathbf{C}^{k-1} + \Delta\tau_k\,\mathbf{g}^k + [h^k]\,\Delta\mathbf{W}^k)\} \\ &= E\{\Delta\mathbf{W}^k\otimes\Delta\mathbf{W}^k\}\,[h^k]^T \\ &= [h^k]^T\Delta\tau_k\,. \end{aligned} \tag{4.21}$$

For all k in $\{2,\dots,K\}$, Eq. (4.20) can be rewritten as

$$E\{\mathbf{C}^k\otimes\mathbf{C}^k\} = ([I_{N_c}] - \Delta\tau_k[A])\,E\{\mathbf{C}^{k-1}\otimes\mathbf{C}^k\} + \Delta\tau_k\,\mathbf{g}^k\otimes E\{\mathbf{C}^k\} + [h^k]\,[h^k]^T\Delta\tau_k\,. \tag{4.22}$$

From Eq. (4.22), it can then be deduced that, for all k in $\{2,\dots,K\}$, the second-order tensor moment equation with weights is written as

$$[F^k([A],\{\mathbf{g}\},\{[h]\})] = [0_{N_c,N_c}]\,, \tag{4.23}$$

in which the function $[F^k]$ with values in $\mathbb{M}_{N_c}(\mathbb{R})$ is defined by

$$[F^k([A],\{\mathbf{g}\},\{[h]\})] = \mathbb{T}^k : \big(E\{\mathbf{C}^k\otimes\mathbf{C}^k\} - ([I_{N_c}]-\Delta\tau_k[A])\,E\{\mathbf{C}^{k-1}\otimes\mathbf{C}^k\} \\ -\Delta\tau_k\,\mathbf{g}^k\otimes E\{\mathbf{C}^k\} - [h^k]\,[h^k]^T\Delta\tau_k\big)\,, \tag{4.24}$$

in which the symbol " : " denotes the double contraction tensor operation. For all i,j,i',j' in $\{1,\dots,N_c\}$, the weights $\{\mathbb{T}^k\}_{iji'j'}$ are introduced for the same reasons as those given for Eq. (4.18). The fourth-order tensor $\mathbb{T}^k$ of these weights is thus defined by

$$\{\mathbb{T}^k\}_{iji'j'} = \frac{\sqrt{\alpha_i\alpha_j}}{E\{C_i^kC_j^k\}}\delta_{ii'}\delta_{jj'}\,, \tag{4.25}$$

in which $\{\alpha_1,\dots,\alpha_{N_c}\}$ are the weights defined in Section 4.4.1 and where $C_1^k,\dots,C_{N_c}^k$ are the components of the random vector $\mathbf{C}^k$.

4.4.3 Second-order cross-tensor moment equation with weights used for constructing the cost function

For each $k=2,\dots,K$ and for $\mu=1,\dots,k-1$, Eq. (4.14) is right-tensorized by $\mathbf{C}^{k-\mu}$ and taking the mathematical expectation yield

$$E\{\mathbf{C}^k\otimes\mathbf{C}^{k-\mu}\} = ([I_{N_c}]-\Delta\tau_k[A])\,E\{\mathbf{C}^{k-1}\otimes\mathbf{C}^{k-\mu}\} + \Delta\tau_k\,\mathbf{g}^k\otimes E\{\mathbf{C}^{k-\mu}\} \\ + [h^k]\,E\{\Delta\mathbf{W}^k\otimes\mathbf{C}^{k-\mu}\}\,. \tag{4.26}$$

As $\Delta\mathbf{W}^k$ and $\mathbf{C}^{k-\mu}$ are statistically independent for all k in $\{2,\dots,K\}$ and μ in $\{1,\dots,k-1\}$, and as $\Delta\mathbf{W}^k$ is centered, it can be deduced that

$$E\{\Delta\mathbf{W}^k\otimes\mathbf{C}^{k-\mu}\} = 0\,, \tag{4.27}$$

$$E\{\mathbf{C}^k\otimes\mathbf{C}^{k-\mu}\} = ([I_{N_c}]-\Delta\tau_k[A])\,E\{\mathbf{C}^{k-1}\otimes\mathbf{C}^{k-\mu}\} + \Delta\tau_k\,\mathbf{g}^k\otimes E\{\mathbf{C}^{k-\mu}\}\,. \tag{4.28}$$

From Eq. (4.28), it can then be deduced that, for all k in $\{2,\dots,K\}$ and for all μ in $\{1,\dots,k-1\}$, the second-order cross-tensor moment equation with weights can be written as

$$[H^{k,k-\mu}([A],\{\mathbf{g}\})] = [0_{N_c,N_c}]\,, \tag{4.29}$$

in which the function $[H^{k,k-\mu}]$ with values in $\mathbb{M}_{N_c}(\mathbb{R})$ is defined by

$$[H^{k,k-\mu}([A],\{\mathbf{g}\})] = \mathbb{T}^k : \big(E\{\mathbf{C}^k\otimes\mathbf{C}^{k-\mu}\} \\ -([I_{N_c}]-\Delta\tau_k[A])\,E\{\mathbf{C}^{k-1}\otimes\mathbf{C}^{k-\mu}\} - \Delta\tau_k\,\mathbf{g}^k\otimes E\{\mathbf{C}^{k-\mu}\}\big)\,, \tag{4.30}$$

in which the components of fourth-order tensor $\mathbb{T}^k$ are defined by Eq. (4.25).

4.4.4 Formulation of the least-squares optimization problem for the identification of the parameters

(i) *Definition of the admissible sets for the optimization problem.* In the framework of the long-term evolution of the track irregularities, one or several components of the vector-valued indicator are not bounded functions when k is increasing. Consequently, for any fixed value of K, it is not necessary to introduce a convergence condition on $\max_k \Delta\tau_k$ as a function of the spectral radius of $[A]$. Therefore, no constraints are introduced for matrix-valued parameter $[A]$ in the optimization problem, and the admissible set for $[A]$ is then defined by

$$\mathcal{C}_A = \{\, [A] \in \mathbb{M}_{N_c}(\mathbb{R}) \,\}\,. \tag{4.31}$$

For all k in $\{1, \ldots, K\}$, the discrete time-dependent diffusion matrix of the Markov chain defined by Eq. (4.14) is written as $[\sigma^k] = [h^k][h^k]^T$ and is a positive-definite matrix, taking into account the hypothesis on $[h^k]$ introduced in Section 4.3.4. The moment equations defined by Eqs. (4.16), (4.23) and (4.29) only give access to the symetric positive-definite matrix $[\sigma^k]$. Then, using the Cholesky decomposition (see [106]), identifying the positive-definite matrix $[h^k]$ in $\mathbb{M}_{N_c}(\mathbb{R})$ is equivalent to identifying the lower triangular positive-definite matrix $[h^k]$ in $\mathbb{M}_{N_c}(\mathbb{R})$. Consequently, the family $\{[h]\} = \{[h^k], k = 2, \ldots, K\}$ must belong to the following admissible set

$$\mathcal{C}_h = \{\, [h^k] \in \mathbb{M}^L_{N_c} \quad \text{for} \quad k = 2, \ldots, K \,\}\,, \tag{4.32}$$

in which $\mathbb{M}^L_{N_c}$ is the set of all the lower triangular $(N_c \times N_c)$ real matrices with positive diagonal entries. No constraints are needed for the family of $\mathbb{R}^{N_c}$-values vectors $\{\mathbf{g}\} = \{\mathbf{g}^k, k = 2, \ldots, K\}$. The admissible set for $\{\mathbf{g}\}$ is thus

$$\mathcal{C}_g = \{\, \mathbf{g}^k \in \mathbb{R}^{N_c} \quad \text{for} \quad k = 2, \ldots, K \,\}\,. \tag{4.33}$$

(ii) *Definition of the target quantities for the optimization problem.* The target quantities introduced in Eqs. (4.16), (4.23), and (4.29) are, for $k = 2, \ldots, K$, the vectors $E\{\mathbf{C}^k\}$ and $E\{\mathbf{C}^{k-1}\}$, and, for $\mu = 0, \ldots, k-1$, the tensors $E\{\mathbf{C}^k \otimes \mathbf{C}^{k-\mu}\}$ and $E\{\mathbf{C}^{k-1} \otimes \mathbf{C}^{k-\mu}\}$. For computing the cost function in the least-squares problem, these target quantities are approximated by $E\{\mathbf{C}^{\rm mod}(\tau_k)\}$, $E\{\mathbf{C}^{\rm mod}(\tau_{k-1})\}$, $E\{\mathbf{C}^{\rm mod}(\tau_k) \otimes \mathbf{C}^{\rm mod}(\tau_{k-\mu})\}$ and $E\{\mathbf{C}^{\rm mod}(\tau_{k-1}) \otimes \mathbf{C}^{\rm mod}(\tau_{k-\mu})\}$, that are estimated using the stochastic computational model of the high-speed train dynamics introduced in Chapter 3 such as

$$E\{\mathbf{C}^k\} = E\{\mathbf{C}^{\rm mod}(\tau_k)\}\,, \tag{4.34}$$

$$E\{\mathbf{C}^k \otimes \mathbf{C}^k\} = E\{\mathbf{C}^{\rm mod}(\tau_k) \otimes \mathbf{C}^{\rm mod}(\tau_k)\}\,, \tag{4.35}$$

$$E\{\mathbf{C}^k \otimes \mathbf{C}^{k-\mu}\} = E\{\mathbf{C}^{\rm mod}(\tau_k) \otimes \mathbf{C}^{\rm mod}(\tau_{k-\mu})\}\,. \tag{4.36}$$

(iii) *Formulation of the optimization problem for the identification of the parameters.* Using Eqs. (4.16), (4.23), and (4.29), the optimal values $[A^{\rm opt}]$, $\{\mathbf{g}^{\rm opt}\}$, and $\{[h^{\rm opt}]\}$ for parameters $[A]$, $\{\mathbf{g}\}$, and $\{[h]\}$ of the stochastic predictive model described by Eq. (4.14) are estimated using the least-squares method with constraints, for which the cost function is defined by

$$J([A],\{\mathbf{g}\},\{[h]\}) = \sum_{k=2}^{K}(\|\mathbf{f}^k([A],\{\mathbf{g}\})\|^2 + \|[F^k([A],\{\mathbf{g}\},\{[h]\})]\|_F^2 + \sum_{\mu=1}^{k-1}\|[H^{k,k-\mu}([A],\{\mathbf{g}\})]\|_F^2)\,, \quad (4.37)$$

in which $\|\cdot\|$ is the Euclidean norm in $\mathbb{R}^{N_c}$ and $\|\cdot\|_F$ is the Frobenius norm in $\mathbb{M}_{N_c}(\mathbb{R})$ (for all matrix M in $\mathbb{M}_{N_c}(\mathbb{R})$, the Frobenius norm is defined by $\|M\|_F^2 = \mathrm{Tr}(M\,M^T)$.) The optimal values $[A^{\mathrm{opt}}]$, $\{\mathbf{g}^{\mathrm{opt}}\}$, and $\{[h^{\mathrm{opt}}]\}$ are constructed as the solution of the following optimization problem.

$$\{[A^{\mathrm{opt}}],\{\mathbf{g}^{\mathrm{opt}}\},\{[h^{\mathrm{opt}}]\}\} = \arg\min_{[A]\in\mathcal{C}_A,\,\{\mathbf{g}\}\in\mathcal{C}_g,\,\{[h]\}\in\mathcal{C}_h} J([A],\{\mathbf{g}\},\{[h]\})\,. \quad (4.38)$$

This optimization problem is solved with the trust-region-reflective algorithm with constraints (see [107] for details on the trust-region-reflective algorithm), for which the initial values, denoted by $[A^0]$, $\{\mathbf{g}^0\}$, and $\{[h^0]\}$, are computed by solving the simplified optimization problem described in the next section.

For this optimization problem, the number of variables is $N_{\mathrm{var}} = N_c^2 + N_c(K-1) + (K-1)N_c(N_c+1)/2$ (and will be 675, in the application presented after). The number of scalar equations is $N_c(K-1)$ in Eq. (4.16), $N_c(N_c+1)(K-1)/2$ in Eq. (4.23), and $N_c^2K(K-1)/2$ in Eq. (4.29), which makes a total of $N_{\mathrm{eq}} = N_c(K-1) + N_c(N_c+1)(K-1)/2 + N_c^2K(K-1)/2$ scalar equations. The problem is well-posed for $N_{\mathrm{eq}} \geq N_{\mathrm{var}}$, which yields, for $N_c = 9$,

$$K \geq 2\,. \quad (4.39)$$

The problem is well posed for $K \geq 2$, as it will be the case for the application presented in Chapter 5, for which $K = 12$.

4.4.5 Simplified optimization problem for computing the initial values

The simplified formulation consists in using Eqs. (4.17), (4.24), and (4.30), in which the full matrix $[A]$ is replaced by a diagonal matrix with real diagonal entries $A_1,\ldots,A_{N_c}$, and for $k = 2,\ldots,K$, the lower triangular matrix $[h^k]$ is replaced by a diagonal matrix with positive diagonal entries $h_1^k,\ldots,h_{N_c}^k$. These hypotheses imply that the N_c stochastic equations in Eq. (4.14) are not coupled. For fixed j in $\{1,\ldots,N_c\}$ and k in $\{2,\ldots,K\}$, Eqs. (4.17), (4.24), and (4.30) become

$$f_j^k(A_j,\{g_j\}) = [\mathbb{N}_f^k]_{jj}\left(E\{C_j^k\} - (1-\Delta\tau_k A_j)E\{C_j^{k-1}\} - \Delta\tau_k\, g_j^k\right)\,, \quad (4.40)$$

$$F_j^k(A_j,\{g_j\},\{h_j\}) = \{\mathbb{T}^k\}_{jjjj}\left(E\{(C_j^k)^2\} - (1-\Delta\tau_k\,A_j)\,E\{C_j^{k-1}\,C_j^k\} - \Delta\tau_k\,g_j^k E\{C_j^k\} - (h_j^k)^2\Delta\tau_k\right)\,, \quad (4.41)$$

and, for $\mu = 1, \ldots, k-1$,

$$H_j^{k,k-\mu}(A_j, \{g_j\}) = \{\mathbb{T}^k\}_{jjjj} \Big(E\{C_j^k C_j^{k-\mu}\} - (1 - \Delta\tau_k\, A_j) E\{C_j^{k-1} C_j^{k-\mu}\} \\ - \Delta\tau_k\, g_j^k\, E\{C_j^{k-\mu}\} \Big) \,, \quad (4.42)$$

in which $[\mathbb{N}_f^k]$ and $\mathbb{T}^k$ are defined by Eqs. (4.18) and (4.25). Let $\mathcal{C}_{g_j}$ and $\mathcal{C}_{h_j}$ be the admissible sets for $\{g_j\}$ and $\{h_j\}$ defined by

$$\mathcal{C}_{g_j} = \{ g_j^k \in \mathbb{R} \quad , \quad \text{for} \quad k = 2, \ldots, K \} \,, \quad (4.43)$$

$$\mathcal{C}_{h_j} = \{ h_j^k > 0 \quad , \quad \text{for} \quad k = 2, \ldots, K \} \,. \quad (4.44)$$

For all j fixed in $\{1, \ldots, N_c\}$, the cost function J_j is introduced such that

$$J_j(A_j, \{g_j\}, \{h_j\}) = \sum_{k=2}^{K} (|f_j^k(A_j, \{g_j\})|^2 + |F_j^k(A_j, \{g_j\}, \{h_j\})|^2 \\ + \sum_{\mu=1}^{k-1} |H_j^{k,k-\mu}(A_j, \{g_j\})|^2) \,, \quad (4.45)$$

in which, for $k = 2, \ldots, K$ and for $\mu = 0, \ldots, k-1$, the quantities $E\{C_j^k\}$, $E\{C_j^{k-1}\}$, $E\{C_j^k C_j^{k-\mu}\}$, and $E\{C_j^{k-1} C_j^{k-\mu}\}$ are replaced by the corresponding quantities $E\{C_j^{\mathrm{mod}}(\tau_k)\}$, $E\{C_j^{\mathrm{mod}}(\tau_{k-1})\}$, $E\{C_j^{\mathrm{mod}}(\tau_k) C_j^{\mathrm{mod}}(\tau_{k-\mu})\}$ and $E\{C_j^{\mathrm{mod}}(\tau_{k-1}) C_j^{\mathrm{mod}}(\tau_{k-\mu})\}$. The optimal values A_j^0, $\{g_j^0\}$, and $\{h_j^0\}$ of parameters A_j, $\{g_j\}$, and $\{h_j\}$ are the solution of the following optimization problem,

$$\{A_j^0, \{g_j^0\}, \{h_j^0\}\} = \arg \min_{A_j \in \mathbb{R},\, \{g_j\} \in \mathcal{C}_{g_j},\, \{h_j\} \in \mathcal{C}_{h_j}} J_j(A_j, \{g_j\}, \{h_j\}) \,. \quad (4.46)$$

This optimization problem is solved using the gradients method with the trust-region-reflective algorithm with constraints, for which the initial values are $A_j^{\mathrm{ini}} = 0$, $g_j^{\mathrm{ini}} = 0$, and $h_j^{\mathrm{ini}} = 10^{-12}$. The solution $\{[A^0], \{\mathbf{g}^0\}, \{[h^0]\}\}$ of the simplified problem is used as initial value to solve the optimization problem defined by Eq. (4.38).

4.5 Prediction of the long-term evolution with the stochastic model

4.5.1 Methodology used for the prediction

For $k = 1, \ldots, K$, the unknowns $[A]$, $\mathbf{g}^k$, and $[h^k]$ introduced in Eq. (4.14) are identified in two steps. First, the simplified optimization problem defined by Eq. (4.46) is solved yielding the optimal values $\{[A^0], \{\mathbf{g}^0\}, \{[h^0]\}\}$. These optimal values are then used as initial values for the multidimensional optimization problem defined by Eq. (4.38), which yields the optimal values $\{[A^{\mathrm{opt}}], \{\mathbf{g}^{\mathrm{opt}}\}, \{[h^{\mathrm{opt}}]\}\}$ for $\{[A], \{\mathbf{g}\}, \{[h]\}\}$.

Once the stochastic predictive model is identified, this model aims at being used for predicting the statistics of the non-Gaussian random vector $\mathbf{C}^{K+1}$. However, the values of $\mathbf{g}^{K+1}$ and $[h^{K+1}]$ are unknown. We then propose to represent $\mathbf{g}^k$ and $[h^k]$ as the values $\mathbf{g}^{\rm aff}(\tau_k)$ and $[h^{\rm aff}(\tau_k)]$ at τ_k of affine functions $\mathbf{g}^{\rm aff}$ and $[h^{\rm aff}]$ (a more higher-degree representations could be introduced, but it has been seen that no gain can be obtained with respect to the one-degree (affine) representation). For the identification of the parameters of such affine representations $\mathbf{g}^{\rm aff}$ and $[h^{\rm aff}]$, two approaches can *a priori* be used. The first one consists in introducing the affine reprensentations in Eq. (4.14) before the identification (as proposed, for instance, in [83]), and then to identify $[A]$ and the parameters involved in the affine representations $\mathbf{g}^{\rm aff}(\tau_k)$ and $[h^{\rm aff}(\tau_k)]$ of $\mathbf{g}^k$ and $[h^k]$. The second one consists in identifying the coefficients $\mathbf{g}^k$ and $[h^k]$ (as explained before) and then approximating $\mathbf{g}^k$ and $[h^k]$ resulting from this identification by the values $\mathbf{g}^{\rm aff}(\tau_k)$ and $[h^{\rm aff}(\tau_k)]$ of these affine functions using the least-squares method with constraints. These two approaches have been analyzed and it has been concluded that the second one is more robust than the first one. Using the second approach, the prediction $\mathbf{C}^{K+1}$ of $\mathbf{C}^{\rm mod}(\tau_{K+1})$ will be denoted by $\mathbf{C}^{{\rm aff},K+1}$.

4.5.2 Identification of affine representations for g and $[h]$

The stochastic model identified in Section 4.4 has to be adapted in order to be able to predict the long-term evolution $\mathbf{C}^{K+1} = \mathbf{C}(\tau_{K+1})$ of the random indicator of the train dynamics at discrete long time τ_{K+1}. In this section, the families $\{\mathbf{g}\}$ and $\{[h]\}$ are considered as the values of the functions $\tau \mapsto \mathbf{g}(\tau)$ and $\tau \mapsto [h(\tau)]$ at discrete long times τ_k, $k = 2, \ldots, K$, such that $\mathbf{g}(\tau_k) = \mathbf{g}^k$ and $[h(\tau_k)] = [h^k]$. Functions $\mathbf{g}$ and $[h]$ are then approximated by

$$\mathbf{g}^{\rm aff}(\tau_k) = \mathbf{a}_g\, \tau_k + \mathbf{b}_g \quad , \quad [h^{\rm aff}(\tau_k)] = [a_h]\, \tau_k + [b_h]\,, \tag{4.47}$$

in which $\mathbf{a}_g$ and $\mathbf{b}_g$ are vectors in $\mathbb{R}^{N_c}$, where $[b_h]$ is a matrix in $\mathbb{M}^L_{N_c}$, and where $[a_h]$ is a lower triangular $(N_c \times N_c)$ real matrix such that $[a_h]\, \tau_k + [b_h]$ is in $\mathbb{M}^L_{N_c}$ for all k in $\{2, \ldots, K\}$. These conditions define the admissible set for $[a_h]$ and $[b_h]$ denoted by $\mathcal{C}_{a_h b_h}$ and ensure that the values of $[h^{\rm aff}]$ are in $\mathcal{C}_h$.

- For $i = 1, \ldots, N_c$, the optimal value $(a^{\rm opt}_{g_i}, b^{\rm opt}_{g_i})$ of (a_{g_i}, b_{g_i}) is given as the solution of the following optimization problem,

$$(a^{\rm opt}_{g_i}, b^{\rm opt}_{g_i}) = \arg \min_{(a_{g_i}, b_{g_i}) \in \mathbb{R}^2} \sum_{k=2}^{K} \Delta\tau_k \, |g_i^{{\rm opt},k} - (a_{g_i}\, \tau_k + b_{g_i})|^2 \,. \tag{4.48}$$

  This unconstrained linear least-squares problem is solved with the trust-region-reflective algorithm without constraints.

- The optimal value $([a_h^{\rm opt}], [b_h^{\rm opt}])$ of $([a_h], [b_h])$ is given as the solution of the following optimization problem,

$$([a_h^{\rm opt}], [b_h^{\rm opt}]) \;=\; \arg \min_{([a_h],[b_h]) \in \mathcal{C}_{a_h b_h}} \sum_{k=2}^{K} \Delta\tau_k \, |[h^{{\rm opt},k}] \;-\; ([a_h]\, \tau_k \;+\; [b_h])|^2 \,. \tag{4.49}$$

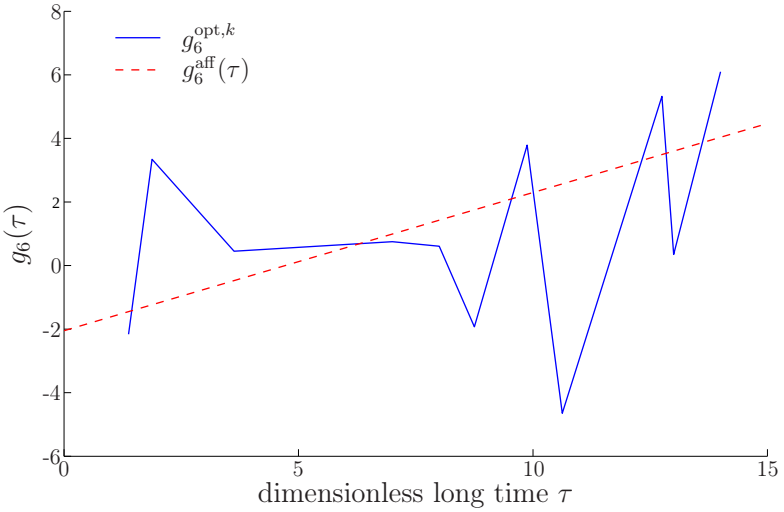

Figure 4.1: Comparison between the optimal values $g_6^{\mathrm{opt},2}, \ldots, g_6^{\mathrm{opt},K}$ identified for g_6 and its affine representation $g_6^{\mathrm{aff}}(\tau_k)$, $k = 1, \ldots, K+1$.

This constrained linear least-squares problem is solved using the trust-region-reflective algorithm with constraints.

The values $\mathbf{g}^{\mathrm{aff}}(\tau_{K+1})$ and $[h^{\mathrm{aff}}(\tau_{K+1})]$ are then calculated by

$$\mathbf{g}^{\mathrm{aff}}(\tau_{K+1}) = \mathbf{a}_g^{\mathrm{opt}}\,\tau_{K+1} + \mathbf{b}_g^{\mathrm{opt}}\ ,\ [h^{\mathrm{aff}}(\tau_{K+1})] = [a_h^{\mathrm{opt}}]\,\tau_{K+1} + [b_h^{\mathrm{opt}}]\,. \tag{4.50}$$

As an illustration, the sixth component of $\mathbf{g}^{\mathrm{opt}}$ and its affine approximation $\mathbf{g}^{\mathrm{aff}}$ are displayed in Figure 4.1. It should be noticed that, for some values of k, $g_6^{\mathrm{opt},k}$ and $g_6^{\mathrm{aff}}(\tau_k)$ are quite distant and the approximation of $\mathbf{g}^{\mathrm{opt}}$ by an affine function is bad. Nevertheless, representing $\mathbf{g}^{\mathrm{opt}}$ by an affine function allows to compute $\mathbf{g}^{\mathrm{opt},k}$ for $k \geq K+1$. The sixth component of the diagonal of $[h^{\mathrm{opt}}]$ and its affine approximation $[h^{\mathrm{aff}}]$ are displayed in Figure 4.2. The observations are the same as for the comparison between g_6^{opt} and g_6^{aff}. It is verified that the values of $[h^{\mathrm{opt},k}]_{6,6}$, $k = 2, \ldots, K$, and of $[h^{\mathrm{aff}}(\tau_k)]_{6,6}$, $k = 1, \ldots, K+1$ are positive.

The prediction $\mathbf{C}^{\mathrm{aff},K+1}$ of the vector-valued random indicator $\mathbf{C}^{K+1} = \mathbf{C}(\tau_{K+1})$ at long time τ_{K+1} , given $\mathbf{C}^{\mathrm{mod}}(\tau_K)$, is then estimated using Eq. (4.14) that yields

$$\mathbf{C}^{\mathrm{aff},K+1} = ([I_{N_c}] - \Delta\tau_{K+1}\,[A^{\mathrm{opt}}])\mathbf{C}^{\mathrm{mod}}(\tau_K) + \Delta\tau_{K+1}\,\mathbf{g}^{\mathrm{aff}}(\tau_{K+1}) + [h^{\mathrm{aff}}(\tau_{K+1})]\,\Delta\mathbf{W}^{K+1}\,. \tag{4.51}$$

Remark. As explained before, Eq. (4.51) correponds to Eqs. (4.14) and (4.13) for which the initial condition is given at time τ_K:

$$\mathbf{C}^{\mathrm{aff},k} = ([I_{N_c}] - \Delta\tau_k\,[A^{\mathrm{opt}}])\mathbf{C}^{\mathrm{aff},k-1} + \Delta\tau_k\,\mathbf{g}^{\mathrm{aff}}(\tau_k) + [h(\tau_k)^{\mathrm{aff}}]\,\Delta\mathbf{W}^k \quad , \quad k = K+1\,, \tag{4.52}$$

with the initial condition

$$\mathbf{C}^{\mathrm{aff},K} = \mathbf{C}^{\mathrm{mod}}(\tau_K)\,, \tag{4.53}$$

in which $\Delta\tau_{K+1} = \tau_{K+1} - \tau_K$.

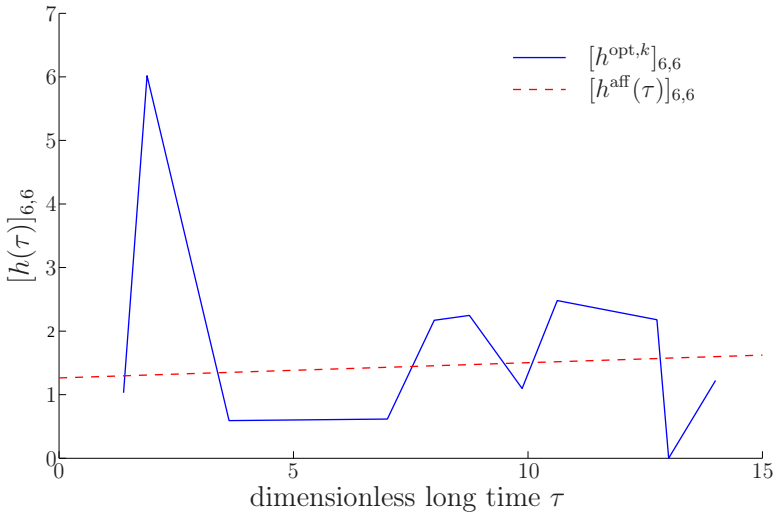

Figure 4.2: Comparison between the optimal values $[h^{\mathrm{opt},2}]_{6,6}, \ldots, [h^{\mathrm{opt},K}]_{6,6}$ identified for $[h]_{6,6}$ and its affine representation $[h^{\mathrm{aff}}(\tau_k)]_{6,6}$, $k = 1, \ldots, K+1$.

4.6 Conclusion

In this chapter, a stochastic predictive model has been developed in order to predict, for a given stretch of the track, the long-term evolution of the vector-valued random indicator $\mathbf{C}$ for the dynamic response of the train. The choice of the stochastic predictive model is relatively restrained by the fact that only a few long time $\tau_1, \ldots, \tau_K$ are known for which the measurements have been performed. Since the vector-valued random indicator is a nonstationary and non-Gaussian time series, a one-order nonstationary vector-valued Markov chain with a non-Gaussian initial condition has been constructed. The stochastic predictive model is identified in two steps. For the first one, the model parameters are identified with a least-squares method with weights using realizations $\mathbf{C}^{\mathrm{mod}}$ of the random indicator, which have been simulated at each long time by using the stochastic computational model of the train dynamics. For the second step, the time-dependent parameters of the stochastic predictive model are fitted by affine functions of long time τ, in order to be able to predict the long-term evolution of the random indicator with the stochastic predictive model.

Chapter 5

Application to a high-speed line of the French railway network

5.1 Introduction

This chapter is devoted to the application of the models and methodologies developed in the previous chapters for a given stretch of the railway track of a French high-speed line. The given track stretch is chosen straight with a significant long-term evolution of the dynamic response of the train. For this track stretch, the measurements performed at the discrete long times show that all the track irregularities present a significant long-term evolution and that the vertical offset reaches a peak value. It is observed that the long-term evolution of the components of the vector-valued indicator, which are related to the vertical direction, is significant, and that the long-term evolution of the components related to the horizontal direction is not.

For the given track stretch, the local stochastic model of the track irregularities is constructed, the dynamic response of the train is numerically simulated, and the vector-valued random indicator is calculated. In the perspective of improving the maintenance strategy, a vector-valued threshold level is defined for the vector-valued random indicator. Then, the stochastic predictive model is identified using the realizations of the random indicator at long times $\tau_1, \ldots, \tau_K$. The predictive model allows for predicting the long-term evolution of the vector-valued random indicator. The relevance of the stochastic predictive model is then analyzed.

Section 5.2 is devoted to the identification of the local stochastic model for the track irregularities of the given track stretch. In Section 5.3, the vector-valued random indicator of the dynamic response of the train is constructed and the vector-valued threshold is defined. The parameters of the stochastic model of the long-term evolution of the indicator are identified in Section 5.4, which allows for predicting the long-term evolution presented in Section 5.5.

All the numerical results presented in the figures diplayed in this chapter are dimensionless concerning the components of the indicator (named as "dimensionless indicator") and the discrete long times. The discrete long times $\tau_1, \ldots, \tau_{K+1}$ are transformed in di-

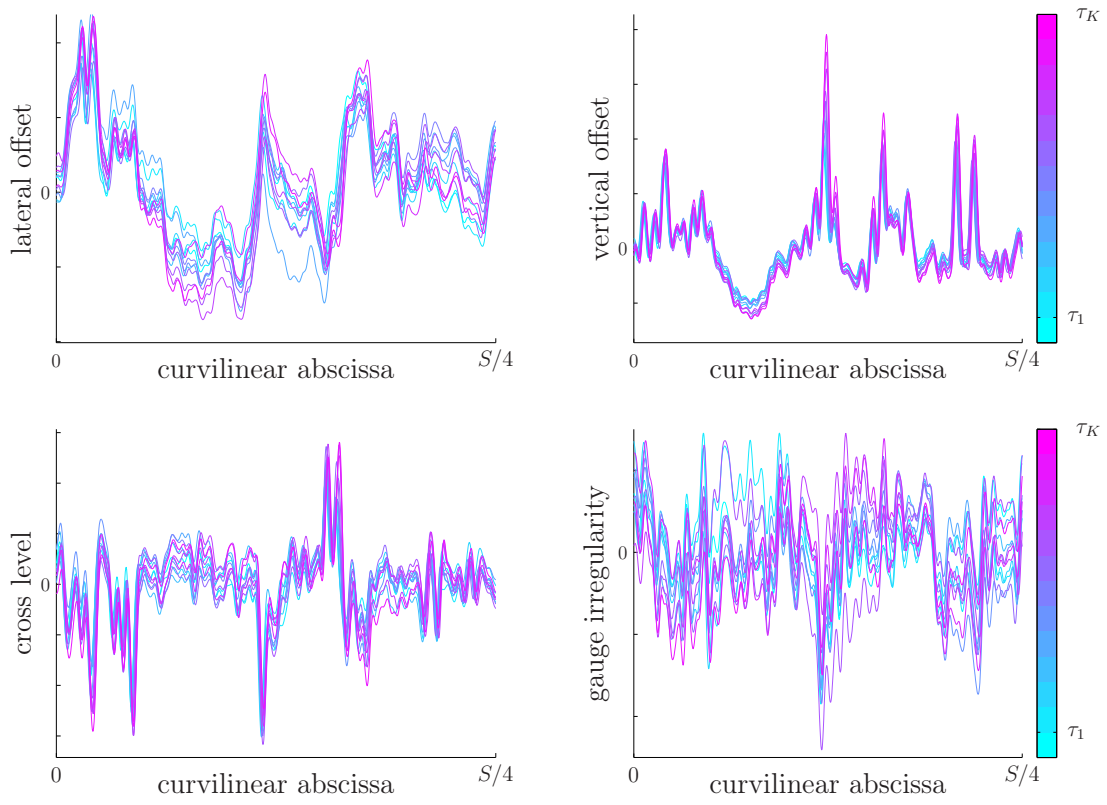

Figure 5.1: long-term evolution of the track irregularities for the given track stretch. In each figure, each curve represents the track irregularities at a given τ_k.

mensionless discrete long times (named as dimensionless long time τ) that are written as $\tau_k/\Delta\tau_{\text{ref}}$ as introduced in Section 4.3.4.

5.2 Identification of the local stochastic model for the track irregularities

5.2.1 Measurements of the track irregularities

For the given track stretch, the track irregularities are measured by the recording train IRIS 320 at discrete long times $\tau_1, \ldots, \tau_K$. For long time τ_k, $k = 1, \ldots, K$, the measured track irregularities vector of the track stretch is denoted by $\mathbf{x}^{\text{meas}}_{\tau_k} = (\mathbf{x}^{1,\text{meas}}_{\tau_k}, \mathbf{x}^{2,\text{meas}}_{\tau_k}, \mathbf{x}^{3,\text{meas}}_{\tau_k}, \mathbf{x}^{4,\text{meas}}_{\tau_k})$ ($K = 12$ measurements are available for this track stretch). Figure 5.1 displays the long-term evolution of the four track irregularities. All the track irregularities present a significant evolution, and this evolution is heterogeneous along the track stretch. Meanwhile, it appears clearly that the vertical offset reaches a peak value.

5.2.2 Local stochastic model for the track stretch

The construction of the local stochastic model for the track irregularities is carried out as explained in Section 2.5. The local stochastic model for the track irregularities of the given track stretch is constructed using Eq. (2.32), such that, for $k = 1, \ldots, K$,

$$\widetilde{\mathbf{X}}^{\kappa}_{\tau_k}(\boldsymbol{\delta}^{\text{opt}}) = [Q^{\kappa}] \left(\boldsymbol{\eta}^{\text{meas}}_{\tau_k} + \delta^{\kappa,\text{opt}}\, \mathbf{G}^{\kappa}\right) \quad , \quad \kappa = 1, 2, 3, 4\,, \tag{5.1}$$

in which, from Eq. (2.31), the projection of the measurement $\mathbf{x}^{\text{meas}}_{\tau_k}$ on matrix $[Q]$, which represents the spatial basis of the global stochastic model, is written as

$$\boldsymbol{\eta}^{\text{meas}}_{\tau_k} = [\lambda]^{-1}\, [Q]^T [\text{Diag}(\mathbf{O})]^2 \mathbf{x}^{\text{meas}}_{\tau_k}\,. \tag{5.2}$$

The optimal value $\boldsymbol{\delta}^{\text{opt}} = (\delta^{1,\text{opt}}, \delta^{2,\text{opt}}, \delta^{3,\text{opt}}, \delta^{4,\text{opt}})$ of hyperparameter $\boldsymbol{\delta}$ for this track stretch is computed using the method that is described in Section 2.5.2. The obtained value is $\boldsymbol{\delta}^{\text{opt}} = (0.05, 0.35, 0.65, 0.65)$. For the four track irregularities ($\kappa = 1, 2, 3, 4$) and at $\tau = \tau_1$, a realization $\widetilde{\mathbf{X}}^{\kappa}_{\tau_1}(\theta')$, for θ' in Θ', of the local stochastic model, the measured irregularity $\mathbf{x}^{\kappa,\text{meas}}_{\tau_1}$, and the confidence region at 90% of $\widetilde{\mathbf{X}}^{\kappa}_{\tau_1}(\boldsymbol{\delta}^{\text{opt}})$ are displayed in Figure 5.2, which confirms that the local stochastic model of the track irregularities preserves the statistical properties of the track geometry for each type of track irregularities.

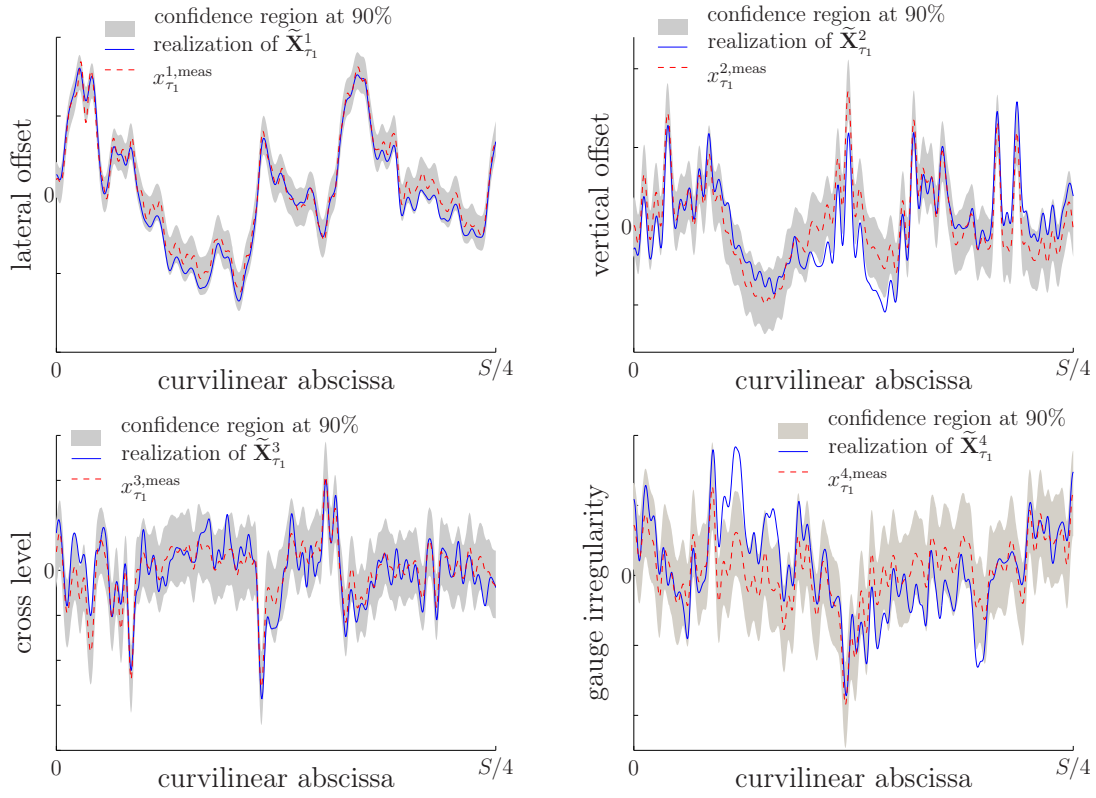

Figure 5.2: At initial long time τ_1, and for $\kappa = 1, 2, 3, 4$, irregularity $x^{\kappa,\text{meas}}_{\tau_1}$, realization $\widetilde{\mathbf{X}}^{\kappa}_{\tau_1}(\theta')$, for θ' in Θ', and confidence region at 90% of $\widetilde{\mathbf{X}}^{\kappa}_{\tau_1}(\boldsymbol{\delta}^{\text{opt}})$ for the given track stretch.

The long-term evolution of the track stretch can also be observed during several cycles of degradation/maintenance operations. In this case, the optimal value for the hyper-parameter $\boldsymbol{\delta}$ has to be identified after each maintenance operation because the track irregularities are deeply modified by the maintenance operations. The values of the components of $\boldsymbol{\delta}^{\text{opt}}$ are displayed in Figure 5.3 for six maintenance cycles. A little modification of $\boldsymbol{\delta}^{\text{opt}}$ is generally observed after a maintenance operation.

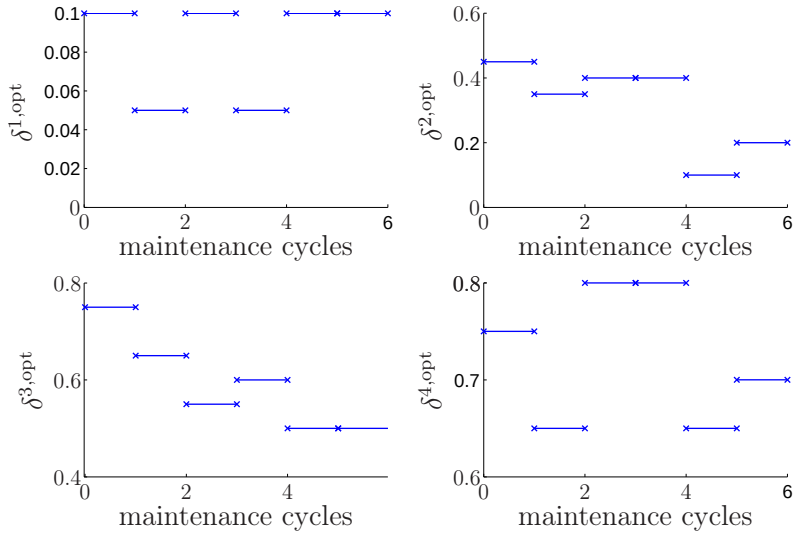

Figure 5.3: Evolution of the optimal value $\boldsymbol{\delta}^{\text{opt}} = (\delta^{1,\text{opt}}, \delta^{2,\text{opt}}, \delta^{3,\text{opt}}, \delta^{4,\text{opt}})$ for a given track stretch after 5 maintenance operations.

5.3 Constructing the vector-valued random indicator $\mathbf{C}^{\text{mod}}$

The dynamic response of the train on the given track stretch is assessed by the vector-valued random indicator $\mathbf{C}^{\text{mod}}$ with values in $\mathbb{R}^{N_c}$, which has been constructed in Section 3.5.1. The number of components of the indicator is $N_c = 9$. The first four components are based on usual comfort criteria for the high-speed trains, whereas the other five components are based on safety criteria such as (see Section 3.4.1)

- C_1 assesses the lateral acceleration of the first bogie in the train.
- C_2 assesses the vertical acceleration of the first bogie in the train.
- C_3 assesses the lateral acceleration of the third bogie in the train.
- C_4 assesses the lateral acceleration of the second coach in the train.
- C_5 assesses the sum of lateral forces on the ninth wheelset in the train.
- C_6 assesses the sum of vertical forces on the first wheelset in the train.

- C_7 assesses the sum of vertical forces of the second wheelset in the train.
- C_8 assesses the sum of vertical forces of the tenth wheelset in the train.
- C_9 assesses the difference between right-wheel and left-wheel vertical forces of the tenth wheelset in the train.

5.3.1 Adopted approach

Once the local stochastic model for the track irregularities has been identified, we are able to generate realizations of the track irregularities for the given track stretch and to compute the dynamic response of the train for these realizations. The Monte-Carlo method is performed with $\nu = 2,000$ independent realizations of the local stochastic model, and is summarized hereinafter.

- $\nu = 2,000$ independent realizations $\mathbf{G}(\theta'_1), \ldots, \mathbf{G}(\theta'_\nu)$ of $\mathbf{G} = (\mathbf{G}^1, \mathbf{G}^2, \mathbf{G}^3, \mathbf{G}^4)$ are generated on the probability space $(\Theta', \mathcal{F}', \mathcal{P}')$ (see Section 2.5.1).
- These ν independent realizations of $\mathbf{G}$ are used for constructing, for each $k = 1, \ldots, K$, the ν independent realizations of random vector $\widetilde{\mathbf{X}}_{\tau_k}(\boldsymbol{\delta}^{\text{opt}}) = (\widetilde{\mathbf{X}}^1_{\tau_k}(\boldsymbol{\delta}^{\text{opt}}), \widetilde{\mathbf{X}}^2_{\tau_k}(\boldsymbol{\delta}^{\text{opt}}), \widetilde{\mathbf{X}}^3_{\tau_k}(\boldsymbol{\delta}^{\text{opt}}), \widetilde{\mathbf{X}}^4_{\tau_k}(\boldsymbol{\delta}^{\text{opt}}))$ by using Eq. (5.1). In order to have realistic initial conditions for the dynamic response of the train, and to avoid a side-effect when filtering the dynamic response of the train, a realistic deterministic track section is added before and after the given track stretch for the simulation. The junction between the added track sections and the given track stretch has to be of $\mathcal{C}^2$-class (the second derivative is continuous). A spline of order 3 is thus chosen to smooth the junction on a few meters.
- For each realization of the track irregularities $\widetilde{\mathbf{X}}_{\tau_k}(\boldsymbol{\delta}^{\text{opt}})$, the deterministic dynamic response of the train induced by this realization of the track irregularities is computed with the computational model (using *Vampire* code), with a train speed of 300 km/h. Using parallel computing, 50 realizations of the dynamic response of the train are computed simultaneously, which gives a computation time between 5 and 6 hours for the train dynamics for each long time τ_k. The ν corresponding independent realizations of the dynamic criteria $Z_1(s, \tau_k), \ldots, Z_9(s, \tau_k)$ introduced in Section 3.4.1 are computed. As an illustration, the mean and the confidence region at 90% of the vertical acceleration of the first bogie of the TGV $Z_2(s, \tau_K)$ are featured in Figure 5.4 as a function of the curvilinear abscissa for $\tau = \tau_K$.
- From the realizations of the criteria $Z_1(s, \tau_k), \ldots, Z_9(s, \tau_k)$, the ν corresponding independent realizations $\mathbf{C}^{\text{sim}}(\tau_k; \theta'_1), \ldots, \mathbf{C}^{\text{sim}}(\tau_k; \theta'_\nu)$ of the vector-valued random indicator $\mathbf{C}^{\text{sim}}(\tau_k)$ are computed (see Eq. (3.2)).
- Then, ν independent realizations of the $\mathbb{R}^{N_c}$-valued non-Gaussian second-order random vector $\mathbf{B}^{\text{out}}$ are generated on the probability space $(\Theta'', \mathcal{F}'', \mathcal{P}'')$ using Eq. (3.11).
- The ν corresponding independent realizations of the family $\boldsymbol{\mathcal{C}}^{\text{mod}}$, constituted of the vector-valued random indicators $\{\mathbf{C}^{\text{mod}}(\tau_1), \ldots, \mathbf{C}^{\text{mod}}(\tau_K)\}$ for all long times

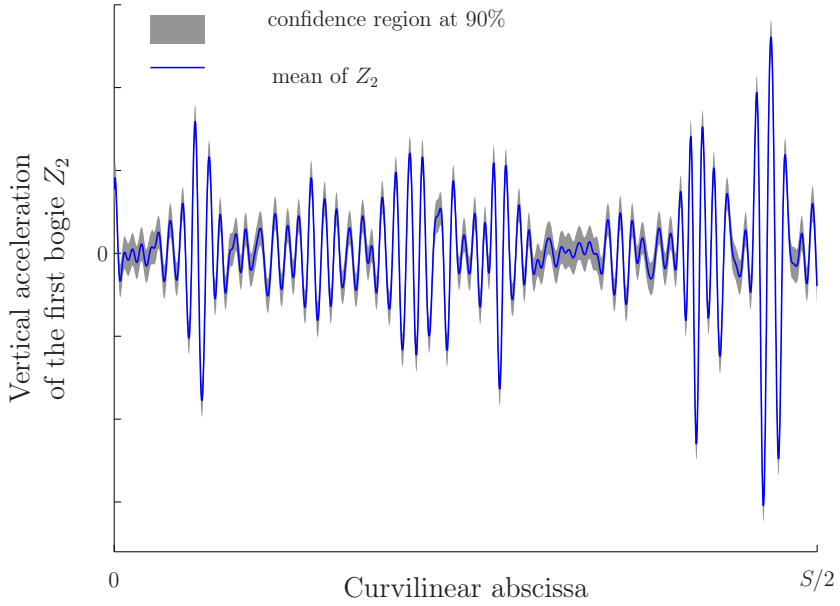

Figure 5.4: Random vertical acceleration of the first bogie of the TGV, Z_2, in output of the numerical simulation.

$\tau_1, \ldots, \tau_K$, are $\boldsymbol{\mathcal{C}}^{\text{mod}}(\theta'_1, \theta''_1), \ldots, \boldsymbol{\mathcal{C}}^{\text{mod}}(\theta'_\nu, \theta''_\nu)$, that are computed using Eq. (3.5), which is rewritten as $C_j^{\text{mod}}(\tau_k; \theta'_\ell, \theta''_\ell) = C_j^{\text{sim}}(\tau_k; \theta'_\ell) \exp(B_j^{\text{out}}(\theta''_\ell))$, with $j = 1, \ldots, N_c$, $k = 1, \ldots, K$, and $\ell = 1, \ldots, \nu$. In order to analyze the results, the probability density functions of the components of $\mathbf{C}^{\text{mod}}(\tau_k)$ and $\mathbf{C}^{\text{sim}}(\tau_k)$ are estimated using the Gaussian kernel estimation method. For the given track stretch, Figure 5.5 displays the probability density functions of the nine components $C_j^{\text{sim}}(\tau_1)$, $C_j^{\text{mod}}(\tau_1)$, $C_j^{\text{sim}}(\tau_K)$, and $C_j^{\text{mod}}(\tau_K)$. The figure shows that the components of $\mathbf{C}^{\text{mod}}$ are more dispersed than the components of $\mathbf{C}^{\text{sim}}$ for these two times τ_1 and τ_K, due to the presence of model uncertainties represented by $\mathbf{B}^{\text{out}}$ in the computational model. For each indicator, the long-term evolution between τ_1 and τ_K can be observed.

- As explained in Section 4.4.4-(ii), we need to estimate the target quantities in order to perform the identification of the parameters of the stochastic predictive model (see Section 5.4). Consequently, for $k = 2, \ldots, K$ and for $\mu = 0, \ldots, k-1$, the vectors $E\{\mathbf{C}^{\text{mod}}(\tau_k)\}$ and $E\{\mathbf{C}^{\text{mod}}(\tau_{k-1})\}$, and the tensors $E\{\mathbf{C}^{\text{mod}}(\tau_k) \otimes \mathbf{C}^{\text{mod}}(\tau_{k-\mu})\}$ and $E\{\mathbf{C}^{\text{mod}}(\tau_{k-1}) \otimes \mathbf{C}^{\text{mod}}(\tau_{k-\mu})\}$, are estimated by using the classical statistical estimator of the mathematical expectation with the independent realizations $\boldsymbol{\mathcal{C}}^{\text{mod}}(\theta'_1, \theta''_1), \ldots, \boldsymbol{\mathcal{C}}^{\text{mod}}(\theta'_\nu, \theta''_\nu)$.

5.3.2 Definition of the threshold level for the random indicator

In order to start off the maintenance operations, the values of the random indicator have to be compared to a vector-valued threshold level denoted by $\mathbf{c}^*$, which has to be defined according to the maintenance strategy that is required by the railway operators.

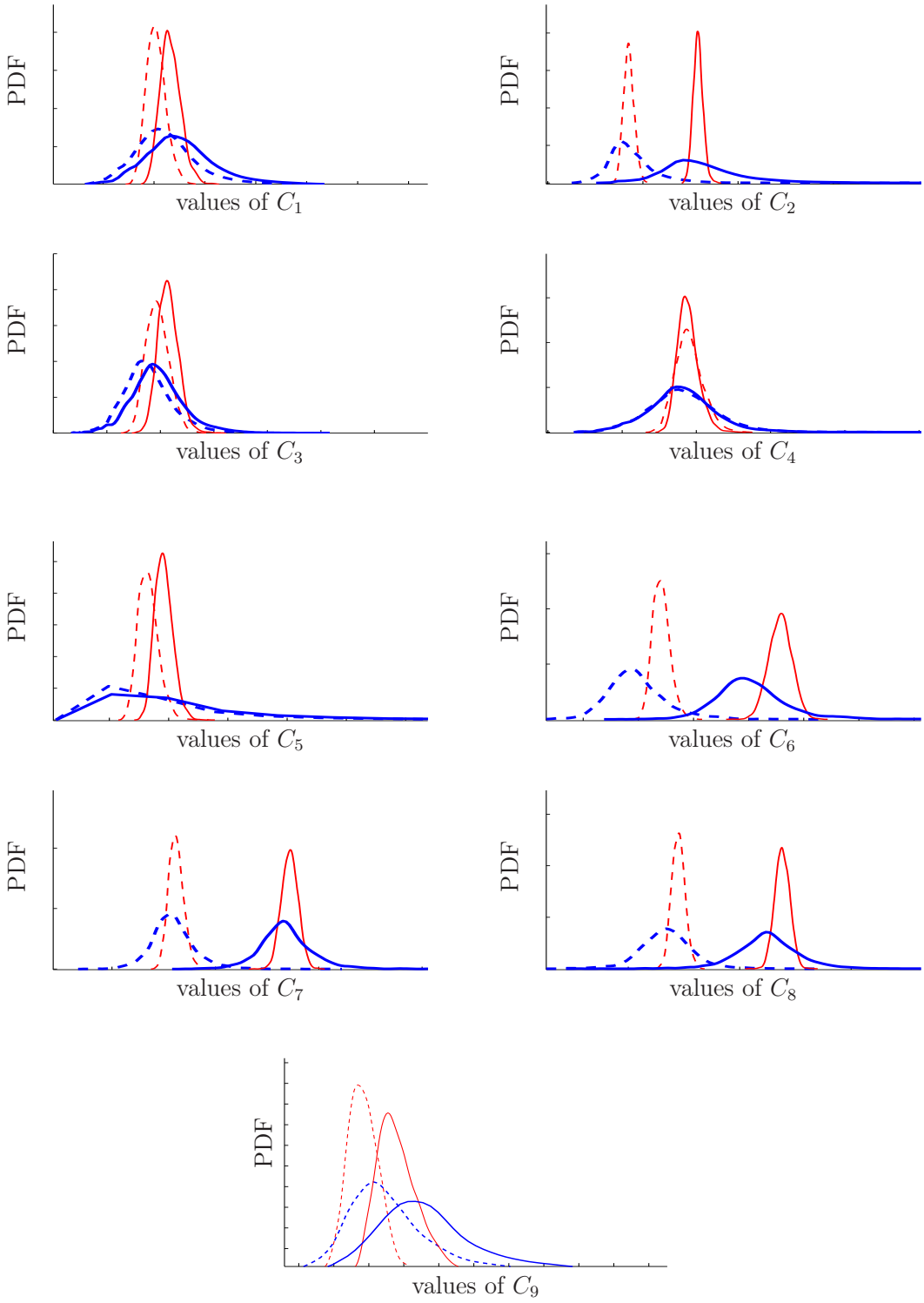

Figure 5.5: For the nine components of the random indicator, $j = 1, \ldots, 9$, comparisons of the probability density functions of $C_j^{\text{sim}}(\tau_1)$ (red dashed line), $C_j^{\text{mod}}(\tau_1)$ (blue dashed line), $C_j^{\text{sim}}(\tau_K)$ (red solid line), $C_j^{\text{mod}}(\tau_K)$ (blue solid line).

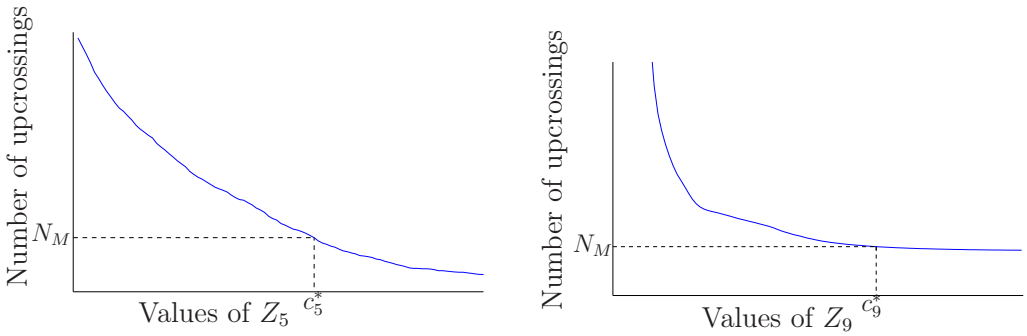

Figure 5.6: Identification of the threshold level for the indicator of the dynamic response of the train. The dashed lines indicate the threshold level c^*.

In order to identify a threshold value for each criteria, since the maintenance operations are currently undertaken depending on a type of irregularities, it has been chosen to associate each criteria $Z_1, \ldots, Z_9$ with a type of irregularities. Criteria Z_1, Z_3, Z_4 (lateral accelerations), and Z_5 (sum of lateral forces) are associated with the lateral offset, Z_2 (vertical acceleration), Z_6, Z_7, and Z_8 (sum of vertical forces) are associated with the vertical offset, and Z_9 (difference of vertical forces) is associated with the cross level. In the same way, the maintenance operations can be associated with the lateral offset, with the vertical offset, or with the cross level. For all the measurements of the track irregularities, the dynamic response of the train is numerically simulated and the criteria $Z_1, \ldots, Z_9$ are computed. The numbers of upcrossings of the criteria are displayed in Figure 5.6 as function of their values. To limit the number of figures, the graphs are only plotted for Z_5 and Z_9. For the criteria $Z_1, \ldots, Z_9$, their threshold values $c_1^*, \ldots, c_9^*$ are defined by a corresponding number of upcrossings, equal to the number of maintenance operations, which is denoted by N_M.

5.3.3 Observation of the long-term evolution of the random indicator

In order to analyze the long-term evolution of the vector-valued random indicator $\mathbf{C}^{\text{mod}}$, the mean function and the confidence region (at 90%) of its components $C_j^{\text{mod}}(\tau_k)$ are calculated as a function of discrete long time τ_k. The mean function and the confidence region, which depend on τ_k, are compared to the threshold level c_j^* that has been defined in the previous section, and are displayed in Figure 5.7. The uncertainties in the computational model of the train dynamics are taken into account, which increases the robustness of the computational predictions of the statistics for the train indicators. For $j = 2, 6, 7, 8$ (components related to the vertical direction), a long-term evolution of the mean value and of the confidence region of the component C_j^{mod} can be observed. For the other values of j, there is no significant long-term evolution. In particular, the lateral acceleration in the second carbody represented by C_4 remains almost constant. This implies that the lateral comfort in the train is not deteriorated by the track irregularities for this track stretch. This result cannot be deduced only in looking at the long-term evolution of the track irregularities (Figure 5.1). It can be concluded that the deterioration of the track irregularities does not have the same influence on all the indicators.

For the given track stretch, it is also possible to observe the long-term evolution of the random indicator taking into account several maintenance operations. Such an observation enables to assess the influence of a maintenance operation on each component of the random indicator. It can be noticed that some maintenance operations cause an improvement on some components, although they have no influence on other components. Figure 5.8 displays the long-term evolution of component C_6^{mod} with six maintenance cycles. It appears that the fourth and fifth maintenance operations did not have any effect on this component (although they may have improved other components).

5.4 Stochastic model for the long-term evolution of the random indicator

The stochastic predictive model defined by Eqs. (4.14) with (4.13) is used to model the long-term evolution of the random indicator:

$$\mathbf{C}^k = ([I_{N_c}] - \Delta\tau_k\,[A])\mathbf{C}^{k-1} + \Delta\tau_k\,\mathbf{g}^k + [h^k]\,\Delta\mathbf{W}^k \quad , \quad k = 2, \ldots, K\,, \tag{5.3}$$

with the initial condition

$$\mathbf{C}^1 = \mathbf{C}^{\text{mod}}(\tau_1)\,, \tag{5.4}$$

in which matrix $[A]$, vectors family $\{\mathbf{g}\} = \{\mathbf{g}^2, \ldots, \mathbf{g}^K\}$, and matrix family $\{[h]\} = \{[h^2], \ldots, [h^K]\}$ are identified using the methodology presented in Section 4.4.

5.4.1 Choice of the family of weight coefficients

The family $\{\alpha_1, \alpha_2, \ldots, \alpha_N\}$ of weight coefficients introduced in Section 4.4 is chosen in order to favor the components $j = 2, 6, 7, 8$ of the vector-valued indicator, which present a significant long-term evolution, while the condition appearing in Eq. (4.19) is fullfilled. The chosen values for $\boldsymbol{\alpha}$ are $\alpha_1 = \alpha_3 = \alpha_4 = \alpha_5 = \alpha_9 = 0.01$, $\alpha_2 = 0.35$, and $\alpha_6 = \alpha_7 = \alpha_8 = 0.2$.

5.4.2 Solving the optimization problem related to the simplified formulation

The first step of computation consists in solving the simplified formulation of the optimization problem as explained in Section 4.4.5.

For $k = 1, \ldots, K$, the ν realizations of $\mathbf{C}^{\text{mod}}(\tau_k)$ that are computed with the Monte-Carlo method, are used to estimate the target quantities introduced in the cost functions $J_j(A_j, \{g_j\}, \{h_j\})$, with $j = 1, \ldots, N_c$, defined by Eq. (4.45). As explained in Section 4.4.5, for $j = 1, \ldots, N_c$, the optimal values A_j^0, $\{g_j^0\}$, and $\{h_j^0\}$ of parameters A_j, $\{g_j\}$, and $\{h_j\}$ are identified by solving the optimization problem defined by Eq. (4.46) using the trust-region-reflective algorithm. The algorithm stops when the cost function is changing by less than 10^{-11} . For instance, the convergence information of the optimizer related to component C_2 is given in Figure 5.9.

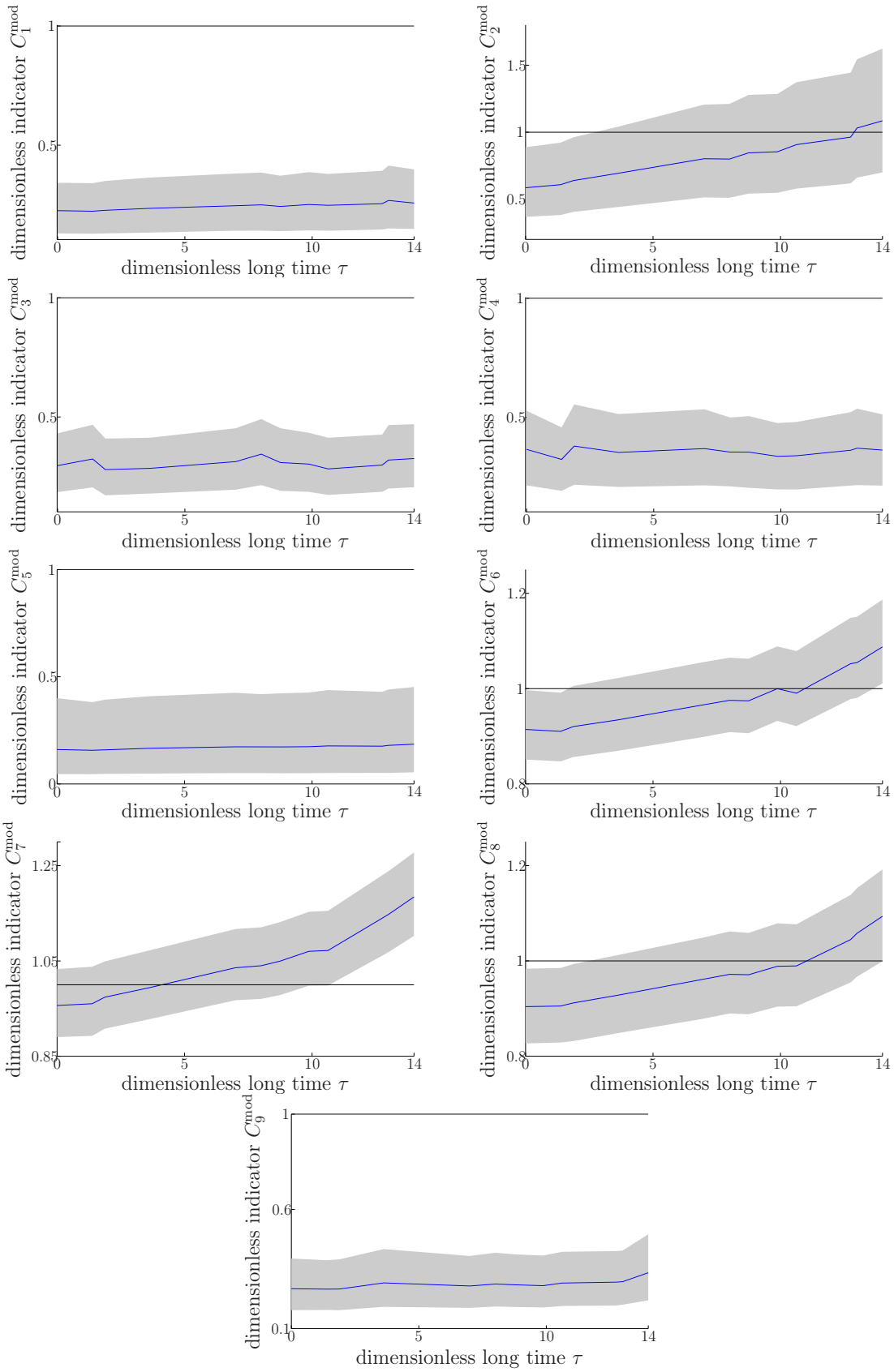

Figure 5.7: Dimensionless long-term evolution of the components of the dimensionless random indicator $\mathbf{C}^{\mathrm{mod}}$. Confidence region with probability 90% (grey region), threshold (horizontal solid line), mean value (solid line).

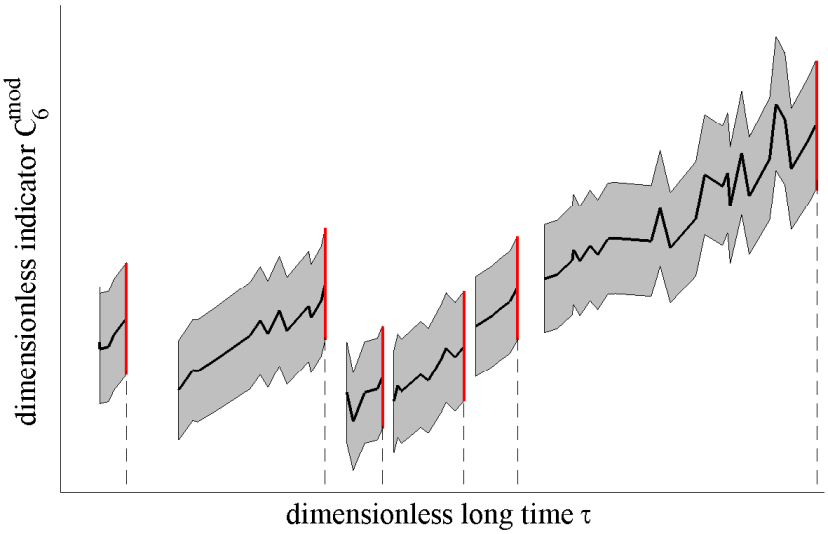

Figure 5.8: Dimensionless long-term evolution of random indicator C_6^{mod} taking into account six maintenance cycles (maintenance times are represented by dashed vertical lines). Confidence region with probability 90% (grey region), mean value (solid line).

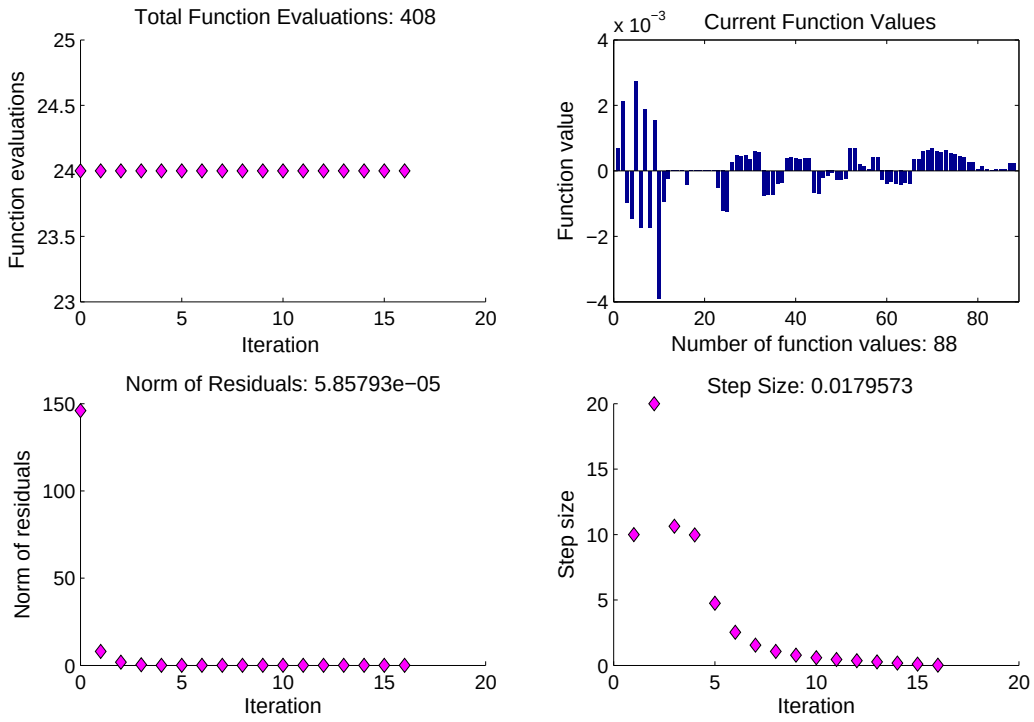

Figure 5.9: *Simplified formulation.* Convergence of the optimizer related to component C_2 using *lsqnonlin* of Matlab (the four figures plot measures of progress while the algorithm executes).

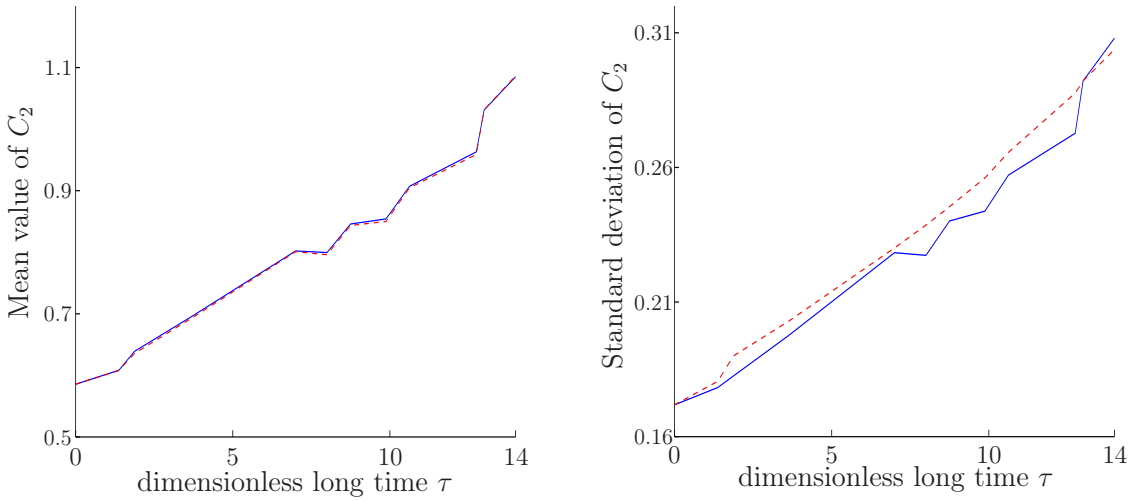

Figure 5.10: *Simplified formulation.* Second-order moments of the dimensionless long-term evolution for the dimensionless indicator $D(\tau_k) = C_2^{\text{mod}}(\tau_k)$ (solid line) and $D(\tau_k) = C_2^k$ (dashed line): mean value (left) and standard deviation (right).

For $k = 2, \ldots, K$ and for each $j = 1, \ldots, N_c$, the values of C_j^k are predicted with A_j^0, $\{g_j^0\}$, and $\{h_j^0\}$, and the simplified modeling is assessed by comparing $C_j^{\text{mod}}(\tau_k)$ with C_j^k. For each quantity, $C_j^{\text{mod}}(\tau_k)$ and C_j^k, denoted hereinafter as $D(\tau_k)$, the long-term evolution of the mean value $E\{D(\tau_k)\}$ and of the standard deviation $E\{(D(\tau_k) - E\{D(\tau_k)\})^2\}^{1/2}$ are estimated using the classical statistical estimator and are displayed in Figure 5.10. The long-term evolution of the probability density function $p_{D(\tau_k)}$ is estimated by the Gaussian kernel density method and is shown in Figure 5.11. Figure 5.12 displays the graph $k \mapsto d^i(\tau_k)$ in which $d^i(\tau_k)$ is such that $P\{D(\tau_k) \leq d^i(\tau_k)\} \geq q^i$, and where q^i is the quantile varying in the interval $[0.4, 0.98]$. This representation allows the value of the indicator to be compared with the threshold c_2^*. These figures show that the simplified evolution model is a good approximation to represent the random indicator and consequently is well adapted as initial condition for the global optimization.

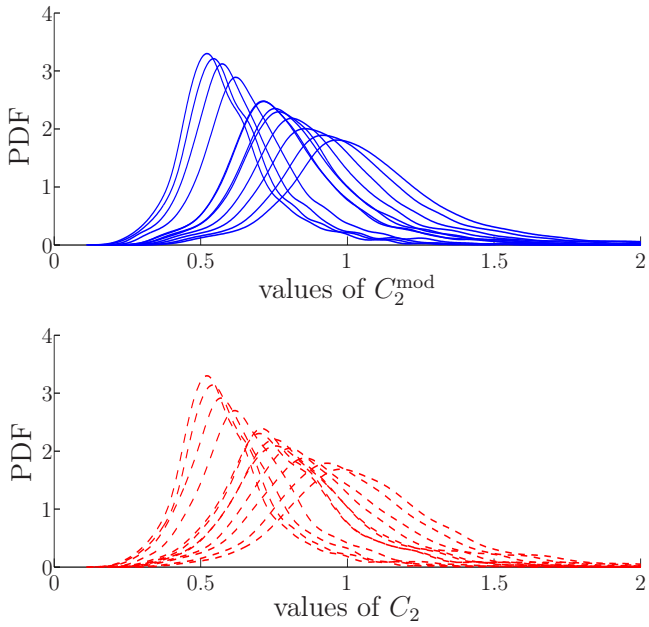

Figure 5.11: *Simplified formulation.* Probability density function (PDF) of the dimensionless long-term evolution for the dimensionless indicator $D(\tau_k) = C_2^{\mathrm{mod}}(\tau_k)$ (up) and $D(\tau_k) = C_2^k$ (down). Each curve corresponds to a given time τ_k. When k is increasing, the curves move to the right.

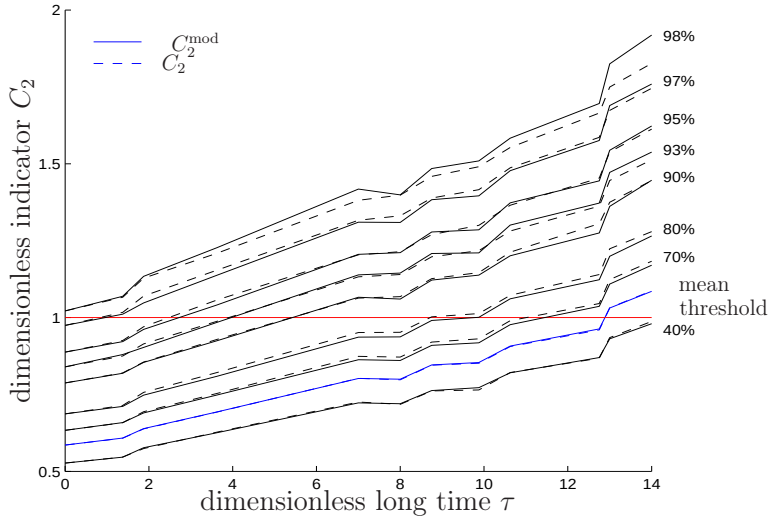

Figure 5.12: *Simplified formulation.* Quantiles of the dimensionless long-term evolution for the dimensionless indicator $D(\tau_k) = C_2^{\mathrm{mod}}(\tau_k)$ (solid line) and $D(\tau_k) = C_2^k$ (dashed line), graphs $k \mapsto d^i(\tau_k)$, in which $d^i(\tau_k)$ is such that $P\{D(\tau_k) \leq d^i(\tau_k)\} \geq q^i$ for different values in percent of the quantile q^i belonging to the interval $[40\%, 98\%]$. The horizontal line corresponds to the threshold level c_2^*.

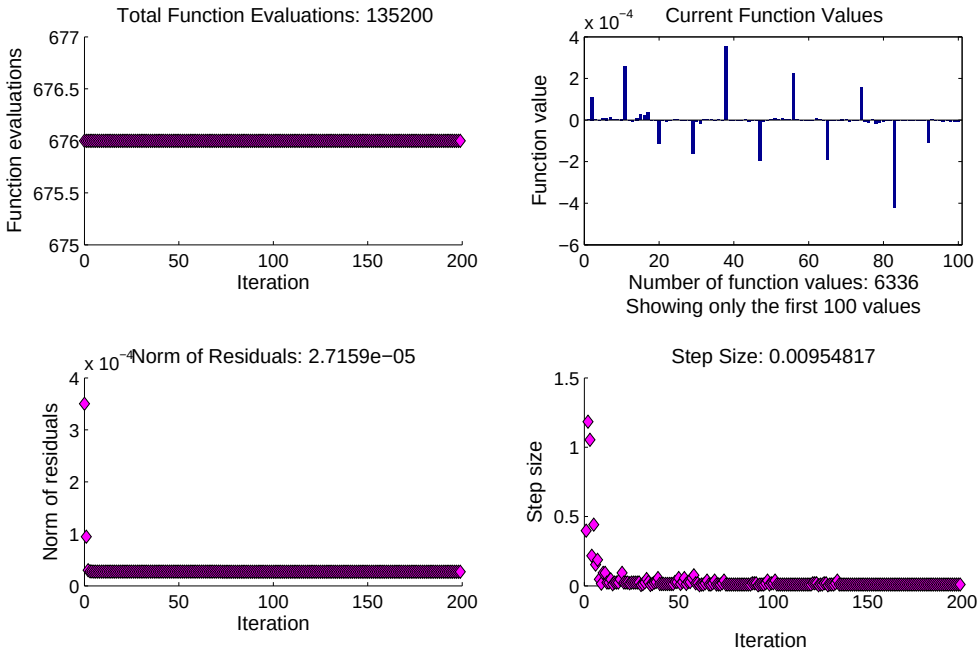

Figure 5.13: Convergence of the optimizer related to $\mathbf{C}$ using *lsqnonlin* of Matlab (the four figures plot measures of progress while the algorithm executes).

5.4.3 Identification of the parameters of the stochastic model for the long-term evolution

The optimal values $\{[A^{\text{opt}}], \{\mathbf{g}^{\text{opt}}\}, \{[h^{\text{opt}}]\}\}$ of the parameters $\{[A], \{\mathbf{g}\}, \{[h]\}\}$ in Eq. (5.3) are computed by using the methodology presented in Section 4.4. The initial values for the optimization are $[A_0]$,$\{\mathbf{g}_0\}$, and $\{[h_0]\}$, that have been identified in the previous section. For $k = 1, \ldots, K$, the ν realizations of $\mathbf{C}^{\text{mod}}(\tau_k)$, which have been computed with the Monte-Carlo method in Section 5.3.1, are used to estimate the target quantities introduced in the cost function $J([A], \{\mathbf{g}\}, \{[h]\})$ defined by Eq. (4.37). For the identification of the optimal values of the $N_c^2 + (K-1)N_c + (K-1)N_c(N_c+1)/2 = 675$ parameters, the trust-region-reflective algorithm is used and stops when the number of iterations is greater than 200 times the number of variables, which yields $135,000$ (this number has been chosen as a compromise between the computational cost and the norm of the residuals). The corresponding norm of the residuals is equal to 2.7×10^{-5}. The convergence information of the optimizer is given in Figure 5.13.

For $k = 2, \ldots, K$, we present a comparison of the vector-valued random indicator $\mathbf{C}^{\text{mod}}(\tau_k)$ computed in Section 5.3.1 with the random indicator $\mathbf{C}^k$ estimated with Eq. (5.3) and with Eq. (5.4) using the optimal parameters $\{[A^{\text{opt}}], \{\mathbf{g}^{\text{opt}}\}, \{[h^{\text{opt}}]\}\}$ that have been identified. For each quantity, $\mathbf{C}^{\text{mod}}(\tau_k)$ and $\mathbf{C}^k$, whose components are denoted hereinafter as $D(\tau_k)$ again, the long-term evolutions of the mean values $E\{D(\tau_k)\}$ are estimated using the classical statistical estimator and are displayed in Figure 5.14. The long-term evolu-

tions of the standard deviations $E\{(D(\tau_k) - E\{D(\tau_k)\})^2\}^{1/2}$ are also estimated using the classical statistical estimator and are displayed in Figure 5.15. The long-term evolutions of the probability density functions $p_{D(\tau_k)}$ are estimated by the Gaussian kernel density method and are shown in Figure 5.16. Figure 5.17 displays the graph $k \mapsto d^i(\tau_k)$, in which $d^i(\tau_k)$ is such that $P\{D(\tau_k) \leq d^i(\tau_k)\} \geq q^i$, where q^i is the quantile varying in the interval $[0.4, 0.98]$.

Figures 5.14, 5.15, 5.16 and 5.17 show that the stochastic model of the long-term evolution defined by Eqs. (4.14) and (4.13) is a very good approximation for representing the long-term evolution of the vector-valued random indicator, in particular for the long-term evolution of the PDF (Figure 5.16) and the long-term evolution of the quantiles (Figure 5.17). Comparing with the results of the previous section for the second component of the indicator, it is noticed that the multidimensional approach is a little better than the simplified approach, thanks to the dependence between the components. In order to limit the number of figures, we restrict the presentation to the components $j = 1, 2, 6$ of the vector-valued random indicator. For the given track stretch, the long-term evolution of components C_3, C_4, C_5 and C_9 is similar to the long-term evolution of C_1, and the long-term evolution of C_7, C_8 is similar to that of C_6.

5.5 Prediction of the long-term evolution of the random indicator

5.5.1 Stochastic predictive modeling of random vector C

- For $k = K + 1$, the prediction of the vector-valued random indicator $\mathbf{C}^k$ is estimated by $\mathbf{C}^{\mathrm{aff},K+1}$, constructed with Eq. (4.51), for which the parameters are $[A^{\mathrm{opt}}]$, $\mathbf{g}^{\mathrm{aff}}(\tau_{K+1}) = \mathbf{a}_g^{\mathrm{opt}}\,\tau_{K+1} + \mathbf{b}_g^{\mathrm{opt}}$, and $[h^{\mathrm{aff}}(\tau_{K+1})] = [a_h^{\mathrm{opt}}]\,\tau_{K+1} + [b_h^{\mathrm{opt}}]$, as explained in Section 4.5 (see Eq. (4.50)). The vector-valued random indicator $\mathbf{C}^{\mathrm{aff},K+1} = \mathbf{C}^{\mathrm{aff}}(\tau_{K+1})$ at long time τ_{K+1} is then estimated using Eq. (4.51):

$$\mathbf{C}^{\mathrm{aff},K+1} = ([I_{N_c}] - \Delta\tau_{K+1}\,[A])\mathbf{C}^{\mathrm{aff},K} + \Delta\tau_{K+1}\,\mathbf{g}^{\mathrm{aff}}(\tau_{K+1}) + [h^{\mathrm{aff}}(\tau_{K+1})]\,\Delta\mathbf{W}^{K+1}\,, \tag{5.5}$$

  with the initial condition $\mathbf{C}^{\mathrm{aff},K} = \mathbf{C}^{\mathrm{mod}}(\tau_K)$.

- For $k \leq K$, we consider $\mathbf{C}^{\mathrm{aff}}(\tau_k) = \mathbf{C}^{\mathrm{mod}}(\tau_k)$. The prediction for the mean and for the confidence region at 90% of $\mathbf{C}^{\mathrm{aff},K+1}$ is displayed in Figure 5.18 for the components C_1^{aff},C_2^{aff}, and C_6^{aff}.

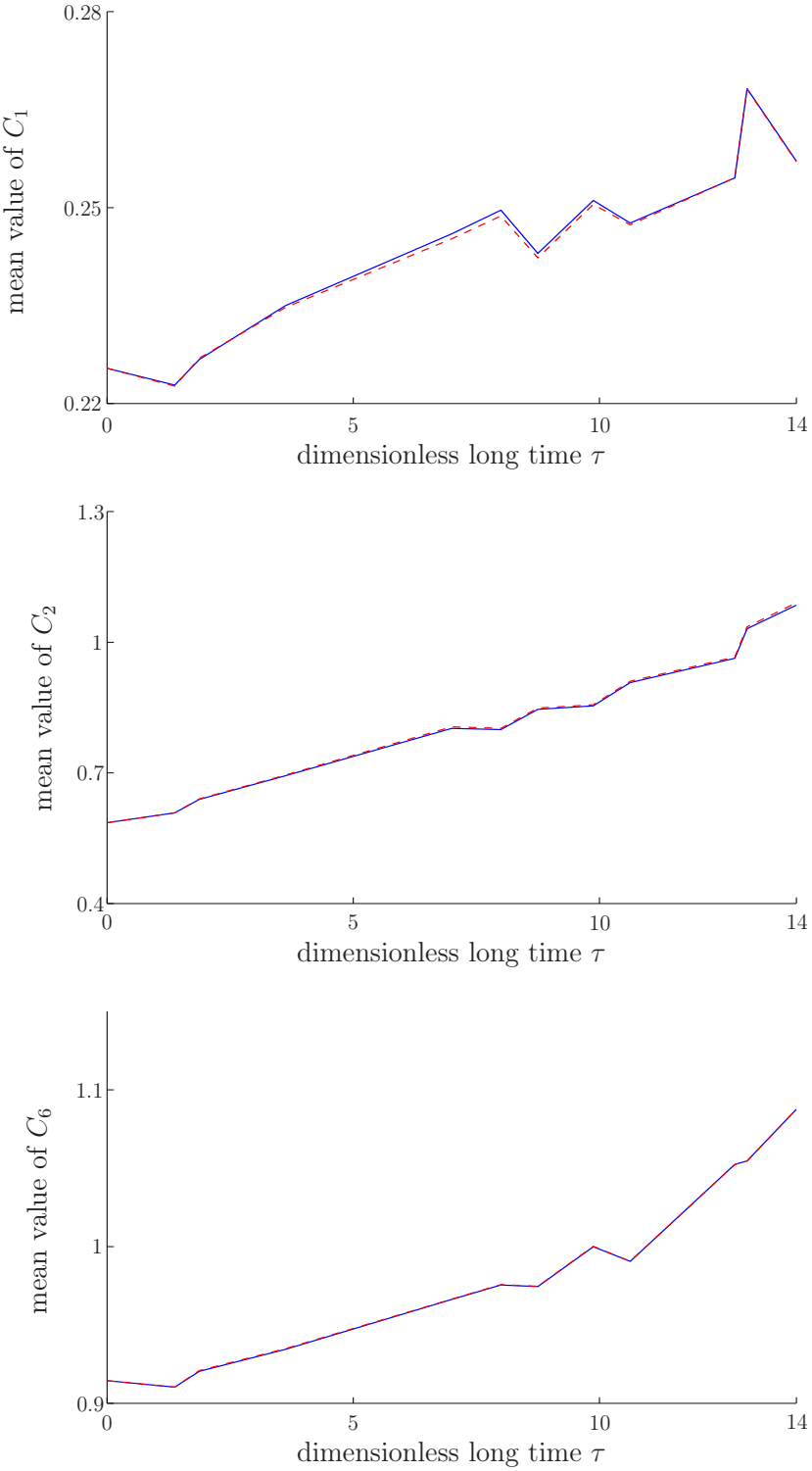

Figure 5.14: Mean values of the long-term evolution for the dimensionless indicator $D(\tau_k) = C_j^{\mathrm{mod}}(\tau_k)$ (solid line) and $D(\tau_k) = C_j^k$ (dashed line), for $j = 1$ (up), $j = 2$ (middle), and $j = 6$ (down).

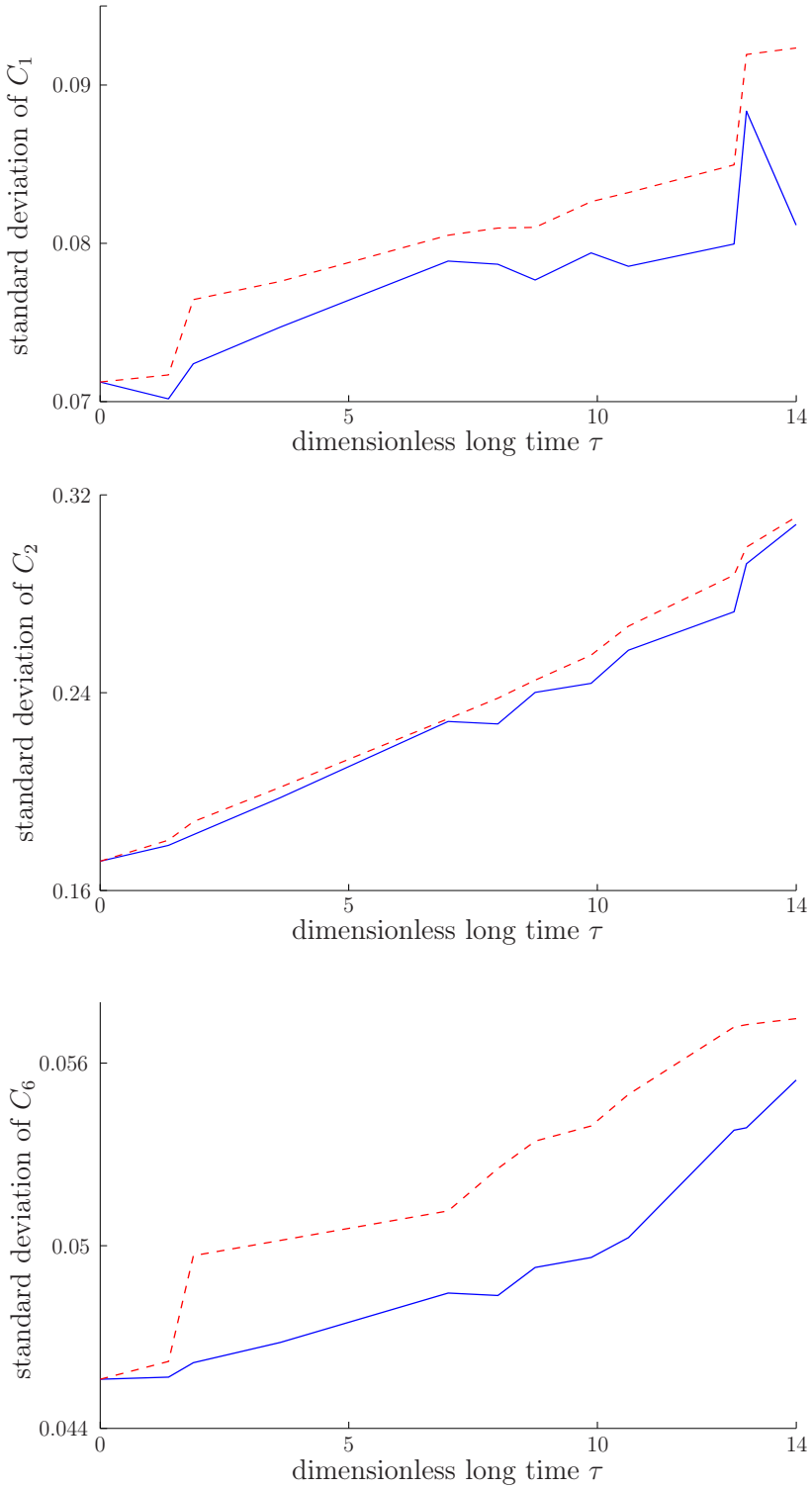

Figure 5.15: Standard deviations of the long-term evolution for the dimensionless indicator $D(\tau_k) = C_j^{\text{mod}}(\tau_k)$ (solid line) and $D(\tau_k) = C_j^k$ (dashed line), for $j = 1$ (up), $j = 2$ (middle), and $j = 6$ (down).

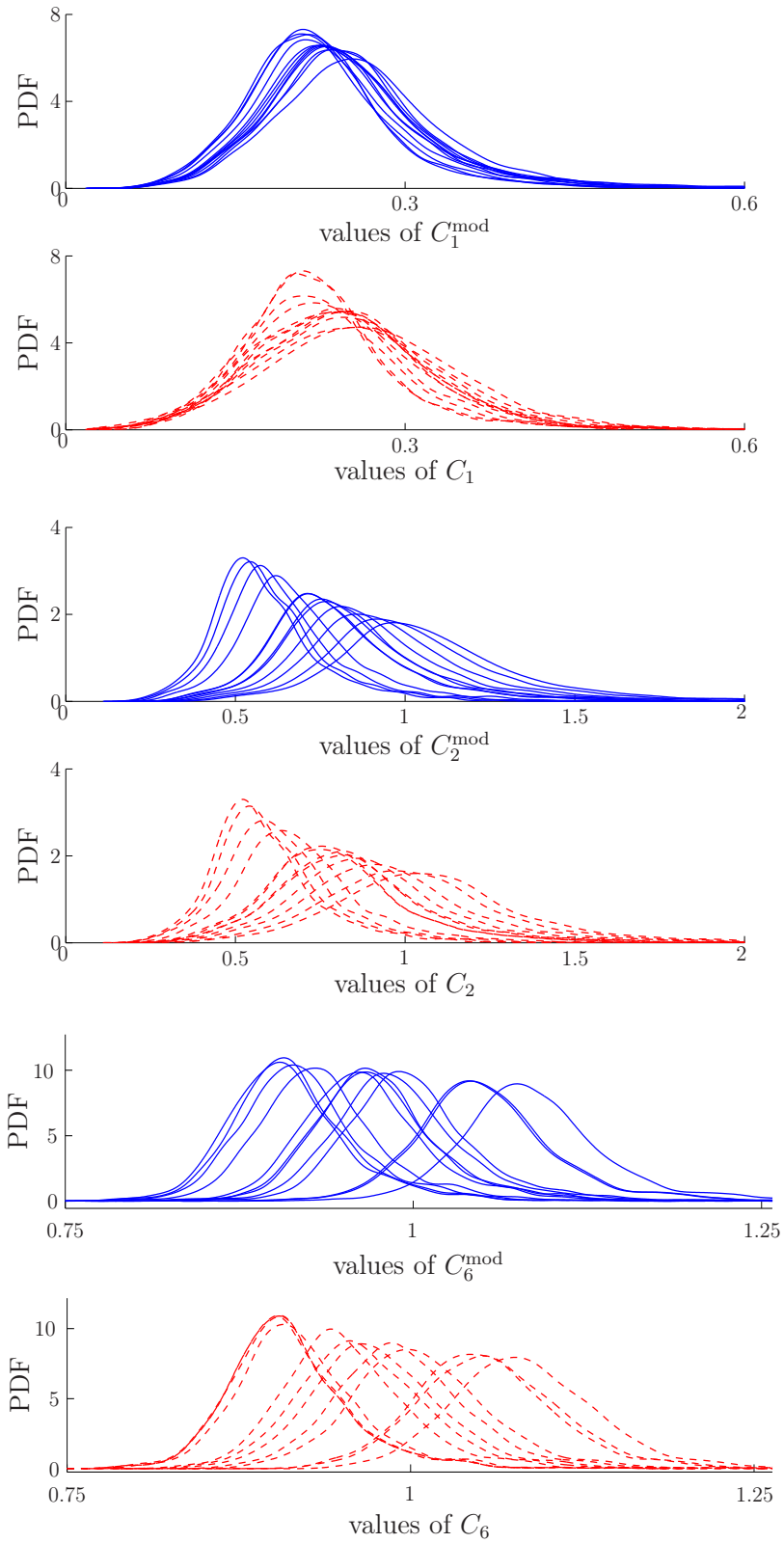

Figure 5.16: Probability density function (PDF) of the dimensionless long-term evolution for the dimensionless indicator $D(\tau_k) = C_j^{\mathrm{mod}}(\tau_k)$ (up, solid line) and $D(\tau_k) = C_j^k$ (down, dashed line): $j = 1$, $j = 2$, and $j = 6$. Each curve corresponds to a given time τ_k. When k is increasing, the curves move to the right.

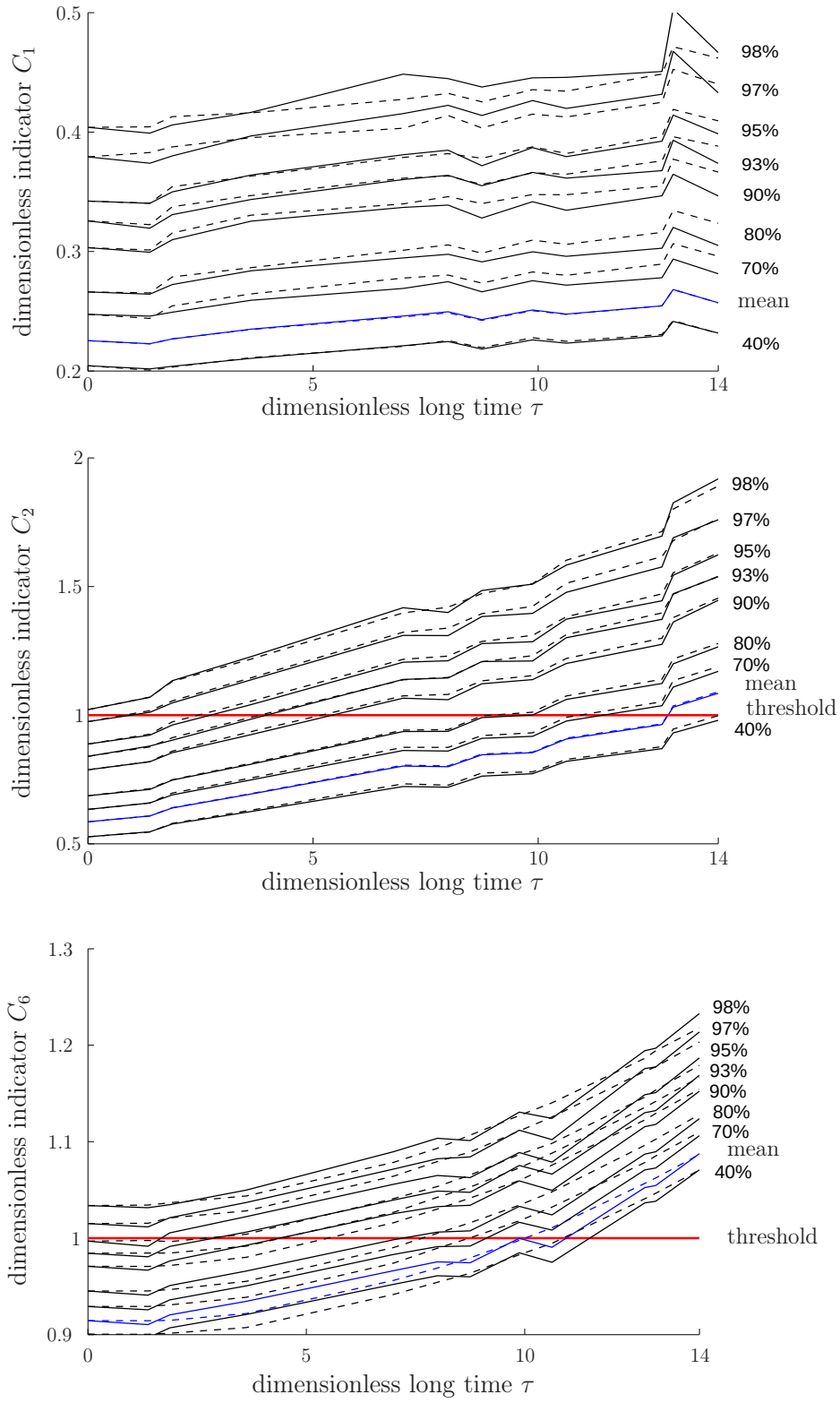

Figure 5.17: Quantiles of the dimensionless long-term evolution for the dimensionless indicator $D(\tau_k) = C_j^{\text{mod}}(\tau_k)$ (solid line) and $D(\tau_k) = C_j^k$ (dashed line): $j = 1$ (up), $j = 2$ (middle) and $j = 6$ (down). Graphs $k \mapsto d^i(\tau_k)$, in which $d^i(\tau_k)$ is such that $P\{D(\tau_k) \leq d^i(\tau_k)\} \geq q^i$ for different values in percent of the quantile q^i belonging to the interval $[40\%, 98\%]$. The horizontal line corresponds to the threshold level c_j^*.

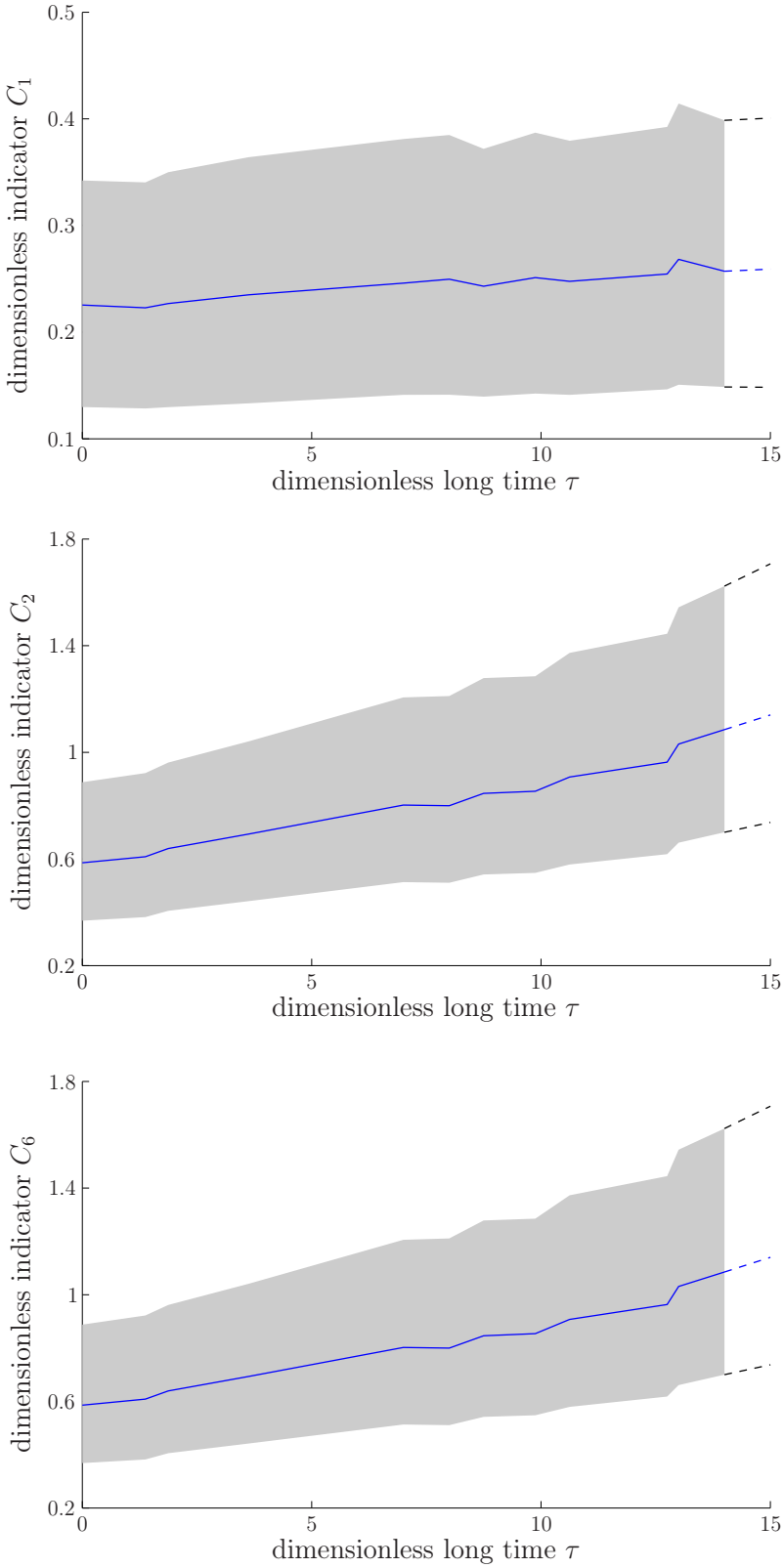

Figure 5.18: Dimensionless long-term evolution and prediction of dimensionless random indicator C_1^{mod}(up), C_2^{mod}(middle), C_6^{mod}(down). Confidence region with probability 90% (grey region), mean value (solid line), prediction (dashed line).

5.5.2 Relevance of the stochastic predictive model

Two criteria are used in order to assess the relevance of the stochastic predictive model that has been identified.

- For the quality assessment, the predictions $\mathbf{C}^{\mathrm{aff},K-1}$ and $\mathbf{C}^{\mathrm{aff},K}$ are performed given the known random vector $\mathbf{C}^{\mathrm{mod}}(\tau_{K-2})$. This prediction is carried out using Eq. (4.50) and Eq. (4.51),

$$\mathbf{C}^{\mathrm{aff},k} = ([I_N] - \Delta\tau_k\,[A^{\mathrm{opt}}])\mathbf{C}^{\mathrm{aff},k-1} + \Delta\tau_k\,\mathbf{g}^{\mathrm{aff}}(\tau_k) + [h^{\mathrm{aff}}(\tau_k)]\,\Delta\mathbf{W}^k \quad , \quad k = K-1, K\,, \tag{5.6}$$

  with the initial condition

$$\mathbf{C}^{\mathrm{aff},K-2} = \mathbf{C}^{\mathrm{mod}}(\tau_{K-2})\,. \tag{5.7}$$

  The quality assessment is then evaluated in comparing firstly $\mathbf{C}^{\mathrm{aff},K-1}$ with $\mathbf{C}^{\mathrm{mod}}(\tau_{K-1})$, and secondly in comparing $\mathbf{C}^{\mathrm{aff},K}$ with $\mathbf{C}^{\mathrm{mod}}(\tau_K)$.

  For the probability density function, the quality assessment of the stochastic predictive model is displayed in Figure 5.19, in which the probability density function of $C_6^{\mathrm{aff},k}$ is compared with the probability density function of $C_6^{\mathrm{mod}}(\tau_k)$ for $k = K-1$ and for $k = K$. For each long times τ_{K-1} and τ_K, the probability density functions of C_6^{aff} and C_6^{mod} are very close. Therefore it should be noted that the stochastic predictive model is good enough.

  For the quantiles of the dimensionless indicator $D(\tau_k) = C_6^{\mathrm{mod}}(\tau_k)$ and $D(\tau_k) = C_6^{\mathrm{aff},k}$ for $k = K-1$ and for $k = K$, the quality assessment can be viewed in Figure 5.20, which displays the graphs $k \mapsto d^i(\tau_k)$, in which $d^i(\tau_k)$ is such that $P\{D(\tau_k) \leq d^i(\tau_k)\} \geq q^i$ for different values in percent of the quantile q^i belonging to the interval $[40\%, 98\%]$. Again this result shows that the stochastic predictive model is good, because the quantiles of $C_6^{\mathrm{aff},k}$ are very close to those of $C_6^{\mathrm{mod},k}$ for $k = K-1$ and for $k = K$.

- The relevance of the stochastic predictive model can be obtained in computing the modeling error induced by both the stochastic predictive model itself (as described in Eq. (4.14)) and the approximations of functions $\mathbf{g}$ and $[h]$ by the affine functions $\mathbf{g}^{\mathrm{aff}}$ and $[h^{\mathrm{aff}}]$. For each $k = 2, \ldots, K$, $\mathbf{C}^{\mathrm{aff},k}$ is computed with Eq. (4.52), using $\mathbf{C}^{\mathrm{mod}}(\tau_{k-1})$ as initial value, that is to say by using the following equation

$$\mathbf{C}^{\mathrm{aff},k} = ([I_N] - \Delta\tau_k\,[A^{\mathrm{opt}}])\mathbf{C}^{\mathrm{mod}}(\tau_{k-1}) + \Delta\tau_k\,\mathbf{g}^{\mathrm{aff}}(\tau_k) + [h^{\mathrm{aff}}(\tau_k)]\,\Delta\mathbf{W}^k\,. \tag{5.8}$$

  The initial condition is given by

$$\mathbf{C}^{\mathrm{aff},1} = \mathbf{C}^{\mathrm{mod}}(\tau_1)\,. \tag{5.9}$$

  For $k = 1, \ldots, K$, for the j-th component of the vector-valued random indicator at time τ_k, the random modeling error denoted by ε_j^k is defined by

$$\varepsilon_j^k = \frac{C_j^{\mathrm{mod}}(\tau_k) - C_j^{\mathrm{aff},k}}{C_j^{\mathrm{mod}}(\tau_k)}\,. \tag{5.10}$$

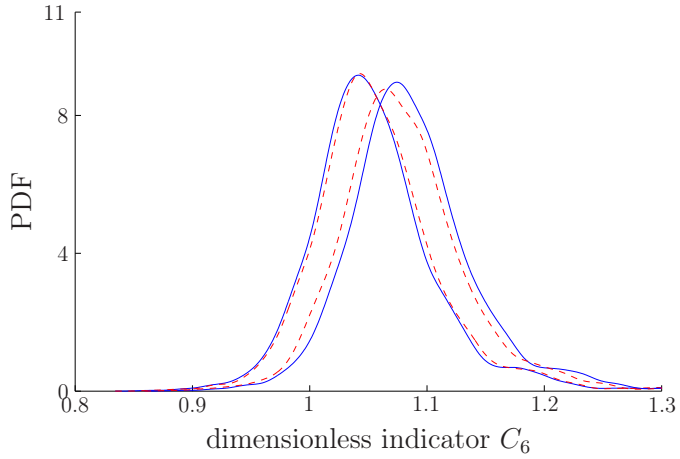

Figure 5.19: Quality assessment of the stochastic predictive model comparing the PDF of $C_6^{\mathrm{aff},k}$ (dashed red line) with the PDF of $C_6^{\mathrm{mod}}(\tau_k)$ (solid blue line) for $k = K - 1$ (left curves) and for $k = K$ (right curves).

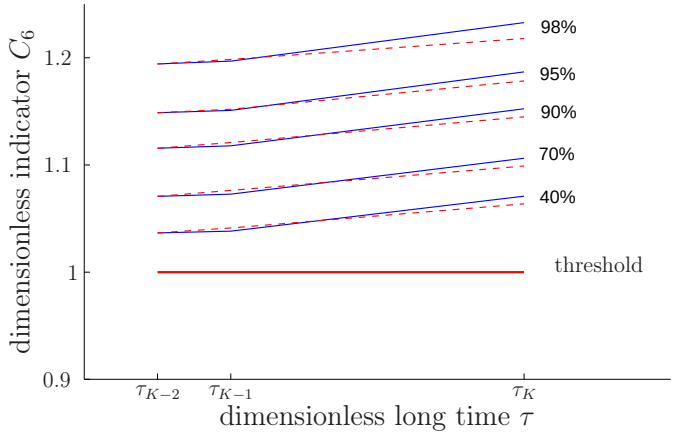

Figure 5.20: Quality assessment of the stochastic predictive model comparing the quantiles of $C_6^{\mathrm{aff},k}$ (dashed red line) with the quantiles of $C_6^{\mathrm{mod}}(\tau_k)$ (solid blue line) for $k = K-1$ and for $k = K$.

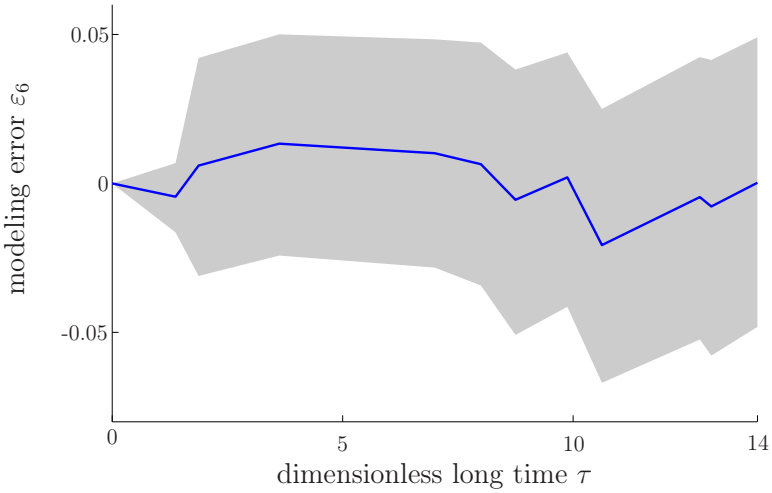

Figure 5.21: Mean value (solid line) and confidence region at 90% (grey region) of the random modeling error ε_6^k.

For the component $j = 6$, the mean value of ε_j^k and its confidence region at 90% are featured in Figure 5.21 for $k = 1, \ldots, K$. It sould be noted that the dispersion is 0 for $k = 1$ corresponding to initial time $\tau_1 = 0$ for which $C_j^{\mathrm{aff},1} = C_j^{\mathrm{mod}}(\tau_1)$. Then, the dispersion slightly increases with long time τ (that is coherent) but stays very small (smaller than 5%).

5.6 Conclusion

In this chapter, the methodology and the models developed in the previous chapters have been applied to the long-term evolution of the dynamic response of the train for a given track stretch. The identified local stochastic model allows us to generate ν realizations of the track irregularities for the given track stretch. Then, for each long time $\tau_1, \ldots, \tau_K$, the dynamic response of the train is numerically simulated by the Monte-Carlo method. After generating ν independent realizations of the multiplicative output noise for the dynamic response of the train, the realizations of the random indicator are computed. These realizations are used to identify the parameters of the stochastic predictive model for the long-term evolution of the random indicator. The prediction of the statistical quantities of the vector-valued random indicator is performed for long time τ_{K+1}, for which no track measurements have been carried out yet. The relevance of the stochastic predictive model is assessed with the quality assessment and with the modeling error induced by the approximations in the stochastic predictive modeling. The obtained results show that the stochastic predictive model is good for the prediction at long time τ_{K+1}.

Chapter 6

Conclusions and prospects

6.1 Summary of the industrial context

For the companies in charge of the maintenance of railway networks, it is of great interest to predict the long-term evolution of the track irregularities of a given stretch of the railway track, in order to be able to anticipate the start off of the maintenance operations. The criteria used for the maintenance of railway tracks have been based, for decades, on the amplitude of chords of the track geometry. Nevertheless, these criteria are not directly linked to safety, ride comfort, or damages of the infrastructure and can be improved using numerical tools. The railway dynamics simulation, achieving the nonlinear link between the track geometry and the dynamic response of the train, offers good opportunities to build criteria that are more representative of safety, comfort, and damages. The numerical simulation actually allows for calculating the accelerations in the vehicles as well as the loads that are applied to the tracks and that lead to the degradation of the track irregularities.

However, concerning the global degradation of the track, the numerical simulation is not sufficient for the identification of degradation laws. The constitutive elements of the track, the substructure, the climatic conditions, and so on, actually are very heterogeneous on the network, such that the construction of a generic degradation law would be very complex and would imply a large number of parameters.

For the French high-speed lines, the track irregularities are regularly measured by the recording train IRIS 320. These measurements provide a large data base that allows for developing a local stochastic modeling of the track irregularities. Combining this local model of the track irregularities with the computational model of the train dynamics, the stochastic dynamic response of the train can be predicted for a given stretch of the track.

To finish with, the construction of a stochastic predictive model for the long-term evolution of the track irregularities allows the anticipation of the maintenance operations in order to optimize the maintenance scheduling.

6.2 Summary of the work achieved

In this thesis, a stochastic predictive model has been developed to predict the long-term evolution of the dynamic response of the train on a given stretch of the track with respect to the long-term evolution of the track irregularities. For the given track stretch, the long-term evolution of the track irregularities is thus characterized by a vector-valued random indicator of the dynamic response of the train.

The track irregularities of the given track stretch have been modeled by introducing a local stochastic model. This local model takes into account the variability of the track irregularities and is specific to each stretch of the track. It has been identified using the measurements of the track irregularities for the given track stretch and using the global stochastic modeling of the track irregularities that has been developed in [19, 6, 20] and which is representative of the track irregularities for the whole track.

A vector-valued random indicator has been defined to assess the dynamic response of the train on the given track stretch, and is estimated by propagating the variability of the track irregularities in a computational model of the train dynamics. Model uncertainties have also been taken into account by introducing a multiplicative output noise in the computation of the vector-valued indicator. This output noise has been characterized by comparing vector-valued indicators computed from the simulated dynamic response of the train with vector-valued indicators calculated from measurements of the dynamic response of the train for a French TGV Duplex. For the given track stretch, the analysis of the long-term evolution of the vector-valued random indicator allows for assessing the criticality of the track stretch. The efficiency of the performed maintenance operation can also be evaluated.

Finally, a stochastic predictive model has been proposed in order to predict the long-term evolution of the vector-valued random indicator for future long times. A Kalman-filter type model with a non-Gaussian initial condition has been identified. The relevance of this stochastic predictive model is analyzed and gives good results. The predictive model allows for anticipating the maintenance operations by comparing the values of the random indicator with a threshold value.

6.3 Scientific and industrial contributions

The originality of this work lays in the application of advanced stochastic techniques on a complex industrial problem. The computational model of the train dynamics is used with a stochastic input and a stochastic output which allow for taking into account the variability of the track irregularities and the model uncertainties in the computational model of the train dynamics.

First, the description of the track irregularities for a given stretch of the track requires to develop a local stochastic model that is specific to each stretch of the track and that preserves the statistical properties identified through the global stochastic model of the track irregularities of the whole railway network. This local stochastic model is constructed in

adding a Gaussian random vector to the global stochastic model, the probability distribution of which is identified by minimizing the statistical distance between the measured track irregularities (for the given track stretch) and the global stochastic model. In addition, the model uncertainties in the computational model of the train dynamics are taken into account by introducing a non-Gaussian multiplicative random vector in output of the computational model. This non-Gaussian random vector has been identified by solving a statistical inverse problem using experimental measurements.

A stochastic predictive model has been proposed in order to model the long-term evolution of the vector-valued random indicator that is represented by a non-Gaussian and nonstationary time series. The stochastic predictive model is a nonstationary Kalman-filter type model for which a non-Gaussian initial condition is given. The identification of this stochastic predictive model depending on a large number of parameters is performed using the known realizations of the vector-valued indicator.

From an industrial point of view, this work, combining mechanics and statistics, gives some tools for performing a local analysis of the track irregularities and for analyzing their long-term evolution. The enrichment of geometrical maintenance criteria with systemic criteria, which are based on the dynamic response of the trains, allows a better understanding of the degradation process as well as a more appropriate maintenance. The developed predictive model will drastically change the maintenance process, which is until now only based on curative operations, allowing predictive maintenance. This model can also give interesting results to set maintenance policies adapted to new trains or new running conditions (for instance higher speeds).

6.4 Prospects

Detection of the causes of the track irregularities. To complete the work achieved in this thesis, the developed tools could be combined with an analysis comparing measured dynamic responses of the train with the shapes and wavelengths of the track irregularities. This could help to determine the origin of the track irregularities. Indeed, some of the track irregularities are caused by rail defects that induce high frequencies accelerations. Others are due to the sliding of soil layers, generating large wavelength evolutions of the geometry. Recurrent track irregularities are moreover often caused by the track substructure: for example uneven track layers or pipes under the ballast. These defects must thus be corrected differently: grinding, drainage, tamping, etc. The knowledge of these origins could therefore drastically improve the maintenance process.

Link between track degradation and track equipment. The intensive use of the developed models on all the available measurements could help to identify a statistical relationship between the track equipment and the long-term evolution of the track irregularities. Furthermore, this analysis would identify construction methods for the track which reduce the degradation of the track irregularities.

Introduction of the traffic in the stochastic predictive model. One of the main drawbacks of the developed model concerns the fact that the long-term evolution of the vector-valued indicator depends only on the measurements carried out at long times and on the simulated realizations of the vector-valued indicator constructed with a stochastic computational model of the train. Any change in the traffic or in the type of trains, which have been used for the identification of the stochastic predictive model, could deteriorate the relevance of the prediction. Instead of the multiplication by a time parameter in the stochastic predictive model, it would thus be relevant to introduce a cumulative rule of the loads induced by the different trains.

6.5 Scientific production

The work achieved in this thesis has brought forward a series of publications and communications, which are listed hereinafter.

Journal publications

- N. Lestoille, C. Soize, C. Funfschilling. Sensitivity of train stochastic dynamics to long-term evolution of track irregularities. Vehicle System Dynamics, *submitted*.
- N. Lestoille, C. Soize, C. Funfschilling. Stochastic prediction of high-speed train dynamics to long-term evolution of track irregularities. Mechanics Research Communications, *submitted*.

Conferences with proceedings

- N. Lestoille, C. Soize, C. Funfschilling. Characterization of the evolution of the train dynamic response under the effect of track irregularities. IAVSD 2015, 24th International Symposium on Dynamics of Vehicles on Roads and Tracks, August 2015, Graz, Austria. Proceedings of IAVSD 2015.
- N. Lestoille, C. Soize, C. Funfschilling. Stochastic modeling of train dynamics under effect of track irregularities and experimental comparisons. USD 2014, 5th International Conference on Uncertainty in Structural Dynamics, September 2014, Leuven, Belgium. Proceedings of ISMA2014-USD2014.
- N. Lestoille, C. Soize, G. Perrin, C. Funfschilling. Long time evolution of train dynamics with respect to track irregularities. Railways 2014, 2nd International Conference on Railway Technology: Research, Development and Maintenance, April 2014, Ajaccio, France. Proceedings of Railways 2014.

Conference without proceedings

- C. Funfschilling, G. Perrin, N. Lestoille, D. Lebel, C. Soize. Influence of the track geometry variability on the dynamics of high speed trains. COMPDYN 2015, 5th ECCOMAS Thematic Conference on Computational Methods in Structural Dynamics and Earthquake Engineering, May 2015, Crete Island, Greece.

- N. Lestoille, C. Soize, G. Perrin, C. Funfschilling. Track geometry degradation under effect of the train dynamics. Railway Track Science and Engineering. 1st International Workshop, December 2013, Paris, France.

Appendix

A Post-processing of the measured track irregularities

Measurement of the track geometry. The French high-speed lines are regularly measured by the recording high-speed train IRIS 320, which provides big data used for characterizing and modeling the track irregularities. Before being used for the stochastic modeling of the track irregularities and for the computation of the dynamic response of the train, the measurements of the track irregularities have to be post-processed. This post-processing is necessary in order to remove the measurement errors and to put the experimental data into the format required for the stochastic modeling of the track irregularities and the numerical simulation of the dynamic response of the train.

In this work, we focus on the high-speed line between Paris and Marseille which is composed of two tracks, denoted by V1 and V2. V1 is used by the trains running from Paris to Marseille, and V2 is used by the trains running from Marseille to Paris. The high-speed trains have two locomotives, one at each end of the train, denoted by M1 and M2. Usually, M1 is at the front of the train when the train runs on V1, and M2 is at the front when the train runs on V2. The total length of the measured track is denoted by S^{tot} and its discrete curvilinear abscissa $s_0 = 0, s_1, \ldots, s_L = S^{\text{tot}}$ is introduced to locate the position of the train on the track. The spatial step of the curvilinear abscissa $h = s_n - s_{n-1}$, for $n = 1, \ldots, L$, is constant. For the measurements of the track irregularities, the curvilinear abscissa is measured by an odometric wheel and is given in output of the measurement system. Each time the recording train passes over a localization sensor on the track, the measured curvilinear asbcissa is rectified. The zero of the measured curvilinear abscissa is situated manually, wich creates a lag with the real curvilinear abscissa. Moreover, since the measurement system with the odometric wheel is not perfect, an error is introduced in the measured data. For each discrete curvilinear abscissa along the track s_n, the following quantities are measured by IRIS 320, and are represented by discrete functions of s_n:

- the curvilinear abscissa s,
- the speed of the train v,
- the horizontal curvature of the track c_H,
- the lateral positions of the left rail e_L and of the right rail e_R,

- the lateral positions of the left rail h_L and of the right rail h_R,

The positions of the rail are measured using two cameras that are fixed under a bogie of the train. At last, it has to be noticed that the measurement is not correctly processed when the train speed is less than 80km/h. Such measurements have then to be removed.

For the modeling of the track irregularities and for the computational model of the train dynamics, the following conventions are used:

- the curvilinear abscissa increases on V1 and decreases on V2.
- the horizontal curvature is positive when the track turns to the right, and negative when the track turns to the left.
- the measured track sections are at least 5 km long.

The track design is known, which allows for comparing the theoretical horizontal curvature with the measured one.

Re-sampling the curvilinear abscissa. The curvilinear abscissa given in output of the measurement system is piecewise constant, with groups of 4 samples with a jump of $4\,h$ between each group of 4 samples, which yields $0, 0, 0, 0,\ 4\,h, 4\,h, 4\,h, 4\,h,\ 8\,h, 8\,h, 8\,h, 8\,h,$ $\ldots, s_{L-1}, s_{L-1}, s_{L-1}, s_{L-1}, s_L$. It is thus re-sampled with a linear interpolation in order to have a linear increasing and continuous curvilinear abscissa.

Removing measurement errors. It happens that the track irregularities are not properly measured by IRIS 320. These measurement errors have to be detected and removed, such that they do not disturb the stochastic modeling of the track irregularities. Three types of measurement errors are identified.

- Sometimes the cameras stop measuring and the value of the position of the rail remains constant during several decades of meters. For this work, the first derivative of the position of the rail is computed. When the value of this derivative stays zero during at least 20 m, the corresponding measurement is removed.
- Some values measured for the rail position are irrelevant because they are too high. A threshold value is chosen, above which the values of the rail position are considered irrelevant. The quantile q_0 at 99.9% of the rail position Y is defined by $P_Y(Y \leq q_0) = 0.999$. The threshold value for irrelevant measured data is chosen as $3\,q_0$ for the rail position at each curvilinear abscissa. Using a quantile prevents us from having to chose an arbitrary threshold, which would not be adapted to all the measurements. The irrelevant values, provided that they represent no more than 3 meters of the track, are removed and substituted by substitution values. The substitution values have to be realistic and to ensure a continuity of the second derivative ($\mathcal{C}^2$-continuity) with existing values. A cubic spline is chosen to compute the substitution values.

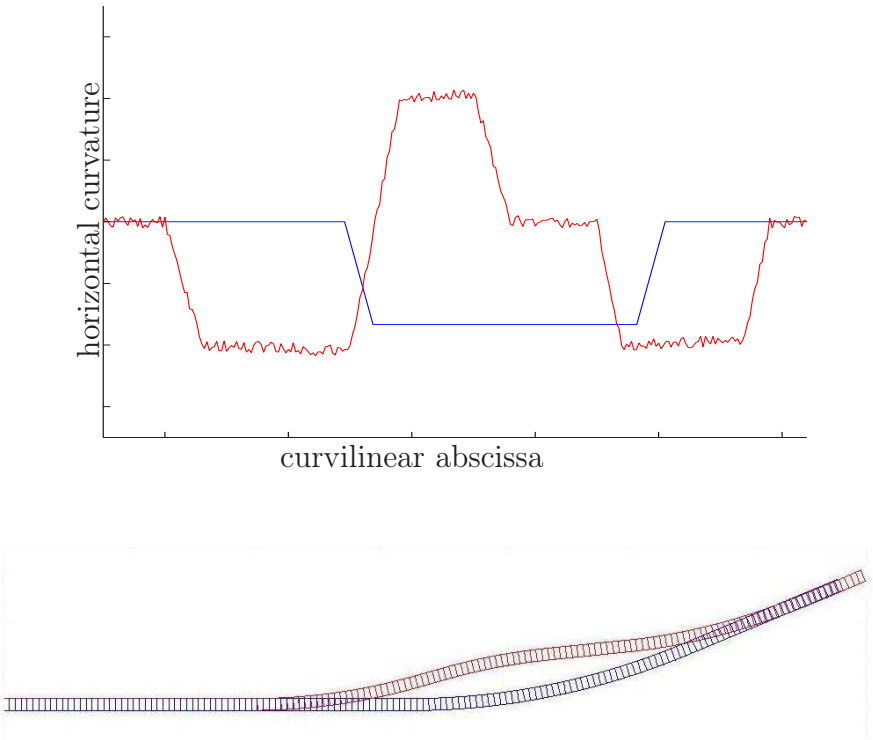

Figure 6.1: Detection of a change of running track by comparing the measured horizontal curvature (blue line) with the theoretical one (red line).

- At last, some jumps in the measurements of the rail position exist. These jumps are detected using the second derivative of the measured rail positions. A threshold value for the values of the second derivative is introduced as $1.5\,q_2$, where q_2 is the quantile at 99.999% of the rail position. The irrelevant values of the rail position are substituted by substitution values computed with a cubic spline, ensuring the continuity of the second derivative for the track irregularities.

Verification of the running direction. When the locomotive M2 is in front of the train on track V1 or the locomotive M1 is in front of the train on track V2, it means that the train runs in the unusual direction on the track. In order to compare these measured data with the usual ones, the measurements for the right and left rails have to be interchanged, so that they correspond to the right and left rails measured in the usual running direction. The sign of the measured horizontal curvature also has to be inverted.

Comparison of the measured horizontal curvature with the theoretical one. It happens that IRIS 320 changes briefly of running track (for example to double another train) or takes a service track. This implies that IRIS 320 briefly measures a track that does not correspond to the principal measured track: this measurement is then removed. Such cases are detected in comparing the measured horizontal curvature with the theoretical one, as displayed in Figure 6.1.

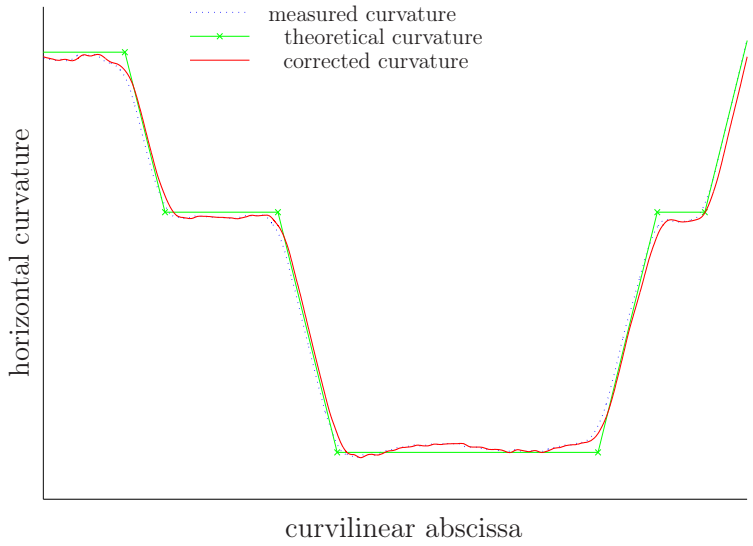

Figure 6.2: Correction of the curvilinear abscissa by comparing the measured horizontal curvature with the theoretical one, yielding the corrected measured curvature.

The curvilinear abscissa given in output of the measurement system does not exactly correspond to the theoretical curvilinear abscissa, because the zero of the measured curvilinear abscissa is given manually. Sometimes the difference between both can be of several decades of meters. The measured curvilinear abscissa has therefore to be rectified in order to correct this difference. The difference is computed by comparing the measured horizontal curvature c_H with the theoretical one c_H^{th}. The measured horizontal curvature, the theoretical curvature, and the measured horizontal curvature taking into account the rectification, are displayed in Figure 6.2.

Smoothing of the rectification done by the localization sensors of the track. The rectification of the curvilinear abscissa by the sensors on the track creates jumps in the measurements. To remove these jumps, the curvilinear abscissa is linearly interpolated in these rectification zones over 3 m. The rail positions for these zones are substituted with cubic splines over three meters, in order to guarantee the continuity of the second derivative of the track irregularities.

Rectification of the curvilinear abscissa for a track stretch. Once the measurement errors are corrected and the curvilinear abscissa is rectified for the whole measured track, the track is partitioned into stretches of length S used for the stochastic modeling of the track irregularities. For a given stretch of the railway track, the measured curvilinear abscissa of the track irregularities s_n, for $n = 0, \ldots, N_s$, can change between two consecutive measurement times τ_{k-1}, τ_k, $k = 2, \ldots, K$. The shift between two consecutive measurement times is corrected by comparing the sum of the track irregularities at τ_k with this sum at τ_{k-1}.

B Construction of the spectral function allowing the cut-off frequency to be defined

Let Z be a time signal, which represents either an experimental measurement or a response predicted with the computational model. This time signal is deduced from the spatial signal using the speed of the train (which is not constant with the time). Let Z^ℓ, $\ell = 1, \ldots, \nu_p$ be the corresponding time signals for ν_p stretches of the track. Let F_s be the sampling frequency that is given. The corresponding time step is $\delta t = 1/F_s$. Let N_ℓ be the given number of time steps for the track stretch ℓ. Consequently, for the track stretch ℓ, the time duration is $T_\ell = N_\ell\, \delta t$. The associated frequency resolution is thus $1/T_\ell$. For each ℓ, the discrete Fourier transform $\{\widehat{Z^\ell}(m), m \in \{0, \ldots, N_\ell - 1\}\}$ of the time series $\{\widetilde{Z^\ell}(n), n \in \{0, \ldots, N_\ell - 1\}\}$ is computed by

$$\widehat{Z^\ell}(m) = \sum_{n=0}^{N_\ell - 1} \widetilde{Z^\ell}(n) \exp(\frac{-2\, i\, \pi\, n\, m}{N_\ell}) \quad , \quad m = 0, \ldots, \max_\ell N_\ell - 1\,, \tag{6.1}$$

in which $\widetilde{Z^\ell}$ is written as

$$\widetilde{Z^\ell}(n) = \frac{1}{F_s}\, W_T(n)\, Z^\ell(n)\, \exp(i\pi n) \quad , \quad n = 0, \ldots, N_\ell - 1\,, \tag{6.2}$$

where $W_T(n)$ is the Hamming time window which is written as

$$W_\ell(n) = \frac{1}{\sqrt{T_\ell}}\, 1.5863\, (0.54 - 0.46\, \cos(\frac{2\pi n}{T_\ell})) \quad , \quad n = 0, \ldots, N_\ell - 1\,. \tag{6.3}$$

We then define the spectral function by the formula

$$D_Z(m) = \frac{1}{2\pi\nu_p} \sum_{\ell=1}^{\nu_p} |\widehat{Z^\ell}(m)|^2 \quad , \quad m = 0, \ldots, \max_\ell N_\ell\,. \tag{6.4}$$

C Correction of the measurements of the train dynamic response

The localization of the measuring TGV Duplex with respect to the track design is performed with an odometric wheel, which is not sufficiently precise, and which introduces a shift between the measured and the real curvilinear abscissa. This shift is corrected as follows.

First, the measured lateral acceleration in the second coach of the train is filtered with a low-pass filter and double-integrated, in order to compute the lateral displacement of the second coach at low frequencies. Because of the rigid bodies movements in the curves of the track, the inverse of the lateral displacement should vary as the track horizontal curvature does. The shift in the measured curvilinear abscissa is computed by comparing the inverse of the lateral displacement with the theoretical track horizontal curvature. This first step provides a large estimation of the shift of the curvilinear abscissa which is refined in a second step.

Then, the dynamic response of the train on the measured track is numerically simulated. The simulated vertical acceleration in the first bogie is compared with the measured one. Since the simulated vertical acceleration is very close to the measured one (because of little modeling errors and little nonlinearities), the comparison of both allows for calculating the shift in the measured curvilinear abscissa.

Bibliography

[1] A. Lopez-Pita, P.F. Teixeira, C. Casas, A. Baschiller, and P.A. Ferreira. Maintenance costs of high-speed lines in Europe. *Transportation Research Record: Journal of the Transport Research Board*, 2043:13–19, 2008.

[2] T. Karis. *Track Irregularities for High-Speed Trains*. Master thesis, KTH University, 2009.

[3] Y. Ben-Haim, S. Cogan, and L. Sanseigne. Usability of mathematical models in mechanical decision processes. *Mechanical Systems and Signal Processing*, 12(1):121–134, 1998.

[4] M. Guedri, S. Cogan, and N. Bouhaddi. Robustness of structural reliability analyses to epistemic uncertainties. *Mechanical Systems and Signal Processing*, 28:458–469, 2012.

[5] S. Kraft. *Parameter Identification for a TGV Model*. PhD thesis, Ecole Centrale Paris, 2012.

[6] G. Perrin. *Random Fields and Associated Statistical Inverse Problems for Uncertainty Quantifications - Applications to Railway Track Geometries for High-Speed Trains Dynamical Responses and Risk Assessment*. PhD thesis, Universite Paris Est, 2013.

[7] D. Clouteau, E. Savin, and D. Aubry. Stochastic simulations in dynamic soil-structure interaction. *Meccanica*, 36(4):379–399, 2001.

[8] A. Hot, G. Kerschen, E. Foltête, and S. Cogan. Detection and quantification of nonlinear structural behavior using principal component analysis. *Mechanical Systems and Signal Processing*, 26(1):104–116, 2012.

[9] D.F. Elliott. *Handbook of Digital Signal Processing: Engineering Applications*. Academic Press, 1987.

[10] S.J. Orfanidis. *Introduction to Signal Processing*. Prentice-Hall, 1995.

[11] P. Stoica and R.L. Moses. *Spectral Analysis of Signals*. Pearson/Prentice Hall, Upper Saddle River, USA, 2005.

[12] R.N. Iyengar and O.R. Jaiswal. Random field modeling of railway track irregularities. *Journal of Transportation Engineering*, 3(August):303–308, 1995.

[13] R.N. Iyengar and O.R. Jaiswal. A new model for non-Gaussian random excitations. *Probabilistic Engineering Mechanics*, 8:281–287, 1993.

[14] X. Lei and N.A. Noda. Analyses of dynamic response of vehicle and track coupling with random irregularity of track vertical profile. *Journal of Sound and Vibration*, 258(1):147–165, 2002.

[15] C. Esveld. Computer-aided maintenance and renewal of track. In *Railroad Conference*, pages 165–170. Technical papers presented at the 1990 ASME/IEEE joint, 1990.

[16] A. Hamid and A. Gross. Track-quality indices and track-degradation models for maintenance-of-way planning. *Transportation Research Record: Journal of the Transport Research Board*, 802:2–8, 1981.

[17] M. El-Sibaie and Y. Zhang. Objective track quality indices. *Transportation Research Record: Journal of the Transport Research Board*, 1863:81–87, 2004.

[18] H.B. Zheng, Q.S. Yan, J.L. Hu, and Z. Chen. Numercial simulation of railway track irregularities based on stochastic expansion method of standard orthogonal basis. *Applied Mechanics and Materials*, 178:1373–1378, 2012.

[19] G. Perrin, C. Soize, D. Duhamel, and C. Funfschilling. Modeling the track geometry variability. In *10th World Congress on Computational Mechanics*, Sao Paulo, Brazil, 2012.

[20] G. Perrin, C. Soize, D. Duhamel, and C. Funfschilling. Track irregularities stochastic modeling. *Probabilistic Engineering Mechanics*, 34:123–130, 2013.

[21] N Wiener. The homogeneous chaos. *American Journal of Mathematics*, 60:897–936, 1938.

[22] R. Ghanem and P.D. Spanos. Polynomial chaos in stochastic finite elements. *Journal of Applied Mechanics*, 57(1):197–202, 1990.

[23] A.J. Bing and A. Gross. Development of railroad track degradation models. *Transportation Research Record: Journal of the Transport Research Board*, 939:27–31, 1983.

[24] C. Esveld. *Modern Railway Track*. 2001.

[25] Y. Zhang, L. Ferreria, and M. Murray. Track degradation prediction: criteria, methodology and models. In *21st Australasian Transport Research Forum*, pages 391–405, Adelaide, 1997.

[26] J. Zhao, A.H.C. Chan, C. Roberts, and A.B. Stirling. Optimizing policies of railway ballast tamping and renewal. *Transportation Research Record: Journal of the Transport Research Board*, 1943:50–56, 2006.

[27] A.P. Patra, P. Soderholm, and U. Kumar. Uncertainty estimation in railway track life cycle cost: a case study from Swedish National Rail Administration. *Proceedings of the Institution of Mechanical Engineers, Part F: Journal of Rail and Rapid Transit*, 223(3):285–293, 2009.

[28] A.R. Andrade and P.F. Teixeira. A Bayesian model to assess rail track geometry degradation through its life-cycle. *Research in Transportation Economics*, 36(1):1–8, 2012.

[29] A.R. Andrade and P.F. Teixeira. Statistical modelling of railway track geometry degradation using hierarchical Bayesian models. *Reliability Engineering and System Safety*, 142:169–183, 2015.

[30] S. Mercier, C. Meier-Hirmer, and M. Roussignol. Bivariate Gamma wear processes for track geometry modelling, with aplication to intervention scheduling. *Structure and Infrastructure Engineering*, 8(4):367–366, 2012.

[31] C. Meier-Hirmer. *Modèles et Techniques Probabilistes pour l'Optimisation des Stratégies de Maintenance : Application au Domaine Ferroviaire*. PhD thesis, Université de Marne-la-Vallée, 2007.

[32] C. Vale and S.M. Lurdes. Stochastic model for the geometrical rail track degradation process in the Portuguese railway Northern Line. *Reliability Engineering and System Safety*, 116:91–98, 2013.

[33] M. Audley and J.D. Prescott. The effects of tamping on railway track geometry degradation. *Proceedings of the Institution of Mechanical Engineers, Part F: Journal of Rail and Rapid Transit*, 2013.

[34] H Guler. Prediction of track railway geometry deterioration using artificial neural networks: a case study for Turkish state railways. *Structure and Infrastructure Engineering*, 10(5):614–626, 2014.

[35] D. Prescott and J. Andrews. Stochastic state space methods for railway network asset management modelling. *Advances in Risk and Reliability Technology Symposium*, 2013.

[36] J. Andrews, D. Prescott, and F. de Rozières. A stochastic model for railway track asset management. *Reliability Engineering and System Safety*, 130:76–84, 2014.

[37] L. Bai, R. Liu, Q. Sun, F. Wang, and P. Xu. Markov-based model for the prediction of railway track irregularities. *Proceedings of the Institution of Mechanical Engineers, Part F: Journal of Rail and Rapid Transit*, 229(2):150–159, 2015.

[38] D. Prescott and J. Andrews. Investigating railway track asset management using a Markov analysis. *Proceedings of the Institution of Mechanical Engineers, Part F: Journal of Rail and Rapid Transit*, 229(4):402–416, 2015.

[39] C. Zhong and Y. Xu. Forecast method study on track longitudinal level irregularity based on most possible similarity model. *Advanced Materials Research*, 779:1705–1710, 2013.

[40] P. Xu, R. Liu, and F. Wang. Novel description method for track irregularity evolution. *International Journal of Computational Intelligence Systems*, 4(6):1358–1366, 2011.

[41] R. Guo and B. Han. Multi-stage linear prediction model for railway track irregularity. *Applied Mechanics and Materials*, 361-363:1811–1816, 2013.

[42] J. Chaolong, X. Weixiang, W. Futian, and W. Hanning. Track irregularity time series analysis and trend forecasting. *Discrete Dynamics in Nature and Society*, 2012, 2012.

[43] H. Chebli, D. Clouteau, and L. Schmitt. Dynamic response of high-speed ballasted railway tracks: 3D periodic model and in situ measurements. *Soil Dynamics and Earthquake Engineering*, 28(2):118–131, 2008.

[44] P. Ferreira. *Modelling and Prediction of the Dynamic Behaviour of Railway Infrastructures at very high Speeds*. PhD thesis, Universidade Tecnica de Lisboa, 2010.

[45] G. Degrande, D. Clouteau, R. Othman, M. Arnst, H. Chebli, R. Klein, P. Chatterjee, and B. Janssens. A numerical model for ground-borne vibrations from underground railway traffic based on a periodic finite element-boundary element formulation. *Journal of Sound and Vibration*, 293(3-5):645–666, 2006.

[46] G. Lombaert, G. Degrande, J. Kogut, and S. François. The experimental validation of a numerical model for the prediction of railway induced vibrations. *Journal of Sound and Vibration*, 297(3-5):512–535, 2006.

[47] G. Lombaert and G. Degrande. Ground-borne vibration due to static and dynamic axle loads of InterCity and high-speed trains. *Journal of Sound and Vibration*, 319(3-5):1036–1066, 2009.

[48] G. Degrande and L. Schillemans. Free field vibrations during the passage of a Thalys high-speed train at variable speed. *Journal of Sound and Vibration*, 247(1):131–144, 2001.

[49] G. Lombaert, P. Galvín, S. François, and G. Degrande. Quantification of uncertainty in the prediction of railway induced ground vibration due to the use of statistical track unevenness data. *Journal of Sound and Vibration*, 333(18):4232–4253, 2014.

[50] A. Al Shaer, D. Duhamel, K. Sab, G. Foret, and L. Schmitt. Experimental settlement and dynamic behavior of a portion of ballasted railway track under high speed trains. *Journal of Sound and Vibration*, 316(1-5):211–233, 2008.

[51] P.A. Ferreira and A. Lopez-Pita. Numerical modelling of high-speed train/track system for the reduction of vibration levels and maintenance needs of railway tracks. *Construction and Building Materials*, 79:14–21, 2015.

[52] S. Iwnicki and S. Grassie. Track settlement prediction using computer simulation tools. *Vehicle System Dynamics*, 33:37–46, 2000.

[53] H. True, A. P. Engsig-Karup, and D. Bigoni. On the numerical and computational aspects of non-smoothnesses that occur in railway vehicle dynamics. *Mathematics and Computers in Simulation*, 95:78–97, 2013.

[54] N. Ananthanarayana. Track irregularity limits from consideration of track-vehicle interaction. *Mathematical and Computer Modelling*, 11:932–935, 1988.

[55] G. Lönnbark. Characterization of Track Irregularities with Respect to Vehicle Response. Technical report, KTH University, Stockholm, 2012.

[56] C. Funfschilling, G. Perrin, and S. Kraft. Propagation of variability in railway dynamic simulations: application to virtual homologation. *Vehicle System Dynamics*, 50:245–261, 2012.

[57] H. Ishii, Y. Fujino, Y. Mizuno, and K. Kaito. The study of train intelligent monitoring system using acceleration of ordinary trains. 2006.

[58] Y. Mizuno, Y. Fujino, K. Kataoka, and Y. Matsumoto. Development of a mobile sensing unit and its prototype implementation. *Tsinghua Science and Technology*, 13:223–227, 2008.

[59] A. Lopez Pita, P.F. Teixeira, C. Casas, A. Bachiller, and M. Sanchez. Deterioration in geometric track quality on high-speed lines. In *TRB 85th annual meeting*, Washington DC, 2006.

[60] D. Cantero and B. Basu. Railway infrastructure damage detection using wavelet transformed acceleration response of traversing vehicle. *Structural Control and Health Monitoring*, 22(1):62–70, 2015.

[61] P. Czop, K. Mendrok, and T. Uhl. Application of inverse linear parametric models in the identification of rail track irregularities. *Archive of Applied Mechanics*, 81:1541–1554, 2011.

[62] G. Perrin, C. Soize, D. Duhamel, and C. Funfschilling. Identification of polynomial chaos representations in high dimension from a set of realizations. *SIAM Journal on Scientific Computing*, 34(6):A2917–A2945, 2012.

[63] G. Perrin, C. Soize, D. Duhamel, and C. Funfschilling. Karhunen-Loève expansion revisited for vector-valued random fields: scaling, errors and optimal basis. *Journal of Computational Physics*, 242:607–622, 2013.

[64] G. Perrin, C. Soize, D. Duhamel, and C. Funfschilling. A posteriori error and optimal reduced basis for stochastic processes defined by a finite set of realizations. *SIAM/ASA Journal of Uncertainty Quantification*, 2:745–762, 2014.

[65] C. Soize. Identification of high-dimension polynomial chaos expansions with random coefficients for non-Gaussian tensor-valued random fields using partial and limited experimental data. *Computer Methods in Applied Mechanics and Engineering*, 199(33-36):2150–2164, 2010.

[66] G. Foeillet, F. Coudert, and V. Delcourt. IRIS 320 is a global concept inspection vehicle merging engineering and R&D tools for infrastructure maintenance. In *Eight World Congress on Railway Research*, Seoul, South Korea, 2008.

[67] F. Coudert and B. Richard. IRIS 320 GEOV: a new track geometry recoding system designed continuing on from the Mauzin track recording coaches. *Revue Generale des Chemins de Fer*, pages 7–22, 2009.

[68] R. Ghanem and P.D. Spanos. *Stochastic Finite Elements: A Spectral Approach, rev. ed.* Dover Publications, New York, 2003.

[69] O. Le Maitre and O. Knio. *Spectral Methods for Uncertainty Quantification.* Springer, New York, 2010.

[70] C. Soize. *Stochastic Models of Uncertainties in Computational Mechanics.* American Society of Civil Engineers, Reston, USA, 2012.

[71] B.Y. George, R. Terrell, and D.W. Scott. Variable kernel density estimation. *The Annals of Statistics*, 20(3):1236–1265, 1992.

[72] A.W. Bowman and W. Azzalini. *Applied Smooting Techniques for Data Analysis.* Oxford University Press, Oxford, 1997.

[73] J.J. Kalker. Wheel-rail rolling contact theory. *Wear*, 144(1):243–261, 1991.

[74] J.J. Kalker. *Three-Dimensional Elastic Bodies in Rolling Contact.* Springer, 2nd edition, 2013.

[75] N. Lestoille, G. Perrin, and C. Funfschilling. Characterization of the influence of rail wear on train dynamics. In *COMPDYN 2013*, Kos Island, Greece, 2013.

[76] UIC. Testing and approval of railway vehicles from the point of view of their dynamic behaviour - Safety - Track fatigue - Running behaviour. *Leaflet 518*, 2009.

[77] E. Capiez-Lernout and C. Soize. Robust updating of uncertain damping models in structural dynamics for low- and medium-frequency ranges. *Mechanical Systems and Signal Processing*, 22(8):1774–1792, 2008.

[78] C. Soize, E. Capiez-Lernout, J.-F. Durand, C. Fernandez, and L. Gagliardini. Probabilistic model identification of uncertainties in computational models for dynamical systems and experimental validation. *Computer Methods in Applied Mechanics and Engineering*, 198(1):150–163, 2008.

[79] P. Whittle. *Hypothesis Testing in Time Series.* PhD thesis, 1951.

[80] G. Box and G.M. Jenkins. *Time Series Analysis: Forecasting and Control.* Holden-Day, San Francisco, 1970.

[81] A Papoulis. *Signal Analysis.* McGraw-Hill, 1977.

[82] M B Priestley. *Spectral Analysis and Time Series.* Academic Press, New York, 1981.

[83] M.B. Priestley. *Nonlinear and Nonstationary Time Series Analysis*. Academic Press, London, 1988.

[84] C. Soize. Fundamentals of Random Signal Analysis - Application to Modal Identification in Structural Dynamics, 1997.

[85] G.C. Reinsel. *Elements of Multivariate Time Series Analysis*. Springer, 2003.

[86] A Schuster. On the periodicities of sunspots. *Philosophical Transactions of the Royal Society of London*, Serie A:69–100, 1906.

[87] G. Groves and E.J. Hannan. Time series regression of sea level on weather. *Reviews of Geophysics*, 6(2):129–174, 1968.

[88] T. Yuzuriha. The autocorrelation curves of schizophrenic brain waves and the power spectrum. *Psych. Neurol. Jap.*, 26:911–924, 1960.

[89] G. Gudmundsson. Time series analysis of imports, exports and other economic variables. *Journal of the Royal Statistical Society*, Series A(General):383–412, 1971.

[90] J. Kaipo and E. Somersalo. *Statistical Computational Inverse Problems*. Springer, New York, 2005.

[91] B.P. Carlin and T.A. Louis. *Bayesian Methods for Data Analysis*. CRC Press, Boca Raton, 3rd edition, 2009.

[92] T.R. Fleming and D.P. Harrington. Estimation for discrete time nonhomogeneous Markov chains. *Stochastic Processes and their Applications*, 7(2):131–139, 1978.

[93] P. Whittle. *Prediction and Regulation by Linear Least-Square Methods*. University of Minnesota Press, 1983.

[94] J.D. Hamilton. *Time Series Analysis*. Princeton University Press, Princeton, USA, 1994.

[95] B. Pfaff. *Analysis of Integrated and Cointegrated Time Series with R*. Springer, New York, 2nd edition, 2008.

[96] R. Dahlhaus. Fitting time series models to nonstationary processes. *The Annals of Statistics*, 25(1):1–37, 1997.

[97] R.E. Kalman. A new approach to linear filtering and prediction problems. *Journal of Fluids Engineering*, 82(1):35–45, 1960.

[98] R.E. Kalman and R.S. Bucy. New results in linear filtering and prediction problems. *Journal of Fluids Engineering*, 83(1):95–108, 1961.

[99] G. Favier. *Filtrage, Modélisation et Identification de Systèmes Linéaires Stochastiques à Temps Discret*. Editions du CNRS, 1982.

[100] A.C. Harvey. *Forecasting, Structural Time Series Models and the Kalman Filter*. Cambridge University Press, Cambridge, 1989.

[101] G. Evensen. *Data Assimilation: The Ensemble Kalman Filter*. Springer-Verlag, Berlin, Heidelberg, 2nd edition, 2009.

[102] L. Guikhman and A.V. Skorokhod. *The Theory of Stochastic Processes*. Springer-Verlag, Berlin, 1979.

[103] R.Z. Hasminskii. *Stochastic Stability of Differential Equations*. Springer, Heidelberg, 2nd edition, 2012.

[104] N. Ikeda and S. Watanabe. *Stochastic Differential Equations and Diffusion Processes*. North-Holland, Asmterdam, 1981.

[105] C. Soize. *The Fokker-Planck Equation for Stochastic Dynamical Systems and its Explicit Steady State Solutions*. World scientific publishing Co Pte Ltd, Singapore, 1994.

[106] P. Ciarlet. *Inroduction à l'Analyse Numérique Matricielle et à l'Optimisation*. Masson, 2nd edition, 2001.

[107] T.F. Coleman and Y. Li. A reflective newton method for minimizing a quadratic function subject to bounds on some of the variables. *SIAM Journal on Optimization*, 6(4):1040–1058, 1996.

Modèle stochastique de la dynamique des trains à grande vitesse pour la prévision de l'évolution à long terme des défauts de géométrie de la voie.

Thèse préparée au laboratoire de Modélisation et Simulation Multi-Echelle :
MSME UMR 8208 CNRS
5, boulevard Descartes
77 454 Marne-la-Vallée
France

Résumé. Les voies ferrées sont de plus en plus sollicitées : le nombre de trains à grande vitesse, leur vitesse et leur charge ne cessent d'augmenter, ce qui contribue à la formation de défauts de géométrie sur la voie. En retour, ces défauts de géométrie influencent la réponse dynamique du train et dégradent les conditions de confort. Pour garantir de bonnes conditions de confort, les entreprises ferroviaires réalisent des opérations de maintenance de la voie, qui sont très coûteuses. Ces entreprises ont donc intérêt à prévoir l'évolution temporelle des défauts de géométrie de la voie pour anticiper les opérations de maintenance, et ainsi réduire les coûts de maintenance et améliorer les conditions de transport.
Dans cette thèse, on analyse l'évolution temporelle d'une portion de voie par un indicateur vectoriel sur la dynamique du train. Pour la portion de voie choisie, on construit un modèle stochastique local des défauts de géométrie de la voie à partir d'un modèle global des défauts de géométrie et de big data de défauts mesurés par un train de mesure. Ce modèle stochastique local prend en compte la variabilité des défauts de géométrie de la voie et permet de générer des réalisations des défauts pour chaque temps de mesure. Après avoir validé le modèle numérique de la dynamique du train, les réponses dynamiques du train sur la portion de voie mesurée sont simulées numériquement en utilisant le modèle stochastique local des défauts de géométrie. Un indicateur vectoriel et aléatoire est introduit pour caractériser la réponse dynamique du train sur la portion de voie. Cet indicateur est construit de manière à prendre en compte les incertitudes de modèle dans le modèle numérique de la dynamique du train. Pour identifier le modèle stochastique des défauts de géométrie et pour caractériser les incertitudes de modèle, des méthodes stochastiques avancées, comme par exemple la décomposition en chaos polynomial ou le maximum de vraisemblance multidimensionnel, sont appliquées à des champs aléatoires non gaussiens et non stationnaires.
Enfin, un modèle stochastique de prévision est proposé pour prévoir les quantités statistiques de l'indicateur, ce qui permet d'anticiper le besoin en maintenance. Ce modèle est construit en utilisant les résultats de la simulation de la dynamique du train et consiste à utiliser un modèle non stationnaire de type filtre de Kalman avec une condition initiale non gaussienne.

Mots clefs : Défauts de géométrie de la voie, dynamique du train, modélisation stochastique, prévision stochastique, problème inverse statistique.

Stochastic model of high-speed train dynamics for the prediction of long-term evolution of the track irregularities.

Abstract. Railway tracks are subjected to more and more constraints, because the number of high-speed trains, the train speed, and the train load keep increasing. These solicitations go towards producing track irregularities. In return, track irregularities influence the dynamic response of the train, inducing a degradation of the comfort. To guarantee good conditions of comfort in the trains, railway companies perform maintenance operations of the track, which are very costly. Consequently, it is of great interest for the railway companies to predict the long-term evolution of the track irregularities for a given stretch of track, in order to be able to anticipate the start off of the maintenance operations, and therefore to reduce the maintenance costs and to improve the running conditions.
In this thesis, the long-term evolution of a given track stretch is analyzed through a vector-valued indicator on the train dynamics. For this given track portion, a local stochastic model of the track irregularities is constructed using a global stochastic model of the track irregularities, as well as big data made of experimental measurements of the track irregularities performed by a measuring train. This local stochastic model takes into account the variability of the track irregularities and allows for generating realizations of the track irregularities at each long time. After validating the computational model of the train dynamics, the dynamic responses of the train on the measured track portion are numerically simulated using the local stochastic model of the track irregularities. A vector-valued random indicator is defined to characterize the dynamic responses of the train on the given track stretch. This random indicator is constructed such that it takes into account the model uncertainties in the computational model of the train dynamics. For the identification of the stochastic model of the track irregularities and the characterization of the model uncertainties, advanced stochastic methods such as the polynomial chaos expansion and the multivariate maximum likelihood are applied to non-Gaussian and nonstationary random fields. Finally, a stochastic predictive model is proposed for predicting the statistical quantities of the random indicator, which allows for anticipating the need for track maintenance. This modeling is constructed using the results of the train dynamics simulation and consists in using a nonstationary Kalman-filter type model with a non-Gaussian initial condition. The proposed model is validated using experimental data from the French railways network for high-speed trains.

Key-words : Track irregularities, train dynamics, stochastic modeling, stochastic prediction, statistical inverse problem.